Lattice QCD determination of weak decays of B mesons

Judd Gavin Ivo Henry Harrison

Robinson College

University of Cambridge

Department of Applied Mathematics and Theoretical Physics

Faculty of Mathematics

Supervisor: Dr Matthew Wingate

This dissertation is submitted for the degree of Doctor of Philosophy.

August 2018

Lattice QCD determination of weak decays and mixing of B mesons

Judd Gavin Ivo Henry Harrison

This thesis uses a variety of numerical and statistical techniques to perform high precision calculations in high energy physics using quantum field theory. It introduces the experimental motivation for the calculation of B meson form factors and includes a discussion of previous work. It then describes the modern theoretical framework describing these phenomena, outlining quantum chromodynamics and electroweak theory, and then illustrating the procedure of gauge fixing, the quantum effective action and background field gauge which is required for subsequent perturbative work. Details of the basic methodology of lattice quantum field theory are given as well as the specific formulation of the relativistic and nonrelativistic models used in this work to describe quantum chromodynamics. A comprehensive calculation of the zero recoil $B \to D^*$ form factor is then presented, using state of the art lattice techniques with relativistic sea charm quarks and light sea quarks with correct physical masses, leading to a discussion of the dominant sources of uncertainty and possible resolutions of experimental tensions. Also included is preliminary work towards the full calculation of nonzero recoil matrix elements, with the aim of outlining possible future work. Finally, this thesis presents the computation of parameters correcting for radiative one loop phenomena and corrections to the kinetic coupling parameters in nonrelativistic quantum chromodynamics in order to achieve a desirable level of precision in future calculations. This is done using Monte-Carlo integration to evaluate integrals from diagrams generated using automated lattice perturbation theory in background field gauge in order to match the coefficients of the effective action between the lattice and the continuum.

Acknowledgements

First and foremost I would like to thank my supervisor Matthew Wingate for the countless hours of discussion, support and guidance he has given so freely. I would also like to thank my collaborators Ciaran Hughes, with whom I was lucky enough to learn from during innumerable afternoons of discussion in one of our adjacent offices, as well as Christine Davies and Ron Horgan for the many insightful conversations we have shared and for their instruction and patience in developing projects together. I would also like to thank Andrew Lytle, Brian Colquhoun, Jonna Koponen, Bipasha Chakraborty and Junko Shigemitsu for the time they spent helping me get up to speed as well as their continuing insights in our work together for the HPQCD collaboration. Finally I would like to thank all of the lattice people at DAMTP; most notably Antoni Woss and Gavin Cheung for making my time in the department so enjoyable and interesting, and for making B2.11 such a friendly place to work.

Declaration

This dissertation is the result of my own work and includes nothing which is the outcome of work done in collaboration except as declared in the Preface and specified in the text. It is not substantially the same as any that I have submitted, or, is being concurrently submitted for a degree or diploma or other qualification at the University of Cambridge or any other University or similar institution except as declared in the Preface and specified in the text. I further state that no substantial part of my dissertation has already been submitted, or, is being concurrently submitted for any such degree, diploma or other qualification at the University of Cambridge or any other University or similar institution except as declared in the Preface and specified in the text.

Signed 

(Judd Harrison)

Date 19/11/2018

List of Publications

- [1] "Lattice QCD calculation of the $B_{(s)} \to D^*_{(s)}\ell\nu$ form factors at zero recoil and implications for $|V_{cb}|$"
  Judd Harrison, Christine T. H. Davies and Matthew Wingate
  HPQCD Collaboration
  Phys. Rev. D 97 (2018) 054502, arXiv:1711.11013

- [2] "Improving the kinetic couplings in lattice non-relativistic QCD"
  Ciaran Hughes, Christine T. H. Davies, Judd Harrison, Ronald R. Horgan, Georg M. von Hippel, and Matthew Wingate (HPQCD Collaboration)
  In preparation

- [3] "Improving the theoretical prediction for the $B_s - \bar{B}_s$ width difference: matrix elements of next-to-leading order $\Delta B = 2$ operators"
  Christine Davies, Judd Harrison, G Peter Lepage, Christopher Monahan, Junko Shigemitsu, and Matthew Wingate
  EPJ Web Conf. 2018, vol. 175, 13023

Abstract

This thesis uses a variety of numerical and statistical techniques to perform high precision calculations in high energy physics using quantum field theory. It introduces the experimental motivation for the calculation of B meson form factors and includes a discussion of previous work. It then describes the modern theoretical framework describing these phenomena, outlining quantum chromodynamics and electroweak theory, and then illustrating the procedure of gauge fixing, the quantum effective action and background field gauge which is required for subsequent perturbative work. Details of the basic methodology of lattice quantum field theory are given as well as the specific formulation of the relativistic theory and nonrelativistic approximations used in this work to describe quantum chromodynamics. A comprehensive calculation of the zero recoil $B \to D^*$ form factor is then presented, using state of the art lattice techniques with relativistic charm sea quarks and light sea quarks with correct physical masses, leading to a discussion of the dominant sources of uncertainty and possible resolutions of experimental tensions. Also included is preliminary work towards the full calculation of nonzero recoil matrix elements, with the aim of outlining possible future work. Finally, this thesis presents the computation of parameters correcting for radiative one loop phenomena and corrections to the kinetic coupling parameters in nonrelativistic quantum chromodynamics in order to achieve a desirable level of precision in future calculations. This is done using Monte-Carlo integration to evaluate integrals from diagrams generated using automated lattice perturbation theory in background field gauge in order to match the coefficients of the effective action between the lattice and the continuum.

Contents

List of Figures

List of Tables

Chapter 1

Introduction

The standard model of particle physics provides a description of the universe in the form of an $SU(3) \times SU(2) \times U(1)$ gauge theory coupling six flavours of spin half fermionic quarks and six leptons. Nuclear physics is encoded in the $SU(3)$ sector known as Quantum chromodynamics (QCD). Of the six quarks, in this thesis, we only concern ourselves with the five lightest, the up, down, strange, charm and bottom, and neglect the top quark which is so relatively massive as to decouple from the physics of interest. The electroweak $SU(2) \times U(1)$ sector of the standard model couples different flavours of quarks and leptons and lepton neutrinos to $W^{\pm}$ and Z bosons as well as coupling the electrically charged quarks and leptons to photons.

When doing perturbative calculations in quantum field theory at energy E, away from the renormalisation scale, μ, one encounters logarithms going like the ratio E/μ which become large when E is much larger or smaller than μ. One could renormalise the theory at a scale μ' closer to E in order to avoid such logarithms. A more powerful procedure is to use the value of the renormalised coupling defined at μ as an initial condition from which to calculate a new coupling defined at the new scale μ' This is done by integrating the $\beta-$function $\beta(g) = \frac{\partial}{\ln\mu} g$. In QCD $\beta(g)$ is negative and therefore as μ increases the magnitude of g decreases and the uncertainty coming from higher order diagrams in perturbation theory decreases. This is known as asymptotic freedom and the perturbative framework has been used extensively in high energy applications at scales well above Λ_{QCD} where the QCD coupling is small.

Flavour changing interactions, which we focus on here, are perturbative in the electroweak interaction but often require the computation of matrix elements of composite quark states when the interaction takes place in the context of mesons. These occur at

energies at which perturbation theory is ineffective and require nonperturbative methods in order to be calculated and related to experiments.

More recently improvements in available computational power have made nonperturbative calculations possible within the framework of lattice QCD, originally outlined by Wilson [12]. Such calculations have seen much success, accurately computing such quantities as hadronic masses [13], form factors [14] and decay constants [15], to name a few. As the procedure of lattice regularisation involves moving the system of interest from a continuus infinite space-time to a discrete four dimensional grid of finite size, it is obviously important that the physics of interest take place on scales which are not so large as to wrap around the grid nor too small to be resolved by the lattice spacing. The first restriction is often avoided by taking artificially large up and down quark masses such that the pion correlation length is small compared to the box. This is a frequent compromise made by lattice theorists e.g. [16, 17], though calculations done with physical or extremely close pion masses are becoming more commonplace [18, 19, 20, 21]. The latter restriction is less straightforward to overcome, since in order for the lattice to remain the same physical volume the number of points must grow as a^{-4}, where a is the lattice spacing. A proven method of overcoming this problem is to use an effective theory for heavy quarks, such as HQET [22] or NRQCD. In this thesis I will use NRQCD, performing a number of the required perturbative matching calculations, together with physical lattices using the modern lattice formalism of highly improved staggered quarks to compute form factors of particular physical interest to a high degree of precision.

Chapter 2

Continuum High Energy Physics

This chapter outlines the aspects of the standard model in the continuum relevant to the physics we will later investigate on the lattice. It explains the origins of the unitarity of the CKM matrix and gives examples of current constraints. Continuing to discuss quantum chromodynamics, a crucial ingredient in making predictions for meson interactions and decays, it outlines the continuum procedure of gauge fixing. It then discusses the quantum effective action and background field gauge, both of which will be utilised in the lattice perturbation theory calculation of one loop improvement parameters in NRQCD in chapter 5.

2.1 Electroweak Theory and the CKM Matrix

The $SU(2)$ gauge interaction of the standard model couples exclusively to left handed fermions. We write

$$Q_L^i = (u_L^i, d_L^i) \tag{2.1}$$

where the i index indicates the generation of quark. The electroweak coupling part of the quark action is given via the gauge covariant derivative by

$$\mathcal{L}_{\text{weak,quark}} = \sum_{i=1,2,3} \bar{Q}_L^i \not{D} Q_L^i + \bar{u}_R^i \not{D} u_R^i + \bar{d}_R^i \not{D} d_R^i. \tag{2.2}$$

D_μ is the $SU(2) \times U(1)_\Upsilon$ gauge covariant derivative given by

$$D_\mu = \partial_\mu + igW_\mu^a t_a + ig' B_\mu \Upsilon, \tag{2.3}$$

where W is the $SU(2)$ gauge field, t_a are the $SU(2)$ generators, B is the $U(1)_\Upsilon$ gauge field and Υ is the $U(1)_\Upsilon$ hypercharge generator. The higgs-quark couplings are given by

$$\mathcal{L}_{\text{quark},\phi} = \sum_{i,j} \lambda_d^{ij} \bar{Q}_L^i \phi d_R^j + \lambda_u^{ij} \epsilon^{\alpha\beta} \bar{Q}_L^{i,\alpha} \phi^{\dagger\beta} u_R^j + \text{hermitian conjugate}, \tag{2.4}$$

where the higgs field ϕ is a scalar $SU(2)$ doublet with hypercharge $1/2$ and the Yukawa couplings λ_u and λ_d are real.

After electroweak symmetry breaking, we transform the quark fields between generations according to the unitary transformation

$$u_R^i \to \sum_j U_R^{ij} u_R^j \tag{2.5}$$

$$d_R^i \to \sum_j D_R^{ij} d_R^j \tag{2.6}$$

$$u_L^i \to \sum_j U_L^{ij} u_L^j \tag{2.7}$$

$$d_L^i \to \sum_j D_L^{ij} d_L^j \tag{2.8}$$

with

$$U_L^\dagger \lambda_u U_R = \Lambda_u \tag{2.9}$$

$$D_L^\dagger \lambda_d D_R = \Lambda_d \tag{2.10}$$

in order to obtain an action with mass terms diagonal in flavour. The flavour changing currents present in $\sum_{i=1,2,3} \bar{Q}_L^i \not{D} Q_L^i$ are not invariant under this transformation to the "mass basis" and transform as

$$j^\mu = \bar{u}_L^i \gamma^\mu d_L^i \to \bar{u}_L^j (U_L^\dagger D_L)^{ij} \gamma^\mu d_L^j \tag{2.11}$$

where the appearance of the new matrix $U_L^\dagger D_L = V_{\text{CKM}}$, known as the Cabibbo-Kobyashi-Maskawa matrix, is responsible for the tree level flavour changing weak interaction. By construction V_{CKM} is unitary, meaning that experimental results for each

element must obey strong constraints if the standard model is to be consistent. The CKM matrix does not have as many degrees of freedom as one would naively expect of a 3×3 unitary matrix, this is a consequence of the fact that the standard model is invariant under global $U(1)$ transformations done on any quark field. Such transformations eliminate relative phases: as such the CKM matrix has four degrees of freedom.

2.2 QCD Action

Quantum chromodynamics is the sector of the standard model which aims to reproduce the dynamics of quarks and the particles built from them known as hadrons. It is an $SU(3)$ Yang-Mills gauge theory coupling the six flavours of spin half quarks to spin one gluons. The fields 'live' on Minkowski spacetime and the Lagrangian is given by

$$\mathcal{L}_{\text{QCD}} = -\frac{1}{2}\text{tr}\left[F_{\mu\nu}F^{\mu\nu}\right] + \sum_f \bar{\psi}_f(i\gamma^\mu D_\mu - m_f)\psi_f. \tag{2.12}$$

The covariant derivative is given by

$$D_\mu = \frac{\partial}{\partial x^\mu} + igA^a_\mu t_a \tag{2.13}$$

where t_a form a hermitian, traceless basis for the Lie algebra of $SU(3)$ and $F_{\mu\nu} = F^a_{\mu\nu}t_a$ with $F^a_{\mu\nu} = \partial_\mu A^a_\nu - \partial_\nu A^a_\mu - g f^a_{bc} A^b_\mu A^c_\nu$ and f^a_{bc} are structure constants $if^a_{bc}t_a = [t_b, t_c]$. This lagrangian is tailored so that we may change ψ and $\bar{\psi}$ locally by an element of the gauge group $SU(3)$ and also make a related change to the gauge fields such that the lagrangian remains invariant. Considering a local, infinitesimal change in the fermion fields $\psi \to (1+i\epsilon^a t_a)\psi$, $\bar{\psi} \to \bar{\psi}(1-i\epsilon^a t_a)$ we see that the fermionic part of the lagrangian transforms like

$$\begin{aligned}\mathcal{L}_q &\to \sum_f \bar{\psi}_f(1 - i\epsilon^a t_a)(i\gamma^\mu\partial_\mu - g\gamma^\mu A^a_\mu t_a - m_f)(1 + i\epsilon^a t_a)\psi_f \\ &= \sum_f \bar{\psi}_f(i\gamma^\mu\partial_\mu - g\gamma^\mu A^a_\mu t_a - m_f - \gamma^\mu\partial_\mu\epsilon^a t_a + g\gamma^\mu f^a_{bc}A^b_\mu\epsilon^c)\psi_f.\end{aligned} \tag{2.14}$$

In order to remain invariant we must therefore also make the change

$$A^a_\mu \to A^a_\mu - \frac{1}{g}\partial_\mu\epsilon^a + f^a_{bc}A^b_\mu\epsilon^c. \tag{2.15}$$

This gauge transformation, and the invariance of quantities under it, forms a useful tool allowing us to simplify many calculations considerably.

2.2.1 Gauge fixing

When we construct quantum field theories using the field integral approach as our template for quantisation we begin by postulating a lagrangian, which we have done, and then proceed to introduce a functional field integral over the fields. The functional integral is usually defined in terms of Feynman diagrams constructed from the propagators coming from the quadratic part of the action and the expansion in terms of coupling parameters of the potential terms. For gauge fields there is an obvious problem, which is that the infinite possible gauge transformations on a given field configuration contribute equally. What we really want to do is integrate over gauge configurations modulo gauge transformations. Using the identity

$$1 = \int \mathcal{D}[\lambda]\delta(G[A^\lambda])\det\Big(\frac{\delta G[A^\lambda]}{\delta\lambda}\Big), \tag{2.16}$$

where A^λ is the field A gauge transformed with the local gauge parameter λ, we find

$$\begin{aligned}&\int \mathcal{D}[A]e^{iS[A]}\\ &= \int \mathcal{D}[\alpha]\int \mathcal{D}[A]e^{iS[A]}\delta(G[A^\alpha])\det\Big(\frac{\delta G[A^\alpha]}{\delta\alpha}\Big).\end{aligned} \tag{2.17}$$

One typically takes a general gauge condition $\partial^\mu A^a_\mu = \omega^a(x)$ such that $G[A] = \partial^\mu A^a_\mu - \omega^a(x)$. The delta function and determinant can then be expressed in terms of bosonic and fermionic integrals

$$\delta(G[A^\alpha]) = \int \mathcal{D}h e^{ihG[A^\alpha]} \tag{2.18}$$

$$\det\Big(\frac{\delta G[A^\alpha]}{\delta\alpha}\Big) = \int \mathcal{D}[\bar{c},c]e^{-i\bar{c}\frac{\delta G[A^\alpha]}{\delta\alpha}c} \tag{2.19}$$

where c and $\bar{c}$ are grassman valued fields in the adjoint representation and h is a real field, also in the adjoint representation. These additional fields are known as Faddeev-Popov ghosts. Using the gauge condition $\partial^\mu A^a_\mu = \omega^a(x)$ it is common to integrate over $\omega(x)$ with gaussian weight $\int \mathcal{D}[\omega]e^{-\frac{\omega^2}{2\epsilon}}$, doing so we find the expression for the gauge

fixed field integral, in terms of the constant gauge parameter ϵ,

$$\begin{aligned} &\int \mathcal{D}[A] e^{iS[A]} \delta(G[A^\alpha]) \det\Big(\frac{\delta G[A^\alpha]}{\delta \alpha}\Big) \\ &= C \int \mathcal{D}[A, h, \bar{c}, c] e^{i(S[A] - \frac{\epsilon}{2}(h_a)^2 + h_a(\partial^\mu A^a_\mu) - \bar{c}\partial^\mu D_\mu c)}. \end{aligned} \tag{2.20}$$

2.3 Quantum Effective Action

When I come to perform the perturbative calculation of improvement factors for the NRQCD action it will be convenient to work with the effective action in background field gauge. I discuss these here, in the context of a general theory. The starting point is the expression of the generating functional of the theory in terms of an exponential of connected diagrams

$$Z[J] = \int \mathcal{D}[\phi] e^{iS[\phi]+i\int dx\phi J} = e^{iW[J]}. \tag{2.21}$$

Since $Z[J]$, the sum of all connected and disconnected diagrams, is equal to the exponential of the sum of connected diagrams, $iW[J]$ is the sum of all connected vacuum diagrams in the presence of the current J. We define the expectation of ϕ in the presence of J

$$\phi_J = \frac{\delta}{\delta J} W[J]. \tag{2.22}$$

We can invert this to find the current J for which $\phi_J = \phi'$, which we call $J_{\phi'}$, and define the quantum effective action via the Legendre transformation

$$\Gamma[\phi] = W[J_\phi] - \int dx \phi J_\phi. \tag{2.23}$$

One may show [23], by considering the use of Γ in place of S in (2.21) with coefficient g^{-1}, that

$$iW[J] = \int_{\text{connected,tree}} \mathcal{D}[\phi] e^{i\left[\Gamma[\phi]+\int dx J\phi\right]} \tag{2.24}$$

where, as in [23], the integral is to be interpreted in the perturbative diagrammatic sense. The connected graphs contributing to $iW[J]$ can be seen as tree graphs whose vertices are one particle irreducible (1PI) subgraphs. For (2.24) to hold the vertices in $\Gamma[\phi]$ must be 1PI connected graphs with ϕ in place of external lines. As such we may write

$$i\Gamma[\phi_0] = \int_{\text{connected,1PI}} \mathcal{D}[\phi] e^{iS[\phi+\phi_0]}. \tag{2.25}$$

2.3.1 Background Field Gauge

In this section I discuss the background field gauge and show, following [23], how the background field effective action is invariant under residual gauge transformations of the background fields.

Consider the QCD action in the presence of a classical background field denoted by a tilde. Integrating out h, taking $A \to A + \tilde{A}$, $\psi \to \psi + \tilde{\psi}$, $c \to c + \tilde{c}$ and $\bar{c} \to \bar{c} + \tilde{\bar{c}}$ and choosing the gauge fixing functional

$$G[A]^a = \tilde{D}_\mu A^{\mu a}, \quad \tilde{D}_\mu A^{\mu a} = \partial_\mu A^{\mu a} + ig f^a_{bc} \tilde{A}^b_\mu A^{\mu c} \tag{2.26}$$

we see that the gauge fixing term $(\tilde{D}_\mu A^\mu)^2$ is invariant under the infinitesimal transformations

$$\begin{aligned} \tilde{A}^a_\mu \to \tilde{A}^{a'}_\mu &= \tilde{A}^a_\mu - \frac{1}{g}\partial_\mu \epsilon^a + f^a_{bc}\epsilon^b \tilde{A}^c_\mu \\ A^a_\mu \to A^{a'}_\mu &= A^a_\mu + f^a_{bc}\epsilon^b A^c_\mu. \end{aligned} \tag{2.27}$$

Taken together, these implement a normal gauge transformation on the field $A + \tilde{A}$, so provided the background and quantum fermionic fields also transform as

$$\begin{aligned} \psi &\to \psi + i t_a \epsilon^a \psi \\ \tilde{\psi} &\to \tilde{\psi} + i t_a \epsilon^a \tilde{\psi} \end{aligned} \tag{2.28}$$

the original action will be invariant. Invariance of the ghost action requires we also take

$$\begin{aligned} c^a &\to c^a - f^a_{bc}\epsilon^b c^c \\ \tilde{c}^a &\to \tilde{c}^a - f^a_{bc}\epsilon^b \tilde{c}^c \\ \bar{c}^a &\to \bar{c}^a - f^a_{bc}\epsilon^b \bar{c}^c \\ \tilde{\bar{c}}^a &\to \tilde{\bar{c}}^a - f^a_{bc}\epsilon^b \tilde{\bar{c}}^c. \end{aligned} \tag{2.29}$$

Referring to the background fields as $\tilde{q}$ and the quantum fields as q we may compute the quantum effective action in the presence of background fields $\tilde{q}$, $\tilde{\Gamma}[q_0, \tilde{q}]$,

$$\tilde{\Gamma}[q_0, \tilde{q}] = \int_{\text{1PI,connected}} \mathcal{D}[q] e^{iS_{GI}[q_0+q+\tilde{q}] + iS_{GF}[q_0+q,\tilde{q}]}. \tag{2.30}$$

Note that we can also compute the conventional effective action $\Gamma[q_0, \tilde{q}]$, treating $\tilde{q}$ as simply a gauge parameter

$$\Gamma[q_0, \tilde{q}] = \int_{\text{1PI,connected}} \mathcal{D}[q] e^{iS_{GI}[q_0+q]+iS_{GF}[q_0+q-\tilde{q},\tilde{q}]} \tag{2.31}$$

where the field $\tilde{q}$ here only enters in the gauge fixing term and the quantum fields q are the full fields. From these definitions it is clear that $\tilde{\Gamma}[0, \tilde{q}] = \Gamma[\tilde{q}, \tilde{q}]$. Using (2.23) we write

$$\frac{\delta\tilde{\Gamma}[q_0, \tilde{q}]}{\delta\tilde{q}} = \frac{\delta\tilde{W}[J, \tilde{q}]}{\delta\tilde{q}}\Big|_{J=J_{q_0\tilde{q}}} = \frac{-i}{\tilde{Z}[J, \tilde{q}]}\frac{\delta\tilde{Z}[J, \tilde{q}]}{\delta\tilde{q}}\Big|_{J=J_{q_0\tilde{q}}}. \tag{2.32}$$

Considering the transformations (2.27), (2.28) and (2.29), which we now write as $q \to q + \epsilon F$ and $\tilde{q} \to \tilde{q} + \epsilon G$, and using (2.21) together with the invariance of the measure we find

$$\tilde{Z}[J, \tilde{q} + \epsilon G] = \int \mathcal{D}[q + \epsilon F] e^{iS[q+\tilde{q}+\epsilon(F+G),B+\epsilon G]+iJ(q+\epsilon F)} \tag{2.33}$$

$$= \int \mathcal{D}[q] e^{iS[q+\tilde{q},\tilde{q}]+J(q+\epsilon F)} = \tilde{Z}[J, \tilde{q}] + i\tilde{Z}\epsilon\langle F\rangle_J J \tag{2.34}$$

and hence

$$G\frac{\delta\tilde{Z}[J, \tilde{q}]}{\delta\tilde{q}} = i\tilde{Z}\langle F\rangle_J J \tag{2.35}$$

and

$$G\frac{\delta\tilde{\Gamma}[q_0, \tilde{q}]}{\delta\tilde{q}} = \langle F\rangle_{J_{q_0\tilde{q}}} J_{q_0\tilde{q}} = -\langle F\rangle_{J_{q_0\tilde{q}}}\frac{\delta\tilde{\Gamma}[q_0, \tilde{q}]}{\delta q_0}. \tag{2.36}$$

The functions F are linear in the fields q_0 and hence on right hand side of (2.36) $\langle F\rangle_{J_{q_0\tilde{q}}} = F(q_0)$. The background field effective action is therefore invariant under the original transformations applied to the background and effective fields:

$$G\frac{\delta\tilde{\Gamma}[q_0, \tilde{q}]}{\delta\tilde{q}} + F\frac{\delta\tilde{\Gamma}[q_0, \tilde{q}]}{\delta q_0} = 0. \tag{2.37}$$

If we set $q_0 = 0$ such that $F = 0$ then these transformations are just conventional gauge transformations on the background field B. The condition that $\tilde{\Gamma}[0, \tilde{q}] = \Gamma[\tilde{q}, \tilde{q}]$ be gauge invariant restricts the number of terms we need to consider when matching

continuum QCD to lattice theories, which we do by matching the coefficients of terms in the background effective action $\Gamma[\tilde{q},\tilde{q}]$.

Following the notation of Itzykson and Zuber [24] the effective action takes the form

$$\Gamma[A,c,\bar{c},\psi,\bar{\psi}] = \mathrm{Tr}\Big\{\frac{1}{2}Z_3^{-1}F^2 + \frac{\lambda}{2}f(A)^2 - gZ_1^{-1}F_{\mu\nu}[A^\mu,A^\nu] + \frac{g^2}{2}Z_4^{-1}[A_\mu,A_\nu][A^\mu,A^\nu]$$
$$+Z_3'^{-1}\partial_\mu\bar{c}\partial^\mu c + g\partial_\mu\bar{c}_b A^\mu_a c_c f_{abc} - Z_2^{-1}\bar{\psi}\partial\!\!\!/\psi + gZ_{1F}^{-1}\bar{\psi}A\!\!\!/\psi - Z_m^{-1}\bar{\psi}\psi\Big\} + \text{higher order terms} \tag{2.38}$$

where $f(A)$ is a general linear gauge fixing functional and the trace is understood to be over implicit indices. Since renormalisation is linear it carries across to the effective action. The renormalised effective fields and couplings are given by

$$\begin{aligned} A_R &= Z_3^{-\frac{1}{2}}A, \quad & g_R &= gZ_{1F}^{-1}Z_2Z_3^{\frac{1}{2}} \\ \psi_R &= Z_2^{-\frac{1}{2}}\psi, & \bar{\psi}_R &= Z_2^{-\frac{1}{2}}\bar{\psi} \\ c_R &= Z_3'^{-\frac{1}{2}}c, & \bar{c}_R &= Z_3'^{-\frac{1}{2}}\bar{c} \end{aligned}$$

together with the following ward identies [24]

$$\frac{Z_4}{Z_1} = \frac{Z_1}{Z_3} = \frac{Z_1'}{Z_3'} = \frac{Z_{1F}}{Z_2} = C. \tag{2.39}$$

In background field gauge the restriction of the effective action to gauge invariant operators requires $Z_{1F} = Z_2$ and that, as in QED, the coupling is only renormalised by the gauge field renormalisation. The combination $gA = g_R A_R$ therefore renormalises automatically and the vertex functions only require renormalisation due to the fermion fields. The result is that in BFG the 1PI vertex function is UV finite.

Chapter 3

Lattice Field Theory

3.1 Correlation Functions and the Path Integral

In order to motivate the formulation of lattice field theory I will begin by discussing the relation between correlation functions of operators and the Euclidean path integral. This relation is fundamental in extracting physical information from lattice QCD and will be discussed later when I come to extract matrix elements and energies from correlation functions computed nonperturbatively using the path integral. Beginning with the (time ordered) trace of some product of operators and, expressing the trace in the basis of eigenstates of $\hat{H}$, we find

$$\frac{1}{Z_T}\mathrm{tr}\left[e^{-T\hat{H}}\hat{O}_1(t_1)\hat{O}_2(t_2)...\right] = \frac{\sum_{n=0}^{\infty}\langle n|\hat{O}_1(t_1)\hat{O}_2(t_2)...|n\rangle e^{-T(E_n-E_0)}}{\sum_{n=0}^{\infty}e^{-T(E_n-E_0)}} \tag{3.1}$$

where

$$\hat{O}_i(t_i) = e^{-t_i\hat{H}}\hat{O}_i(0)e^{t_i\hat{H}} \tag{3.2}$$

and

$$Z_T = \mathrm{tr}[e^{-T\hat{H}}].$$

In the limit that $T \to \infty$ all terms in the sum in the denominator go to zero, except for the $n = 0$ term which gives 1. Similarly in the numerator terms with $n \neq 0$ are exponentially suppressed. This gives the first necessary relation for relating the Euclidean path integral to correlation functions

$$\lim_{T\to\infty}\frac{1}{Z_T}\mathrm{tr}\left[e^{-T\hat{H}}\hat{O}_1(t_1)\hat{O}_2(t_2)...\right] = \langle 0|\hat{O}_1(t_1)\hat{O}_2(t_2)...|0\rangle. \tag{3.3}$$

The second relation involves relating the trace to a path integral. For lattice QCD the relation is

$$\frac{1}{Z}\mathrm{tr}\left[e^{-T\hat{H}}\hat{O}_1(t_1)\hat{O}_2(t_2)...\right] = \frac{1}{Z}\int \mathcal{D}[\psi,\bar{\psi},U]e^{-S_E[\psi,\bar{\psi},U]}O_1(t_1)O_2(t_2)... \tag{3.4}$$

where the $O_i(t_i)$ on the right hand side are now functionals of the field variables ψ, $\bar{\psi}$ and U, U is in $SU(3)$ and ψ and $\bar{\psi}$ are grassman valued. The functional S_E is the Euclidean action and may be found one of two ways; either by wick rotating the Minkowski action or by considering the derivation of (3.4). For the sake of clarity I present the latter.

3.1.1 Euclidean Field Integral for Free Fermions

We begin considering the trace on the left hand side of (3.4), with the Dirac Hamiltonian operator expressed in terms of the anticommuting fields operators $\hat{\psi}$ and $\hat{\psi}^\dagger$

$$\hat{H} = \int dx\hat{\psi}^\dagger\hat{\gamma}^0\left(-i\hat{\gamma}^i\partial_i + m\right)\hat{\psi} \tag{3.5}$$

and we have that

$$\left\{\hat{\psi}_a(x),\hat{\psi}_b^\dagger(y)\right\} = \delta_{a,b}\delta(x-y). \tag{3.6}$$

We define $\hat{\bar{\psi}} = \hat{\psi}^\dagger\hat{\gamma}^0$, as well as coherent states

$$|\phi\rangle = e^{-\int dx\phi_\alpha(x)\hat{\psi}_\alpha^\dagger(x)}|-\rangle \tag{3.7}$$

$$\langle\phi| = \langle-|e^{\int dx\phi_\alpha^\dagger(x)\hat{\psi}_\alpha} \tag{3.8}$$

with $\hat{\psi}|-\rangle = \langle-|\hat{\psi}^\dagger = 0$, ϕ and $\phi^\dagger$ independent grassman variables and with the sum over repeated indices implicit such that

$$\hat{\psi}_\alpha(x)|\phi\rangle = \phi_\alpha(x)|\phi\rangle \tag{3.9}$$

$$\langle\phi|\hat{\bar{\psi}}_\alpha(x) = \langle\phi|\bar{\phi}_\alpha(x) \tag{3.10}$$

$$\langle\phi'|\phi\rangle = e^{\int dx\phi'^\dagger_\alpha(x)\phi_\alpha(x)} \tag{3.11}$$

$$\int \mathcal{D}\left[\phi^\dagger,\phi\right]e^{-\int dx\phi_\alpha^\dagger\phi_\alpha}|\phi\rangle\langle\phi| = 1. \tag{3.12}$$

The state $|-\rangle$ annihilated by the field operator may seem suspect at first, but if one considers the deconstruction of the field operator into particle and antiparticle creation and annihilation operators then one finds it is simply the state in which every particle momentum and spin state is empty and every antiparticle state is full. The next step involves breaking the trace in (3.4) into the product of many time steps of length Δt. using the completeness relation (3.12) we have

$$\begin{aligned} &\mathrm{tr}\left[e^{-T\hat{H}}\hat{O}_1(t_1)\hat{O}_2(t_2)...\right] = \\ &\int\prod_i \mathcal{D}[\phi^\dagger(t^i),\phi(t^i)]e^{-\int\phi^\dagger_\alpha(t^i)\phi_\alpha(t^i)}\sum_n\langle n|\phi(t^N)\rangle\langle\phi(t^N)|e^{-\Delta t\hat{H}}|\phi(t^{N-1})\rangle... \\ &\qquad\times\langle\phi(t^k)|e^{-\Delta t\hat{H}}\hat{O}_k(t^k)...|n\rangle = \\ &\int\prod_i \mathcal{D}[\phi^\dagger(t^i),\phi(t^i)]e^{-\int\phi^\dagger_\alpha(t^i)\phi_\alpha(t^i)}\sum_n\langle\phi(t^N)|e^{-\Delta t\hat{H}}|\phi(t^{N-1})\rangle... \\ &\qquad\times\langle\phi(t^k)|e^{-\Delta t\hat{H}}\hat{O}_k(t^k)...|n\rangle\langle n|-\phi(t^N)\rangle \end{aligned} \tag{3.13}$$

where in the final line the minus sign originates from the commutation of $\langle n|\phi(t^N)\rangle$, defined in (3.7) as grassman valued, through the final $\langle\phi(t^0)|n\rangle$. This may be seen by considering the state $|n\rangle$ as a sum over different products of field operators applied to the state $|-\rangle$

$$\begin{aligned}
\langle n|\phi(t^N)\rangle =&\langle -|\hat{\psi}(x_1)\hat{\psi}(x_2)...|\phi(t^N)\rangle \\
=&\phi(x_1,t^N)\phi(x_2,t^N)... \qquad (3.14)\\
\langle \phi(t^0)|n\rangle =&\langle \phi(t^0)|...\hat{\psi}^\dagger(x_2)\hat{\psi}^\dagger(x_1)|-\rangle \\
=&...\phi^\dagger(x_2,t^0)\phi^\dagger(x_1,t^0) \qquad (3.15)\\
\langle n|\phi(t^N)\rangle\langle \phi(t^0)|n\rangle =& \\
=&\phi(x_1,t^N)\phi(x_2,t^N)...\phi^\dagger(x_2,t^0)\phi^\dagger(x_1,t^0) \\
=&\phi(x_1,t^N)\phi^\dagger(x_1,t^0)\phi(x_2,t^N)\phi^\dagger(x_2,t^0)... \\
=&...\phi^\dagger(x_2,t^0)(-\phi(x_2,t^N))\phi^\dagger(x_1,t^0)(-\phi(x_1,t^N)) \\
=&...\phi^\dagger(x_2,t^0)\phi^\dagger(x_1,t^0)(-\phi(x_1,t^N))(-\phi(x_2,t^N))... \\
=&\langle \phi(t^0)|n\rangle\langle n|-\phi(t^N)\rangle. \qquad (3.16)
\end{aligned}$$

The intermediate $\langle\phi|e^{-\Delta t\hat{H}}|\phi'\rangle$ terms do not contribute a sign as they are even products of grassman numbers and therefore commute with $\langle n|\phi\rangle$. The minus sign within the rightmost state in (3.13), $|-\phi(t^N)\rangle$, tells us that when performing the fermionic integral with finite time extent T we must take $\phi(x,T)=-\phi(x,0)$. This requirement is known as taking antiperiodic timelike boundary conditions.

In the limit $\Delta t\to\infty$ we may evaluate the exponential of the Hamiltonian against the coherent states, as well as using (3.11) to evaluate the inner products, to find

$$\begin{aligned}
&\mathrm{tr}\left[e^{-T\hat{H}}\hat{O}_1(t_1)\hat{O}_2(t_2)...\right] = \qquad (3.17)\\
&\lim_{\Delta t\to\infty}\int_{\phi(t^N)=-\phi(t^0)}\prod_i \mathcal{D}[\phi^\dagger(t^i),\phi(t^i)]O_1[\phi^\dagger,\phi]O_2[\phi^\dagger,\phi]... \\
&\times e^{-\sum_i \Delta t(\psi^\dagger(t^i)(\psi(t^i)-\phi(t^{i-1}))/\Delta t+H[\phi^\dagger(t^i),\phi(t^i+1)])} \\
&=\int_{\phi(T)=-\phi(0)}\mathcal{D}[\phi^\dagger,\phi]O_1O_2...e^{-\int dt\phi^\dagger\partial_t\phi+H[\phi^\dagger,\phi]} \\
&=\int_{\phi(T)=-\phi(0)}\mathcal{D}[\bar{\phi},\phi]O_1O_2...e^{-\int dt\bar{\phi}(\hat{\gamma}^0\partial_t-i\hat{\gamma}^i\partial_i+m)\phi}.
\end{aligned}$$

Defining Euclidean gamma matrices $\gamma^i = -i\hat{\gamma}^i$, $\gamma^0 = \hat{\gamma}^0$ we identify the Euclidean action

$$S_E[\bar{\phi}, \phi] = \int d^4x \bar{\phi}(\gamma^\mu \partial_\mu + m)\phi \tag{3.18}$$

and arrive at

$$\mathrm{tr}\big[e^{-T\hat{H}}\hat{O}_1(t_1)\hat{O}_2(t_2)...\big] = \int_{\phi(T)=-\phi(0)} \mathcal{D}[\bar{\phi}, \phi] O_1 O_2 ... e^{-S_E[\bar{\phi},\phi]}. \tag{3.19}$$

This is just (3.4) without the gauge fields U. One can also arrive at this expression for euclidean correlation functions by starting with the standard Minkowski action and making the replacement $x_0 = -ix_4$.

3.1.2 Lattice Regularisation

In order to perform calculations using (3.4) and (3.3) we must find some way of evaluating the path integral. In conventional perturbation theory this would be done by expanding in the couplings, the coefficients of the greater than quadratic terms in the action, and by adding counterterms to the action to cancel off infinities coming from loops in some regularisation scheme. In lattice QCD, as the name suggests, we modify the space so that instead of being infinite the dimension of the integral is finite. We typically take a hypercubic lattice with N_x points in each of the spatial directions and N_t points in the timelike direction with isotropic lattice spacing a. In our simulations we take periodic boundary conditions in time when computing propagators e.g. $\phi(x, T) = \phi(x, 0)$ as opposed to (3.13). For the mesons we are concerned with here we may neglect effects coming from this choice. For the D^* meson for example, on our lattices, $M_{D^*}T \approx 60$ is typical and so uncertainties coming from choosing periodic time boundary conditions are extremely small.

The simplest action one typically thinks of which will naively reproduce the Dirac action in the limit $a \to 0$ on the lattice is found by approximating the derivative as a finite difference.

$$S_{\text{naive}}[\bar{\psi},\psi] = \sum_x a^4 \bar{\psi}(x)(\gamma^i \Delta_i + m_0)\psi(x) \tag{3.20}$$

where

$$\Delta_i \psi(x) = \left(\psi(x+\hat{i}a) - \psi(x-\hat{i}a)\right)/2a. \tag{3.21}$$

The Dirac operator now takes the form of a finite matrix which can be inverted exactly. If we write this naive lattice action as

$$S_{\text{naive}}[\bar{\psi},\psi] = \sum_x a^4 \bar{\psi}(x)(\gamma^i \Delta_i + m_0)\psi(x) = \sum_{x,y} \bar{\psi}(x) D(x,y)\psi(y) \tag{3.22}$$

then we can compute correlation functions of fermion operators exactly. Suppose we have some correlation function

$$\langle 0|\hat{\bar{\psi}}(x_1)\hat{\psi}(x_2)...|0\rangle = \frac{1}{Z}\int \mathcal{D}[\bar{\psi},\psi]\bar{\psi}(x_1)\psi(x_2)...e^{-\bar{\psi}D\psi} \tag{3.23}$$

where we now include the antisymmetric time boundary conditions in the operator D. The path integral on the right hand side of (3.23) may be evaluated analytically, the result is found by replacing pairs of $\psi(x)$ and $\bar{\psi}(y)$ with $D^{-1}(x,y)$, and including appropriate factors of the determinant. The reason for this can be seen by writing the path integral as a set of derivatives applied to the generating functional,

$$\begin{aligned}
&\frac{1}{Z}\int \mathcal{D}[\bar{\psi},\psi]\bar{\psi}(x_1)\psi(x_2)...e^{-\bar{\psi}D\psi} \\
&= \frac{1}{Z}\int \mathcal{D}[\bar{\psi},\psi]\frac{d}{d\nu(x_1)}\frac{d}{d\nu(x_2)}...e^{-\bar{\psi}D\psi+\bar{\nu}\psi-\bar{\psi}\nu}\Big|_{\nu=0} \\
&= \frac{1}{Z}\frac{d}{d\nu(x_1)}\frac{d}{d\nu(x_2)}...\int \mathcal{D}[\bar{\psi},\psi]e^{-(\bar{\psi}-\bar{\nu}D^{-1})D(\psi+D^{-1}\nu)-\bar{\nu}D^{-1}\nu}\Big|_{\nu=0} \\
&= \frac{1}{Z}\frac{d}{d\nu(x_1)}\frac{d}{d\nu(x_2)}...\text{Det}[D]e^{-\bar{\nu}D^{-1}\nu}\Big|_{\nu=0}.
\end{aligned} \tag{3.24}$$

So we may evaluate fermionic correlation functions provided we can invert D.

3.1.3 Bosons

Constructing a Euclidean action for the gauge fields using coherent states is complicated somewhat by the requirement that we must fix the gauge. For lattice calculations it is

also not particularly useful as the discretisation of space would require us to use gauge fields valued in the Lie algebra in the form of complicated nonlinear operators in order to maintain gauge invariance. Instead we take the field integral as a quantisation procedure and choose a suitable Euclidean gauge action on the lattice with fields U in the gauge group which transform in such a way as to make the gauge invariance of the total action clear. Of course, the physics we aim to describe is all encoded in the Hilbert space of states and the Hamiltonian. The requirement that a theory defined in terms of a Euclidean action can be continued back to minkowski space and that a positive semi-definite self adjoint Hamiltionian exists can be expressed as the requirement that the Euclidean correlation functions obey reflection positivity [25]. There are additional subtleties associated with using a lattice, such as choosing whether to reflect about a point or the midpoint of a link, though I will not discuss these here.

As for performing the integral over the bosonic gauge fields let us consider the general case in which $D(x, y, U)$ is some function of the gauge fields U and we have some gauge action $S_{\mathrm{g}}[U]$. The integral over the gauge fields is a large multidimensional integral over real variables for which exact evaluation is practically infeasible. We instead perform the field integral over gauge fields using monte carlo methods. This is done by generating a random distribution of field configurations for which the probability of each configuration is

$$P(U) \propto \mathrm{Det}[D(U)]e^{-S_{\mathrm{g}}[U]}. \tag{3.25}$$

We can then calculate correlation functions, including gauge fields, as expectation values of our contractions of D^{-1} on the set of gauge configurations

$$\langle\bar{\psi}(x_1)\psi(x_2)...\rangle = \int \mathcal{D}[U]\mathrm{Det}[D(U)]e^{-S_{\mathrm{g}}[U]}\langle\bar{\psi}(x_1)\psi(x_2)...\rangle_U \approx \frac{1}{n}\sum_n \langle\bar{\psi}(x_1)\psi(x_2)...\rangle_{U_n} \tag{3.26}$$

where we use the subscript U on the correlation function to indicate that only the path integral over fermionic fields is evaluated and the sum is over n field configurations distributed according to (3.25).

3.1.4 Correlation functions

The expectation of the mean on the right hand side of (3.26) is just the full correlation function, however since we evaluate it for only n field configurations what we have has an associated error. This error has physical significance, which I will discuss shortly, for now let us just note that for some pair of operators O and $O^\dagger$ it goes like

$$\sigma^2 = \frac{1}{n}\sum_n (\langle OO^\dagger\rangle_{U_n})^2 - \left(\frac{1}{n}\sum_n \langle OO^\dagger\rangle_{U_n}\right)^2 \tag{3.27}$$

and that the left part of the right hand side of (3.27), $(\langle OO^\dagger\rangle_U)^2$, is one of the contractions we would have to evaluate in computing $\langle OO^\dagger OO^\dagger\rangle$.

Returning to (3.3), we now have all the tools required to compute $\langle 0|\hat{O}_1(t_1)\hat{O}_2(t_2)...|0\rangle$, provided we take T large enough. For QCD the exponential suppression in (3.1) is governed by the lowest energy eigenstate above the ground state. As such we can use (3.3) without taking the limit as long as $TM_\pi \gg 1$.

In order to extract physical information from (3.3) we again use the eigenstates of the Hamiltonian as a basis. Let us consider a single operator and its hermitian conjugate, with the same quantum numbers as some meson of interest, $\hat{O} = \hat{\bar{\psi}}_a \Gamma \hat{\psi}_b$

$$\begin{aligned}\langle 0|\hat{O}(t_1)\hat{O}^\dagger(0)|0\rangle &= \sum_n \langle 0|\hat{O}(t_1)|n\rangle\langle n|\hat{O}^\dagger(0)|0\rangle \\ &= \sum_n \langle 0|\hat{O}(0)|n\rangle e^{-t_1 E_n}\langle n|\hat{O}^\dagger(0)|0\rangle \\ &= \sum_n A_n A_n^* e^{-t_1 E_n}.\end{aligned} \tag{3.28}$$

We can now compute the correlation function for many values of t_1, using the methods described above, and fit our data using Bayesian statistics against a template fit function of the form

$$\sum_n A_n A_n^* e^{-t_1 E_n}. \tag{3.29}$$

We can also compute matrix elements, provided we also compute two point functions for each meson operator as above, by inserting a basis of energy eigenstates in a similar manner.

Considering (3.28) the variance (3.27) will contain a piece that has the form:

$$\sum_n \langle 0|\hat{O}(0)\hat{O}(0)|n\rangle e^{-t_1 E'_n} \langle n|\hat{O}^\dagger(0)\hat{O}^\dagger(0)|0\rangle. \tag{3.30}$$

where E'_n is the energy of the n^{th} state created by the combined operator $\hat{O}^\dagger(0)\hat{O}^\dagger(0)$. Taking t_1 to be large we find that the error divided by the correlator signal goes like

$$e^{\frac{1}{2}t_1(E'_0 - 2E_0)}. \tag{3.31}$$

This means that for large times if the operator $\hat{\mathcal{O}}^\dagger\hat{\mathcal{O}}^\dagger$ overlaps with a state with energy less than twice the energy of the lowest energy state $\hat{\mathcal{O}}^\dagger$ creates then the fractional error of our correlation function will grow exponentially. This is usually the case, and it restricts the size of correlation functions we can use to extract information.

It is important to understand that it is not possible to directly compute S matrix elements using the lattice since we do not compute analytical expressions for Euclidean correlation functions. Our fits include large errors for the contributions of high energy states which while exponentially suppressed in the Euclidean theory would contribute some relevant unknown phase in the Minkowski theory. Indirect determinations of scattering information from lattice data is still possible, but one must look at the finite volume dependence of mass spectra. Lüscher showed that the shift in energy spectrum of two identical particles with zero total momentum confined to a finite periodic volume is proportional to the elastic scattering amplitude [26]. This work has since been extended considerably, for example [27, 28, 29, 30].

3.2 Symanzik Improvement

If we consider higher orders in the expansion of the naive discretisation of the Dirac operator (3.32) we find

$$\Delta_i\psi(x) = \Big(\psi(x+\hat{i}a) - \psi(x-\hat{i}a)\Big)/2a = \frac{\partial}{\partial x_i}\psi(x) + \frac{a^2}{6}\frac{\partial^3}{\partial x_i^3}\psi(x) + \mathcal{O}(a^4). \tag{3.32}$$

There is no reason why we should not add terms to our discrete derivative in order to cancel these additional higher order a^2 terms. We add a term which approximates a third derivative

$$S_{\text{improved}}[\bar{\psi},\psi] = \sum_x a^4\bar{\psi}(x)(\gamma^i(\Delta_i - \frac{a^2}{6}\Delta_i^3) + m_0)\psi(x). \tag{3.33}$$

Such an addition generates higher order corrections, at $\mathcal{O}(a^4)$ in this case, which could be removed by introducing a higher derivative term. While in principle one could continue this improvement indefinitely it is not typically done beyond a few orders since moving to the quantum theory, as will be discussed later, generates n-loop corrections at lower orders in a^2. In the work done here I deal with 1-loop improved fermionic actions. The two loop corrections potentially enter at $\mathcal{O}(\alpha^2 a^2)$. Typically $\alpha \approx a\Lambda_{\text{QCD}}$, as such it does not make sense to perform the tree level Symanzik improvement beyond $\mathcal{O}(a^4)$.

3.3 Gauge Fields on the Lattice

3.3.1 Gauge covariant derivatives

For the purpose of introducing gauge fields let us consider the naively discretised Dirac action (3.20)

$$S_{\text{naive}}[\bar{\psi},\psi] = \sum_x a^4 \bar{\psi}(x)(\gamma^i \Delta_i + m_0)\psi(x). \tag{3.34}$$

All of the considerations made here will generalise to the improved fermion actions to be discussed later. We wish to find an action with gauge fields that is invariant under local $SU(3)$ transformations $\psi(x) \to \Omega(x)\psi(x)$, $\bar{\psi}(x) \to \bar{\psi}(x)\Omega^\dagger(x)$ with Ω in $SU(3)$. The mass term is already invariant, only the kinetic term requires modification. This term mixes the field at one lattice site with those at adjacent sites. In order to be invariant we must insert something that looks like a gauge transporter, in the continuum this would be the path ordered exponential of the gauge fields

$$U_P(x,y) = \mathcal{P}\text{exp}\left[ig\int_y^x dx' \cdot A(x')\right] \tag{3.35}$$

which transforms as $U_P(x,y) \to \Omega(x)U_P(x,y)\Omega^\dagger(y)$. In the limit that x and y are very close, seperated by the lattice spacing a in the direction μ, this is approximately

$$U_\mu(y) = \exp\left[iagA_\mu(y)\right]. \tag{3.36}$$

We therefore investigate the gauge covariant derivative

$$D_i\psi(x) = \left(U_i^\dagger(x)\psi(x+\hat{i}a) - U_i(x-\hat{i}a)\psi(x-\hat{i}a)\right)/2a. \tag{3.37}$$

Taking the limit $a \to 0$ we find

$$\begin{aligned}\lim_{a\to 0} D_i\psi(x) &= \left[(1-igaA_i)(\psi + a\partial_i\psi) - (1+igaA_i)(\psi - a\partial_i\psi)\right]/2a \\ &= \partial_i\psi(x) - igA_i(x)\psi(x)\end{aligned} \tag{3.38}$$

which is just the continuum covariant derivative of ψ. This method of producing a gauge covariant lattice derivative, using the gauge transported finite difference, will be used in the highly improved actions discussed later, though we will also apply smearings to the gauge links in order to suppress unwanted high energy modes.

3.3.2 Wilson Gauge Action

We require an action for U which reproduces the continuum gauge action, together with some appropriate measure, such that taken together (and ideally individually) they are gauge invariant. The simplest action one can take for these gauge fields is a trace over a plaquette summed over possible routes,

$$S_g[U] = \sum_x \sum_{\mu<\nu} \frac{2N_c}{g^2} \left[1 - \frac{1}{N_c} \text{Re tr} U_{\mu\nu}(x)\right]. \tag{3.39}$$

The plaquette is defined as

$$U_{\mu\nu} = U_\mu(x) U_\nu(x + a\hat{\mu}) U_\mu^\dagger(x + a\hat{\nu}) U_\nu^\dagger(x). \tag{3.40}$$

This object acts to transport gauge transformations at x to $x + \mu$ then to $x + \mu + \nu$ to $x + \nu$ then back to x. It closely resembles a curvature tensor and is effectively a small discrete wilson loop. Expanding this in a and derivatives as before we find that

$$S_g[U] = \frac{1}{2} \sum_x a^4 \sum_{\mu,\nu} \text{tr} \left[F_{\mu\nu}(x)^2\right] + \mathcal{O}(a^2) \tag{3.41}$$

which is exactly what we want. This simple action is known as the Wilson gauge action [31].

3.3.3 Symanzik Improved gauge action

Note that since there are no gauge invariant dimension five operators, corrections to (3.41) must enter at order $\mathcal{O}(a^2)$. The corresponding dimension six operators are [32]:

$$\begin{aligned}\mathcal{O}_1 &= \sum_{\mu\nu} \mathrm{tr}\left[D_\mu F_{\mu\nu} D_\mu F_{\mu\nu}\right], \\ \mathcal{O}_2 &= \sum_{\mu\nu\sigma} \mathrm{tr}\left[D_\mu F_{\nu\sigma} D_\mu F_{\nu\sigma}\right], \\ \mathcal{O}_3 &= \sum_{\mu\nu\sigma} \mathrm{tr}\left[D_\mu F_{\mu\sigma} D_\nu F_{\nu\sigma}\right].\end{aligned} \tag{3.42}$$

Dimension six gauge link operators which allow cancellation of the $\mathcal{O}(a^2)$ discretisation errors are added to the lattice action. The resultant action is [33]

$$\begin{aligned}S &= \sum_x \frac{2N_c}{g^2}\Big[c_0 P_0(x) + c_1 P_1(x) + c_2 P_2(x)\Big] \\ P_0(x) &= \sum_{\mu<\nu}\left[1 - \frac{1}{N_c}\mathrm{Re\ tr}\Big(U_{\mu\nu}(x)\Big)\right] \\ P_1(x) &= \sum_{\mu<\nu}\left[1 - \frac{1}{N_c}\mathrm{Re\ tr}\Big(U_{\mu\mu\nu}(x) + U_{\mu\nu\nu}(x)\Big)\right] \\ P_2(x) &= \sum_{\mu<\nu<\rho}\left[1 - \frac{1}{N_c}\mathrm{Re\ tr}\big(U_{\mu\nu\rho}(x) + U_{\mu\rho\nu}(x) + U_{\rho\mu\nu}(x) + U_{\rho-\mu\nu}(x)\big)\right]\end{aligned} \tag{3.43}$$

where $-\mu$ indicates a Hermitian conjugated gauge link. At tree level the coefficients take values $c_0 = \frac{5}{3},\ c_1 = -\frac{1}{12},\ c_2 = 0$.

3.3.4 Quantum Gauge fields

In order to discuss the gauge action in a quantum sense we must first define a measure of integration for the gauge links. The unique measure for a compact group is given by the Haar measure [31]. If we write the gauge fields as $A^a_\mu t_a$ where now A^a_μ are real fields and t_a are a basis for the Lie algebra then we can define a metric ds^2 on the Lie group

as

$$ds^2 = \mathrm{tr}\left[\frac{\partial U_\mu(A_\mu)}{\partial A^a_\mu}U^\dagger_\mu(A_\mu)\Big(\frac{\partial U_\mu(A_\mu)}{\partial A^b_\mu}U^\dagger_\mu(A_\mu)\Big)^\dagger\right]dA^a_\mu dA^b_\mu \tag{3.44}$$

we may interpret the trace on the right hand side of 3.44 as a metric tensor

$$g_{ab} = \mathrm{tr}\left[\frac{\partial U_\mu(A_\mu)}{\partial A^a_\mu}U^\dagger_\mu(A_\mu)\Big(\frac{\partial U_\mu(A_\mu)}{\partial A^b_\mu}U^\dagger_\mu(A_\mu)\Big)^\dagger\right]. \tag{3.45}$$

The integral over U_μ is then equal to an integral over A_μ in the Lie algebra with gauge invariant measure

$$\int DU_\mu = \int \sqrt{\det[g(A_\mu)]}\prod_a dA^a_\mu. \tag{3.46}$$

In relation to section 2.3.1 the background field gauge is then given by taking $U_\mu(x) = Q_\mu(x)B_\mu(x)$, with Q_μ and B_μ also in $SU(3)$. The background field gauge transformation on these fields is realised as $Q_\mu(x) \to \Omega(x)Q_\mu(x)\Omega^\dagger(x)$ and $B_\mu(x) \to \Omega(x)B_\mu(x)\Omega^\dagger(x+\mu)$. Since the Haar measure is invariant under the conjugation transformation applied to Q the resultant background effective action is invariant under the remaining transformations of B, which are themselves just gauge transformations.

3.3.5 Tadpole Improvement

During the development of lattice QCD there was a period during which lattice perturbation theory and nonperturbative numerical calculations were found to be in disagreement when calculating short distance quantities that one would expect to agree [34]. The perturbative coupling used in such calculations was the bare coupling $\alpha_{\mathrm{latt}} = g^2/4\pi$. This was motivated by the idea that in a cutoff theory the running coupling evaluated at the cutoff scale, $\alpha_s(\pi/a)$, was typically roughly equal to the bare coupling, α_{latt}. In practice however this is not the case, $\alpha_s(\pi/a)$ is much larger than α_{latt} [35]. This is known as the tadpole problem. We constructed our action (3.43) considering the classical expansion of $U_\mu(y) = \exp[iaA_\mu(y)]$. Higher orders in a of the expansion of this exponential, which contain equally many powers of A, contain divergences coming from diagrams in which multiple gauge fields are contracted together which exactly cancel the factors of a. As such rather than being suppressed by $\mathcal{O}(\alpha_s^n a^{2n})$ such terms contribute at $\mathcal{O}(\alpha_s^n)$.

Fortunately tadpole contributions are generally process independent [35] and so can be removed by considering a rescaling of the gauge links

$$U \to \frac{U}{u_0}. \tag{3.47}$$

Several common choices for u_0 exist, one definition is $u_0 = \langle \frac{1}{3}\mathrm{Tr}(U_\mu)\rangle$ which requires gauge fixing since the gauge links are not gauge invariant. A more convenient gauge invariant choice is $u_0 = \langle \frac{1}{3}\mathrm{Tr}(U_{\mu\nu})\rangle^{\frac{1}{4}}$ where $U_{\mu\nu}$ is the plaquette [33]. One can see immediately from the plaquette term in the gauge action that this replacement takes $\alpha_{\mathrm{latt}} \to \alpha'_{\mathrm{latt}} = \frac{\alpha_{\mathrm{latt}}}{u_0^4}$, which is generally much closer to $\alpha_s(\pi/a)$.

3.3.6 The tadpole and symanzik improved Luscher and Weisz gauge action

Since the lattice theory omits modes with momenta $p > \pi/a$ it can be considered as an effective field theory taken with a cutoff of π/a. As with any effective field theory the coefficients in the action must be functions of the cutoff so that physical observables remain fixed. This dependence enters through the lattice spacing dependence of the coupling, whose bare value determines the measured lattice spacing in our simulations [25]. QCD is asymptotically free, so the dependence on the cutoff can be calculated perturbatively provided π/a is well above Λ_{QCD}, the typical QCD scale. The corrections, which enter at $\mathcal{O}(a^2\alpha_s)$ and change the coefficients c_i at $\mathcal{O}(\alpha_s)$, are calculated in [36], where also the one loop contributions of the highly improved staggered quark (HISQ) action [37] to the coefficients c_i are included. Subsuming the factor of c_0/u_0^4 into the gauge coupling we define $\beta_0 = 2c_0N_c/(g^2u_0^4)$. The coefficients in (3.43) multiplying P_1 and P_2 respectively are, to one loop,

$$\begin{aligned}\beta_1 &= -\frac{\beta_0}{20u_0^2}\left[1 - \big(\frac{12\pi}{5}c_0^{(1)} + 48\pi c_1^{(1)} + 2u_0^{(1)}\big)\alpha_s\right] \\ \beta_2 &= \frac{12\pi\beta_0}{5u_0^2}c_2^{(1)}\alpha_s.\end{aligned} \tag{3.48}$$

These coefficients are modified by sea quark loops. For the HISQ action, which will be discussed later, with N_f massless quarks the modified coefficients are

$$\begin{aligned}\beta_1 &= -\frac{\beta_0}{20u_0^2}\left[1 + (0.4805 - 0.899(52)N_f)\alpha_s\right] \\ \beta_2 &= -\frac{\beta_0}{u_0^2}\left[0.033 - 0.0121(23)N_f\right]\alpha_s\end{aligned} \tag{3.49}$$

The procedure for generating gauge fields is then to first choose a principal parameter β_0, as well as a starting guess for u_0. Then using the action 3.43 with coefficients given by (3.49) measure u_0 and adjust the value used in the action accordingly. This tuning procedure can be done very quickly using small lattice volumes [35]. Then using a larger lattice, whose dimensions are chosen with the aim of achieving the desired physical dimensions based on the expected lattice spacing predicted by the running of β, measure the lattice spacing a.

3.4 Fermions on the Lattice

3.4.1 The doubling problem

Let us turn to discuss the naively discretised fermionic action, the problems illustrated will be the same regardless of whether the Dirac operator is Symanzik improved so for clarity I will discuss the simple action (3.20)

$$S_{\text{naive}}[\bar{\psi}, \psi] = \sum_x a^4 \bar{\psi}(x)(\gamma^i \Delta_i + m_0)\psi(x). \tag{3.50}$$

The fermionic propagator is then given by, in momentum space,

$$D^{-1}(p) = \frac{m - \frac{i}{a}\sum_\mu \gamma_\mu \sin(p_\mu a)}{m^2 + \frac{1}{a^2}\sum_\mu \sin(p_\mu a)^2}. \tag{3.51}$$

Provided $|p| \ll \pi/a$ the limit $a \to 0$ recovers the continuum Dirac propagator. However since $-\pi/a < p < \pi/a$ in practical simulations, with opposite edges of the hypercubic Brillouin zone identified, instead taking $a \to 0$ yields a propagator with poles in p_0 near 0 with $p^2 = -m^2$ as well as near multiples of π/a at the corners of the hypercube. The simplest process through which an on shell particle at one corner of the Brillouin zone may change corner is the emission, and absorption by another particle which must also change taste, of a gluon with momenta $p \approx \xi\pi/a$. Such a gluon would be highly virtual and perturbative at current lattice spacings. The interaction therefore looks like an effective four quark operator which should be suppressed by p^2a^2 following from the fact that a four quark operator has dimension six and p is the typical external momenta. Therefore, in the continuum limit, the sixteen *tastes* (one for each possible vector $\xi\pi/a$) decouple and one has fifteen more physical quarks than were intended. In 1981 Nielsen and Ninomiya formulated a no-go theorem [38] which states that it is not possible to remove the unphysical species while maintaining a chirally invariant, doubler-free, local, translationally invariant, action.

Instead of removing the unphysical tastes at the expense of losing approximate chiral symmetry or the introduction of highly nonlocal operators we instead aim to account

for them. In order to do so we take the sixteenth root of the fermion determinant and wherever we contract quarks in a loop we must divide the loop by sixteen. The validity of this trick has been discussed in much depth [39] and while there is no conclusive proof that taking the root before taking the continuum limit is valid there is a great deal of evidence that this procedure reproduces continuum QCD, see for example [37, 40, 5, 41, 10, 42].

3.4.2 Highly Improved Staggered Quarks

Taste can also be considered in terms of doubling operators acting on the naive fermion fields [37]. The naive discretisation:

$$\mathcal{S} = \sum_x \bar{\psi}(x)(\gamma \cdot \Delta(U) + m_0)\psi(x) \tag{3.52}$$

with

$$\Delta_\mu(U)\psi(x) = \frac{1}{2a}\left(U_\mu(x)\psi(x+\hat{\mu}) - U^\dagger_\mu(x-\hat{\mu})\psi(x-\hat{\mu})\right) \tag{3.53}$$

has a discrete, space time dependent symmetry

$$\begin{aligned}\psi(x) &\to \mathcal{B}_\xi(x)\psi(x)\\ \bar{\psi}(x) &\to \bar{\psi}(x)\mathcal{B}^\dagger_\xi(x)\end{aligned} \tag{3.54}$$

where

$$\mathcal{B}_\xi(x) = \gamma^{\bar{\xi}}(-1)^{\xi\cdot x} \tag{3.55}$$

and

$$\begin{aligned}\gamma^m &= \prod_{i=0}^{3}(\gamma^i)^{m_i}\\ m^<_\mu &= \sum_{\eta<\mu} m_\eta \bmod 2\\ m^>_\mu &= \sum_{\eta>\mu} m_\eta \bmod 2\\ \overline{m}_\mu &= \sum_{\eta\neq\mu} m_\eta \bmod 2 = m^>_\mu + m^<_\mu.\end{aligned} \tag{3.56}$$

In momentum space this then gives the relation for the naive quark propagator:

$$S_F(p,q) = \mathcal{B}_\xi(0)S_F(p+\xi\pi, q+\xi\pi)\mathcal{B}_\xi(0) \tag{3.57}$$

telling us that the naive quark propagator contains only one sixteenth the information we would naively expect. One can diagonalise the naive action in spin indices using a

position dependent transformation of the fields. There are several choices for such a transformation, here I use:

$$\begin{aligned} \psi(x) &\to \Omega(x)\chi(x) \\ \bar{\psi}(x) &\to \bar{\chi}(x)\Omega^{\dagger}(x) \end{aligned} \tag{3.58}$$

with $\Omega(x) = \gamma^x$ this yields the action

$$\mathcal{S} = \sum_{x,i} \bar{\chi}_i(x)(\alpha(x) \cdot \Delta(U) + m_0)\chi_i(x) \tag{3.59}$$

with propagator

$$\langle \chi_\kappa(x)\bar{\chi}_\delta(y)\rangle = s(x,y)\delta_{\kappa\delta}. \tag{3.60}$$

This operation, known as staggering, simplifies calculations considerably. We need only do the inversion for a single component of χ and the full naive propagator can be reconstructed trivially by inserting Ω matrices:

$$S_F(x,y)_{\alpha\beta} = \langle \psi_\alpha(x)\bar{\psi}_\beta(y)\rangle = \Omega_{\alpha\kappa}(x)\langle \chi_\kappa(x)\bar{\chi}_\delta(y)\rangle\Omega^{\dagger}_{\delta\beta}(y) = \Omega_{\alpha\delta}(x)\Omega^{\dagger}_{\delta\beta}(y)s(x,y). \tag{3.61}$$

Since in the naive case we take the sixteenth root, using the staggered action with only one component retained we take only the fourth root of the determinant. In order to remove discretisation errors and taste exchange violations the operator $\Delta_\mu(U)$ used in simulations is more elaborate. It retains the feature that $\Delta_\mu(U)\psi(x)$ only contains fields $\psi(x')$ located an odd number of lattice sites away from x in the μ direction, ensuring that the spin-diagonalisation (3.59) still works. We also smear the gauge fields in order to suppress high momentum gluons which change taste. The full, Highly Improved Staggered $SU(3)$ covariant derivative operator is [37]:

$$\mathcal{D}^{\mathrm{HISQ}}_\mu = \Delta_\mu(W) - \frac{a^2}{6}(1+\epsilon)\Delta^3_\mu(X) \tag{3.62}$$

with

$$\begin{aligned} W_\mu &= \mathcal{F}_\mu^{\text{HISQ}} U_\mu \\ X_\mu &= \mathcal{U}\mathcal{F}_\mu U_\mu \\ \mathcal{F}_\mu^{\text{HISQ}} &= \left(\mathcal{F}_\mu - \sum_{\rho\neq\mu} \frac{a^2\delta_\rho^2}{2}\right)\mathcal{U}\mathcal{F}_\mu \\ \mathcal{F}_\mu &= \prod_{\rho\neq\mu}\left(1+\frac{a^2\delta_\rho^{(2)}}{4}\right)_{\text{symm}} \end{aligned} \tag{3.63}$$

where 'symm' indicates that the product ordering is symmetrised in ρ, $\mathcal{U}$ is a reuinitarisation, δ_ρ approximates a covariant first derivative on the gauge links and $\delta_\rho^{(2)}$ approximates a second covariant derivative:

$$\begin{aligned} \delta_\rho U_\mu(x) =& \frac{1}{a}\big(U_\rho(x)U_\mu(x+a\hat{\rho})U_\mu^\dagger(x+a\hat{\mu}) \\ & - U_\rho^\dagger(x-a\hat{\rho})U_\mu(x-a\hat{\rho})U_\mu(x-a\hat{\rho}+a\hat{\mu})\big) \\ \delta_\rho^{(2)} U_\mu(x) =& \frac{1}{a^2}\big(U_\rho(x)U_\mu(x+a\hat{\rho})U_\mu^\dagger(x+a\hat{\mu}) \\ & + U_\rho^\dagger(x-a\hat{\rho})U_\mu(x-a\hat{\rho})U_\mu(x-a\hat{\rho}+a\hat{\mu}) - 2U_\mu(x)\big). \end{aligned} \tag{3.64}$$

The third covariant derivative term originates from the Symanzik improvement discussed in section 3.2 and removes order a^2 discretisation errors coming from the approximation of the derivative. Without the epsilon term, tree level discretisation errors appear going as $(ap_\mu)^4$. For the mesons we are interested in quarks are typically nonrelativistic, and so the error is dominated by the energy, and ultimately the mass contribution going as $(am)^4$. For light quarks this is negligible, but for charm physics this must be included since current lattice spacings have $am_c \approx 0.5$. The epsilon term can be calculated straightforwardly as an expansion in $(am)^2$ by requiring the tree level dispersion relation $\lim_{p\to 0}\frac{E^2(p)-m^2}{p^2} = 1$ to a given order. The expansion is [37]:

$$\epsilon = -\frac{27}{40}(am)^2 + \frac{327}{1120}(am)^4 - \frac{5843}{53760}(am)^6 + \mathcal{O}((am)^8). \tag{3.65}$$

The smearings $\mathcal{F}_\mu$ (unrelated to smearings in the context of sources and sinks) applied to the gauge links remove taste changing interactions, since $\delta_\rho^{(2)} \approx -4/a^2$ when applied to

a link carrying momentum $q_\rho \approx \pi/a$. The μ direction needn't be smeared as the original interaction vanishes in this case anyway. The smearing $\mathcal{F}_\mu$ introduces new $\mathcal{O}(a^2)$ errors. These are removed by replacing $\mathcal{F}_\mu$ with [43]

$$\mathcal{F}_\mu^{\text{ASQTAD}} = \mathcal{F}_\mu - \sum_{\rho\neq\mu} \frac{a^2\delta_\rho^2}{4} \tag{3.66}$$

where $\mathcal{F}_\mu^{\text{ASQTAD}}$ is the gauge link smearing employed in the widely used a-squared tadpole improved action. Note that similar errors originating from the smearing on the third derivative term needn't be corrected as these errors go as $\mathcal{O}(a^4)$. A single smearing introduces perpendicular gauge links which are themselves unsmeared. To further suppress taste exchange we use multiple smearings. Once such smearing is:

$$\mathcal{F}_\mu^{\text{ASQTAD}}\mathcal{U}\mathcal{F}_\mu^{\text{ASQTAD}}$$

where $\mathcal{U}$ is a reunitarisation. This combination ensures that each smearing does not introduce any additional $\mathcal{O}(a^2)$ errors and that there is no growth in the size of two gluon vertices, since the unitarision ensures it is bounded by unity. In the HISQ operator defined in (3.63) we have moved the entirety of the $\mathcal{O}(a^2)$ corrections to the outermost smearing.

In order to check the taste exchange violations in HISQ one can check for taste-splittings of the pion masses. However since there are more allowed effective taste exchange vertices than there are degenerate pion multiplets this does not guarantee the theory is free of taste exchange. A better check is the explicit calculation of the effective couplings of the vertices which would be required to remove taste exchange interactions. These are given in [37] in which it is clear that the HISQ action is a significant improvement over the older ASQTAD action.

The use of multiple flavours of staggered quark as well as NRQCD heavy quarks, which I will discuss shortly, complicates the form of correlation functions described in section 3.1.4. Suppose we are interested in the two point function made from the

operator $\mathcal{O} = \sum_x \bar{\psi}\Gamma\Phi(x)$ where Φ is an NRQCD quark

$$\langle \mathcal{O}(t)\mathcal{O}^\dagger(0)\rangle = \frac{1}{Z}\int \mathcal{D}[\psi,\Phi,U]\sum_{x,y}\bar{\psi}\Gamma\Phi(t,x)\bar{\Phi}\Gamma\psi(0,y)e^{-S[\Phi,\psi,U]}. \tag{3.67}$$

Fourier transforming the fields we have

$$\langle \mathcal{O}(t)\mathcal{O}^\dagger(0)\rangle = \frac{1}{Z}\int \mathcal{D}[\psi,\Phi,U]\sum_{\vec{p},p_0,q_0} e^{i(p_0-q_0)t}\bar{\psi}_{p_0,\vec{p}}\Gamma\Phi_{q_0,\vec{p}}\sum_{\vec{p'},p'_0,q'_0}\bar{\Phi}_{p'_0,\vec{p'}}\Gamma\psi_{q'_0,\vec{p'}}e^{-S[\Phi,\psi,U]} \tag{3.68}$$

$$= \int e^{-S[\Phi,\psi,U]}\sum_{p,q_0,\xi} e^{i(p_0+\xi_0-q_0)t}\bar{\psi}_{p_0+\xi_0,\vec{p}+\vec{\xi}}\Gamma\Phi_{q_0,\vec{p}+\vec{\xi}}\sum_{p,q'_0,\zeta}\bar{\Phi}_{q'_0,\vec{p'}+\vec{\zeta}}\Gamma\psi_{p'_0+\zeta_0,\vec{p'}+\vec{\zeta}} \tag{3.69}$$

where in the second line we have broken the sum over naive quark momenta, p and p', into sixteenths of the hypercubic brillouin zone labelled by ξ and ζ. The heavy quark resists large energies which drive it far off shell, therefore the dominant contribution to this sum will come from the pieces in which $\vec{\xi} = \vec{\zeta} = 0$ by virtue of the spatial sum. If we suppose that our action does indeed contain no taste changing interactions then also we will have that $\xi_0 = \zeta_0$. The Correlation function then has the form

$$\langle \mathcal{O}(t)\mathcal{O}^\dagger(0)\rangle = \int e^{-S[\Phi,\psi,U]}\sum_{p,q_0,\xi_0} e^{i(p_0+\xi_0-q_0)t}\bar{\psi}_{p_0+\xi_0,\vec{p}}\Gamma\Phi_{q_0,\vec{p}}\sum_{p,q'_0}\bar{\Phi}_{q'_0,\vec{p'}}\Gamma\psi_{p'_0+\xi_0,\vec{p'}}. \tag{3.70}$$

when $\xi_0 = 0$ this is just the correlation function of the normal low energy quark. In order to interpret the correlation function when $\xi = \pi/a$ we must use the doubling symmetry, which leaves the action invariant, to transform the high energy quark field to a low energy field. The doubling symmetry (3.54) has the momentum space form

$$\psi_p \to M_\kappa \psi_{p+\kappa\pi/a} \tag{3.71}$$

$$\bar{\psi}_p \to \bar{\psi}_{p+\kappa\pi/a} M_\kappa^\dagger \tag{3.72}$$

where $M_\kappa = \gamma^{\bar{\kappa}}$. The $\xi_0 = \pi/a$ piece of the two point function then has the form

$$\langle \mathcal{O}(t)\mathcal{O}^\dagger(0)\rangle|_{\xi_0=\pi/a} = (-1)^t\int e^{-S[\Phi,\psi,U]}\sum_{p,q_0} e^{i(p_0-q_0)t}\bar{\psi}_{p_0,\vec{p}}M_\xi^\dagger\Gamma\Phi_{q_0,\vec{p}}\sum_{p,q'_0}\bar{\Phi}_{q'_0,\vec{p'}}\Gamma M_\xi\psi_{p'_0,\vec{p'}} \tag{3.73}$$

which is just a normal two point function constructed from low energy quarks made using the operator $\bar{\Phi}\Gamma\gamma^0\gamma^5\psi$, with the additional complication that there is now a factor of $(-1)^t$ oscillating in time. Were we to have used two different tastes of staggered quark the calculation would have been very similar, except that the oscillating piece would come from the case when exactly one quark contributes a nonzero taste piece and the case in which both are doubled gives us the extra factor of two bringing the total up to sixteen times the naively expected correlation function that we expect from the loop made of staggered quarks. In such a case the phases made from conjugating the meson spin matrix Γ by M_κ cancel between the source and sink.

3.5 NRQCD

While the u, d, s and c quarks can be modelled well using the relativistic HISQ action, the b quark is too heavy. The lattice can only be expected to simulate physics involving energies less than $1/a$, since this is the order of magnitude of the maximum physical energy on the lattice. The heavy quark mass is typically of the same order of magnitude as this, with $am_b \approx 1$ and so relativistic heavy quark simulations are not feasible on current lattices, on which $a \approx 0.1$fm.[1] The additional constraint $LM_\pi \gg 1$, required to ensure the absence of finite volume effects, prevents us from reducing the number of lattice sites in order to make calculations with finer lattices feasible. In order to get around this problem we use the observation that in the heavy-light hadrons we are interested in simulating the typical momentum transfer between heavy and light quarks is of the order Λ_{QCD}.

3.5.1 Foldy-Wouthuysen-Tani Transformation

In order to construct a non-relativistic action we must decouple the quark and antiquark degrees of freedom, to some order in the inverse heavy quark mass $1/m_b$. This is done by acting on the quark fields with sequential transformations, known as a Foldy-Wouthuysen-Tani transformation, to remove the terms which do not commute with γ^0. The first is straightforward to see, starting with the continuum relativistic action:

$$S_b = \int d^4x \bar{\psi}_b(x)\big[i\gamma^0 D_0 + i\gamma^i D_i - m\big]\psi_b(x) \tag{3.74}$$

[1] That being said, some work [44] has been carried out using HISQ quarks by using large masses on lattices with $a \approx 0.09, 0.06$ and 0.045fm and extrapolating to the physical b mass. This procedure, while computationally expensive, eliminates several of the systematic uncertainties induced by using an effective theory such as NRQCD for simulating heavy quarks.

we make the change of variables in the fields

$$\psi_b(x) = e^{i\gamma^i D_i/2m}\psi'_b(x) \tag{3.75}$$

$$\bar{\psi}_b(x) = \bar{\psi}'_b(x)e^{i\gamma^i D_i/2m} \tag{3.76}$$

Such a change has determinant unity, since the exponent is traceless, and so leaves the measure invariant. The resultant action is

$$\begin{aligned}
S_b &= \int d^4x \bar{\psi}'_b(x) e^{i\gamma^i D_i/2m}\big[i\gamma^0 D_0 + i\gamma^i D_i - m\big] e^{i\gamma^i D_i/2m}\psi'_b(x) \\
&= \int d^4x \bar{\psi}'_b(x)\big[i\gamma^0 D_0 - m - (\{\gamma^i D_i, \gamma^0 D_0\} + \{\gamma^i D_i, \gamma^j D_j\} \\
&+ (\gamma^i D_i)^2/2)/2m + \mathcal{O}(1/m^2)\big]\psi'_b(x) \\
&= \int d^4x \bar{\psi}'_b(x)\big[i\gamma^0 D_0 - m - \left(ig\gamma^i\gamma^0 F_{i0} + \frac{ig}{4}[\gamma^i,\gamma^j]F_{ij} + D_i D^i\right)/2m \\
&+ \mathcal{O}(1/m^2)\big]\psi'_b(x)
\end{aligned}$$

We may now make the change

$$\psi'_b(x) = e^{-ig\gamma^i\gamma^0 F_{i0}/2m^2}\psi''_b(x) \tag{3.77}$$

$$\bar{\psi}'_b(x) = \bar{\psi}''_b(x)e^{-ig\gamma^i\gamma^0 F_{i0}/2m^2} \tag{3.78}$$

in order to remove all terms of order $\mathcal{O}(1/m)$ which do not commute with γ^0. We may continue in such a manner to remove higher order terms which do not commute with γ^0. Ultimately the field we end up with, removing non-commuting terms to $\mathcal{O}(1/m^3)$, is:

$$\psi(x) = T_{\rm FWT}e^{-imx^0\gamma^0}\Psi(x) \tag{3.79}$$

with

$$\begin{aligned}
T_{\rm FWT} =& e^{i\gamma^i D_i/2m} \\
&\times e^{-ig\gamma^i\gamma^0 E_i/2m^2} \\
&\times e^{\left(\frac{g}{4}\gamma^i(D_0^{\rm ad}E_i) + \frac{1}{3}(i\gamma^i D_i)^3\right)/2m^3}
\end{aligned}$$

where we have written the instances of the field strength in terms of the QCD equivalent of electric and magnetic fields. The last redefinition removes the mass term, which just shifts the definition of the energy of the meson states relative to the physical energy. This step is necessary for our simulations as it ensures we do not run into large discretisation errors associated with aE_m being greater than unity, as it would be for meson states constructed using b quarks had we left the mass term in the lagrangian. We still require that $Lmv^2 \gg 1$, where mv^2 is the typical kinetic energy, estimated from the mass splitting of the $\Upsilon(1S)$ and $\Upsilon(2S)$ states. Studies of the Υ gives $v^2 \approx 0.1$[45], which means on current lattices $Lmv^2 \approx 6$.

The heavy quark lagrangian we end up with is then, decoupling the quark field into its top two and bottom two components as $\Psi = (\psi, \xi)$,

$$\begin{aligned}\mathcal{L}_b = \psi^\dagger \Big[iD_0 + \frac{D^2}{2m} + \frac{g}{2m}\sigma \cdot B + \frac{g}{8m^2}\big(D^{\mathrm{ad}} \cdot E + i\sigma \cdot (D \times E - E \times D)\big)\Big]\psi \\ + \xi^\dagger \Big[iD_0 - \frac{D^2}{2m} - \frac{g}{2m}\sigma \cdot B + \frac{g}{8m^2}\big(D^{\mathrm{ad}} \cdot E + i\sigma \cdot (D \times E - E \times D)\big)\Big]\xi \\ + \mathcal{O}(1/m^3) \end{aligned} \tag{3.80}$$

3.5.2 Power Counting for Heavy-Light Mesons

For systems involving only a single heavy quark, as we are concerned with here, the remaining light degrees of freedom are governed by the nonperturbative gluon dynamics and hence characterised by the scale Λ_{QCD}. For hadrons at rest we find that the covariant derivative acting on the heavy-quark field is of order

$$D\psi \sim \Lambda_{\mathrm{QCD}}\psi. \tag{3.81}$$

Similarly for the gluon fields

$$\begin{aligned} |gA| &\sim \Lambda_{\mathrm{QCD}} \\ |gE| \sim |gB| &\sim \Lambda^2_{\mathrm{QCD}}. \end{aligned} \tag{3.82}$$

Dimensional analysis then tells us that each term in (3.80) which comes with a factor of $1/m$ also comes with a factor of Λ_{QCD} relative to the first. The heavy quark action

therefore receives corrections of order $\mathcal{O}((\Lambda_{\rm QCD}/m)^3)$.

3.5.3 Lattice NRQCD and the Evolution Equation

The next step is to discretise the NRQCD action. A convenient definition for the NRQCD quark lattice action is:

$$S = a^3 \sum_x \Big[\psi^\dagger(x)\psi(x) \\ -\psi^\dagger(x+a\hat{t})\Big(1-\frac{aH_0}{2n}\Big)^n\Big(1-\frac{a\delta H}{2}\Big)U_t^\dagger(x)\Big(1-\frac{a\delta H}{2}\Big)\Big(1-\frac{aH_0}{2n}\Big)^n\psi(x)\Big].$$

The quark propagator then satisfies the simple evolution equation

$$G(x+a\hat{t},z) = \delta(x+a\hat{t},z) + \Big(1-\frac{aH_0}{2n}\Big)^n\Big(1-\frac{a\delta H}{2}\Big)U_t^\dagger(x)\Big(1-\frac{a\delta H}{2}\Big)\Big(1-\frac{aH_0}{2n}\Big)^n G(x,z) \tag{3.83}$$

with $G(x,y) = 0$ for $x_t < y_t$. n is referred to as the stability parameter and ensures numerical stability when computing propagators using 3.83. Since the quark part of the action is first order in D_0 the propagator has no pole at $-E(p)$ and so is only the retarded part of the full propagator. This may be derived straightforwardly from the inverse relation

$$D(x,y)G(y,z) = \delta(x,z) \tag{3.84}$$

taking the Dirac operator D directly from the action:

$$D(x,y) = \delta(x,y) - \Big(1-\frac{aH_0}{2n}\Big)^n\Big(1-\frac{a\delta H}{2}\Big)U_t^\dagger(y)\Big(1-\frac{a\delta H}{2}\Big)\Big(1-\frac{aH_0}{2n}\Big)^n\delta(x,y-a\hat{t}). \tag{3.85}$$

In simulations we neglect the NRQCD determinant, since the energy scales at which the creation of $b\,\bar{b}$ pairs will be relevant are well above $\Lambda_{\rm QCD}$ and well outside the range of validity of NRQCD. None the less the terms appearing in the NRQCD lattice action will be renormalised away from the values obtained from the FWT transformation in the continuum. We might treat it like any effective field theory and compute the coefficients by matching to experiment, but this would result in a substantial reduction of the predictive power of the theory. Another method is to use perturbation theory: since the

corrections are dominated by momenta of order π/a and π/a is typically several GeV in simulations, we expect that these quantities can be calculated using perturbation theory, provided we tadpole improve appropriately. The full, tadpole and Symanzik improved, NRQCD quark action has

$$aH_0 = -\Delta^{(2)}/2am \tag{3.86}$$

$$a\delta H = a\delta H_{v^4} + a\delta H_{v^6} \tag{3.87}$$

$$\begin{aligned} a\delta H_{v^4} =& -c_1\frac{(\Delta^{(2)})^2}{8(am)^3} + c_2\frac{ig}{8(am)^2}\left(\Delta^{(\pm)}\cdot\tilde{E} - \tilde{E}\cdot\Delta^{(\pm)}\right) \\ & - c_3\frac{g}{8(am)^2}\sigma\cdot\left(\tilde{\Delta}^{(\pm)}\times\tilde{E} - \tilde{E}\times\tilde{\Delta}^{(\pm)}\right) \\ & - c_4\frac{g}{2am}\sigma\cdot\tilde{B} + c_5\frac{a^2\Delta^{(4)}}{24am} - c_6\frac{a(\Delta^{(2)})^2}{16n(am)^2} \end{aligned} \tag{3.88}$$

$$\begin{aligned} \delta H_{v^6} =& -f_1\frac{g}{8(am)^3}\left\{\Delta^{(2)}, \sigma\cdot\tilde{B}\right\} \\ & - f_2\frac{3g}{64(am)^4}\left\{\Delta^{(2)}, \sigma\cdot\left(\tilde{\Delta}^{(\pm)}\times\tilde{E} - \tilde{E}\times\tilde{\Delta}^{(\pm)}\right)\right\} \\ & - f_3\frac{ig^2}{8(am)^3}\sigma\cdot\tilde{E}\times\tilde{E} \end{aligned} \tag{3.89}$$

where the tilded quantities are the tadpole improved versions and at tree level $f_i = 1$. We also replace the U_t appearing in (3.83) with its tadpole improved version. In the simulations I perform here the stability parameter takes the value $n = 4$, following [10].

The evolution equation gives a straightforward way to compute the NRQCD propagator. As an initial value problem, as opposed to the boundary value problem of relativistic QCD, the propagator can be computed efficiently and quickly requiring far less memory or computation time than its relativistic counterpart.

Chapter 4

$B \to D^*$

4.1 $B \to D^*$

Precise measurements of quark flavour-changing interactions offer one way to uncover physics beyond the Standard Model. As successful as the Standard Model appears to be so far, there will continue to be progress reducing experimental and theoretical uncertainties, as well as making new measurements. Existing tensions in the global fits to the Cabibbo-Kobyashi-Maskawa (CKM) parameters may become outright inconsistencies, or new measurements of rare decays may differ significantly from Standard Model predictions.

Measurements of the exclusive semileptonic decay $\bar{B}^0 \to D^{*+}\ell^-\bar{\nu}$ provided the first estimations of the magnitude of CKM matrix element V_{cb} [46]. This channel still provides one of three precise methods of determining $|V_{cb}|$. Measurements for the differential branching fraction are fit to a function of q^2, the lepton invariant mass-squared, and extrapolated to the zero-recoil point (maximum q^2). Then lattice QCD results for the relevant hadronic matrix element are used to infer $|V_{cb}|$. The most recent HFLAV experimental average [47] combined with the Fermilab/MILC lattice result [4] gives $|V_{cb}| = (38.71 \pm 0.47_{\text{exp}} \pm 0.59_{\text{th}}) \times 10^{-3}$.

Measurements of the inclusive $b \to c$ decays $B \to X_c\ell\nu$, combined with an operator product expansion offer a complementary method. The latest estimate is $|V_{cb}| = (42.21 \pm 0.78) \times 10^{-3}$ [48, 49]. The discrepancy between the inclusive and exclusive result described above is at the 3σ level.

One can also use the exclusive decay $B \to D\ell\nu$ to estimate $|V_{cb}|$. Historically this has

not given as precise a determination due to having to contend with background from $B \to D^* \ell\nu$. Recent progress has come from new measurements and joint fits to experimental and lattice [50, 51] data over a range of q^2 using so-called z-parametrizations [52, 53]. The latest result using $B \to D\ell\nu$ results is $|V_{cb}| = (40.85 \pm 0.98) \times 10^{-3}$ [54], in acceptable agreement with either the $B \to D^*\ell\nu$ or $B \to X_c\ell\nu$ determinations.

In this chapter I present the details and results of a lattice calculation of the zero-recoil form factor needed to extract $|V_{cb}|$ from experimental measurements of the $B \to D^*\ell\nu$ and $B_s \to D_s^*\ell\nu$ decay rates. This work differs from the Fermilab/MILC calculation [4] in the following respects: (1) the gauge field configurations are the next generation MILC ensembles [55, 56, 57] which include effects of $2 + 1 + 1$ flavours of sea quarks using the highly improved staggered quark (HISQ) action [58]; (2) the fully relativistic HISQ action is used for valence light, strange, *and* charm quarks; (3) the nonrelativistic QCD (NRQCD) action [59] is used for the bottom quark. Therefore, this work represents a statistically independent, complementary calculation to [4], with different formulations in many respects. The two main advantages of using the HISQ action is that discretization errors are reduced and that the MILC HISQ ensembles include configurations with physically light u/d quark effects. Preliminary results were reported in recent proceedings [8].

4.2 Form factors

This section simply summarizes standard notation relating the differential decay rate, the relevant hadronic matrix elements, and the corresponding form factors. Throughout the section I refer to $\bar{B}^0 \to D^{*+}\ell^-\bar{\nu}$ decay, but the expressions for $\bar{B}_s^0 \to D_s^{*+}\ell^-\bar{\nu}$ are the same, substituting $u \to s$.

The differential decay rate, integrated over angular variables, is given in the Standard Model by

$$\begin{aligned}\frac{d\Gamma}{dw}(\bar{B}^0 \to D^{*+}l^-\bar{\nu}_l) &= \frac{G_F^2 M_{D^*}^3 |\bar{\eta}_{EW} V_{cb}|^2}{4\pi^3} \\ &\times (M_B - M_{D^*})^2 \sqrt{w^2-1}\,\chi(w)|\mathcal{F}(w)|^2 \end{aligned} \tag{4.1}$$

where $w = v \cdot v'$ is the scalar product of the B and D^* 4-velocities, and $\chi(w)$ is a known kinematic function normalized so that $\chi(1) = 1$ [4]. The coefficient $\bar{\eta}_{EW}$ accounts for electroweak corrections due to box diagrams in which a photon or Z boson is exchanged in addition to a W boson as well as the Coulomb attraction of the final-state charged particles [60, 61, 62]. The form factor $\mathcal{F}(w)$ is a linear combination of hadronic form factors parametrizing the matrix elements of the $V - A$ weak current, i.e.

$$\begin{aligned}\langle D^*(p',\epsilon)|\bar{c}\gamma^\mu b|B(p)\rangle &= \frac{2iV(q^2)}{M_B + M_{D^*}}\,\epsilon^{\mu\nu\rho\sigma}\epsilon^*_\nu p'_\rho p_\sigma \\ \langle D^*(p',\epsilon)|\bar{c}\gamma^\mu\gamma^5 b|B(p)\rangle &= 2M_{D^*}A_0(q^2)\frac{\epsilon^*\cdot q}{q^2}q^\mu \\ &+ (M_B + M_{D^*})A_1(q^2)\Big[\epsilon^{*\mu} - \frac{\epsilon^*\cdot q}{q^2}q^\mu\Big] \\ &- A_2(q^2)\frac{\epsilon^*\cdot q}{M_B + M_{D^*}}\Big[p^\mu + p'^\mu - \frac{M_B^2 - M_{D^*}^2}{q^2}q^\mu\Big]. \end{aligned} \tag{4.2}$$

The only contribution to $\mathcal{F}(w)$ at zero recoil, $w = 1$, is from the matrix element of the axial vector current; this reduces to

$$\langle D^*(p,\epsilon)|\bar{c}\gamma^j\gamma^5 b|B(p)\rangle = (M_B + M_{D^*})A_1(q^2_{\max})\epsilon^{*j} \tag{4.3}$$

for $j = 1, 2, 3$. It is sometimes conventional to work with form factors defined within

heavy quark effective theory (HQET). Of relevance to this work, I write

$$h_{A_1}(w) = \frac{2\sqrt{M_B M_{D^*}}}{M_B + M_{D^*}} \frac{A_1(q^2)}{1 - \frac{q^2}{(M_B + M_{D^*})^2}} \,. \tag{4.4}$$

At zero recoil, where $w = 1$ and $q^2 = q^2_{\rm max}$,

$$\mathcal{F}(1) = h_{A_1}(1) = \frac{M_B + M_{D^*}}{2\sqrt{M_B M_{D^*}}} A_1(q^2_{\rm max}) \,. \tag{4.5}$$

I will usually use the h_{A_1} notation. When I wish to specifically refer to the $B_s \to D_s^*$ form factor, I write $h^s_{A_1}$, so

$$\mathcal{F}^{B\to D^*}(1) = h_{A_1}(1) \;\text{ and }\; \mathcal{F}^{B_s\to D_s^*}(1) = h^s_{A_1}(1) \,. \tag{4.6}$$

These are the quantities I calculate here.

4.3 Lattice parameters and methodology

Here I give specific details about the lattice calculation. Once again many of the expressions will refer to $B \to D^*$ matrix elements, but they apply for any spectator quark mass.

The gluon field configurations that I use were generated by the MILC collaboration and include 2+1+1 flavours of dynamical HISQ quarks in the sea and include 3 different lattice spacings [55, 56, 57]. The u and d quarks have equal mass, $m_u = m_d \equiv m_l$, and in these calculations I use the values $m_l/m_s = 0.2$, 0.1 and the physical value 1/27.4 [42]. The s and c quarks in the sea are also well-tuned [7] and included using the HISQ action. The gauge action is the Symanzik improved gluon action with coefficients correct to $\mathcal{O}(\alpha_s a^2, n_f \alpha_s a^2)$ [36]. Table 4.1 gives numerical values for the lattice spacings, quark masses, and other parameters describing the ensembles used.

In calculating correlation functions, I use valence s and c masses tuned slightly closer to their physical values [7]. The d, s, and c quark propagators were computed using the MILC code [63]. The b quark is simulated using v^4 perturbatively improved non-relativistic QCD [45, 5], including terms up to $\mathcal{O}(\alpha_s v^4)$ given by $a\delta H_{v^4}$ in (3.88), which takes advantage of the non-relativistic nature of the b quark dynamics in B mesons and produces very good control over discretization uncertainties. The parameters used in calculating quark propagators are recorded in table 4.2.

In order to extract the form factor from lattice calculations I compute the set of Euclidean correlation functions

$$\begin{aligned} C_{B2pt}(t)_{ij} &= \langle \mathcal{O}(t)_{Bi} \mathcal{O}^\dagger(0)_{Bj} \rangle \\ C^{\mu\nu}_{D^*2pt}(t)_{ij} &= \langle \mathcal{O}^\mu(t)_{D^*i} \mathcal{O}^{\dagger\nu}(0)_{D^*j} \rangle \\ C^{\mu\kappa}_{3pt}(\tau, t, 0)_{ij} &= \langle \mathcal{O}^\mu(\tau)_{D^*i} J^\kappa(t) \mathcal{O}^\dagger(0)_{Bj} \rangle \end{aligned} \tag{4.7}$$

where each interpolating operator $\mathcal{O}_i$ is projected onto zero spatial momentum by summing over spatial lattice points and the current J^κ is one of several lattice currents (see

Table 4.1: Details of the gauge configurations used in this work. I refer to sets 1, 2 and 3 as 'very coarse', sets 4, 5 and 6 as 'coarse' and sets 7 and 8 as 'fine'. The lattice spacings were determined from the $\Upsilon(2S-1S)$ splitting in [5]. Sets 3, 6 and 8 use light quarks with their physical masses. u_0 is the tadpole improvement factor; here the Landau gauge mean link is used. M_π and $M_\pi L$ are also given, computed in [6]. The final column specifies the total number of configurations multiplied by the number of different start times used for sources on each. In order to improve statistical precision I use random wall sources.

Set	a(fm)	$L/a \times T/a$	am_l	am_s	am_c	u_0	M_π/MeV	$M_\pi L$	$n_{\rm cfg} \times n_{\rm t}$
1	0.1474	16×48	0.013	0.065	0.838	0.8195	302.4(2)	3.8	960×16
2	0.1463	24×48	0.0064	0.064	0.828	0.8202	215.5(1)	4.0	960×4
3	0.1450	32×48	0.00235	0.0647	0.831	0.8195	133.0(1)	3.3	960×4
4	0.1219	24×64	0.0102	0.0509	0.635	0.8341	304.5(1)	4.6	960×4
5	0.1195	32×64	0.00507	0.0507	0.628	0.8349	216.5(1)	4.3	960×4
6	0.1189	48×64	0.00184	0.0507	0.628	0.8341	132.7(0)	3.9	960×4
7	0.0884	32×96	0.0074	0.037	0.440	0.8525	306.1(2)	4.5	960×4
8	0.08787	64×96	0.00120	0.0363	0.432	0.8518	128.4(0)	3.7	540×4

section 4.4). The indices i and j label different smearing functions. I use three different smearing operators on each of the B and D^* interpolating operators.

In implementing $\mathcal{O}^\mu(t)_{D^*i}$ I use an unsmeared operator and two gauge covariant Gaussian smearings, implemented by applying $\left(1 - \frac{r_{D^*}^2 \nabla^2}{n}\right)^n$ to the field. Here the derivative is stride-2 in order not to mix the staggered-taste meson multiplets. r_{D^*} is the radius (in lattice units) chosen to give good overlap with the ground state, and n is chosen to give a good approximation to a Gaussian while maintaining numerical stability. For the B I use a local operator as well as two Gaussian smearings, implemented as $\frac{1}{N} e^{-(x-y)^2/r_B^2}$, where again r_B is a radius in lattice units and N is an overall normalization. Since the B smearings are not gauge invariant, the gauge fields are fixed to Coulomb gauge. I

Table 4.2: Valence quark masses and parameters used to calculate propagators. The s and c valence masses were tuned using results from [7] and the b mass was taken from [5]. $(1 + \epsilon_{\text{Naik}})$ is the coefficient of the charm Naik term and c_i are the perturbatively improved coefficients appearing in the NRQCD action correct through $\mathcal{O}(\alpha_s v^4)$ [5]. The last column gives the τ values used in three point functions. These have changed from those presented in [8] on the very coarse ensembles as it was found that $\tau = 10, 11, 12, 13$ resulted in excessive noise on Set 3, which resulted in poor fit stability and the relatively low value of $\mathcal{F}(1)$ on this ensemble.

Set	am_s^{val}	am_c^{val}	am_b	ϵ_{Naik}	c_1,c_6	c_5	c_4	τ
1	0.0641	0.826	3.297	−0.345	1.36	1.21	1.22	6,7,8,9
2	0.0636	0.828	3.263	−0.340	1.36	1.21	1.22	6,7,8,9
3	0.0628	0.827	3.25	−0.345	1.36	1.21	1.22	6,7,8,9
4	0.0522	0.645	2.66	−0.235	1.31	1.16	1.20	10,11,12,13
5	0.0505	0.627	2.62	−0.224	1.31	1.16	1.20	10,11,12,13
6	0.0507	0.631	2.62	−0.226	1.31	1.16	1.20	10,11,12,13
7	0.0364	0.434	1.91	−0.117	1.21	1.12	1.16	15,18,21,24
8	0.0360	0.4305	1.89	−0.115	1.21	1.12	1.16	10,13,16,19

refer to the local operator as l and the Gaussian smearings as $g2$ and $g4$ corresponding to radii of $2a$ and $4a$ respectively. I use the same choices of radii for both B and D^* smearings. The smearing parameters are given in table 4.3. Figures 4.1 and 4.2 in section 4.5 show the effectiveness of using combinations of smearings in reducing the uncertainty of the computed form factor. The typical reduction of statistical uncertainty by a factor of between 2 and 4 is gained for the cost of computing more propagators and performing additional contractions. In practice, these additional contractions are fast, and the increase in computational cost by a factor of approximately 3 is favourable compared to using all 16 available time sources on each configuration. Using all 16 time

Table 4.3: Values of r, taken to be the same, for the $B_{(s)}$ and $D^*_{(s)}$ Gaussian smearings on each set and the accompanying n values for the $D^*_{(s)}$ smearings. I chose to fix the radii in lattice units rather than physical units as this seemed to result in more consistent numerical stability of the covariant Gaussian smearing operator when moving between lattices.

Set	r_{g2}/a	r_{g4}/a	n_{g2}	n_{g4}
1,2,3	2	4	30	30
4,5,6	2	4	30	30
7,8	2	4	30	40

sources would yield an improvement in statistical uncertainty of less than a factor of 2 due to correlations between time sources, while increasing the computational cost by a factor of 4. The interpolating operators themselves are

$$\begin{aligned} \mathcal{O}_B(x) &= \sum_y \bar{\psi}_u(x)\gamma^5\Delta(x,y)\Psi_b(y) \\ \mathcal{O}^i_{D^*}(x) &= \sum_y \bar{\psi}_u(x)\gamma^i\Delta(x,y)\psi_c(y+a\hat{i}) \end{aligned} \tag{4.8}$$

where $\Delta(x,y)$ is the appropriate smearing function discussed above and the D^* interpolating operator is point split. In distinction to the continuum quark fields b, c, s, and u of section 4.2, here I denote the NRQCD b field by Ψ_b and the staggered fields, written as 4-component Dirac spinors (see 3.4.2), by ψ with the appropriate flavour subscript.

I checked both the point-split and local D^* interpolating operators on the very coarse, physical point ensemble (Set 3) and found no significant difference in statistical noise or central value of either the D^* mass or the matrix element. I primarily used the point-split current as it was simpler to implement in our framework. The results quoted below for the $B \to D^*$ fits use the point-split vector current, except for Set 3 where results are given for the local vector current. The results below for $B_s \to D^*_s$ form factors were obtained using the local vector current.

In order to improve statistics I multiply the smeared sources with random walls to produce, on average, the effect of multiple sources. [64] compares ground state energies for the Υ computed using random wall sources to those computed without and demonstrates a reduction in statistical uncertainty by a factor of ≈ 4 with a low computational cost. Taking the 2-point function, projected onto zero momentum and with symmetric smearings as we use here, as an example:

$$\begin{aligned} C_{2pt}(t,0)_{ij} =& \sum_{xy,\delta} \langle \bar{\psi}_1(x,t)\Gamma\psi_2(x+\delta_{sink},t)\times \\ & \bar{\psi}_2(y,0)\Gamma\psi_1(y+\delta_{src},0)\rangle \Delta_i(\delta_{sink})\Delta_j(\delta_{src}) \\ =& \sum_{xy,\delta} \mathrm{tr}\Big[\Gamma G_2(x,t;y,0)\Gamma\Delta_j(\delta_{src})\times \\ & G_1(y+\delta_{src},0;x+\delta_{sink},t)\Delta_i(\delta_{sink})\Big]\,. \end{aligned} \tag{4.9}$$

Exact computation requires an inversion for each value of y being summed over. Instead I generate N random vectors ξ satisfying

$$\lim_{N\to\infty} \sum_{l=1}^{N} \xi_{al}(x)\xi_{bl}(y)^* = \delta(x,y)\delta_{ab}\,. \tag{4.10}$$

l labels the N random colour vector sources and a and b are colour indices. The average over configurations further suppresses violations of this relation; in practice a single random wall per colour, setting $N = N_c = 3$, is sufficient. Inserting the above relation into the 2-point function

$$\begin{aligned} C_{2pt}(t,0)_{ij} =& \sum_{xyz,\delta,l} \mathrm{tr}\Big[\Gamma G_2(x,t;z,0)\xi_l(z)\Gamma\times \\ & \Delta_j(\delta_{src})\xi_l^\dagger(y+\delta_{src})G_1(y,0;x+\delta_{sink},t)\Delta_i(\delta_{sink})\Big] \\ =& \sum_{xyz,\delta,l} \mathrm{tr}\Big[\Gamma G_2(x,t;z,0)\xi_l(z)\Gamma\times \\ & \gamma^5\big[\Delta_i(\delta_{sink})G_1(x+\delta_{sink},t;y,0)\Delta_j(\delta_{src})\xi_l(y+\delta_{src})\big]^\dagger\gamma^5\Big] \end{aligned} \tag{4.11}$$

where γ^5 hermiticity has been used. The naive propagators G are built from staggered quarks and the full form of the correlation function contractions in terms of NRQCD and staggered propagators is given in Appendix A.

These correlation functions can be expressed in terms of amplitudes and decaying exponentials by inserting a complete basis of states. Projecting onto zero momentum and setting $q = (M_B - M_{D^*}, 0, 0, 0)$ this gives

$$\begin{aligned} C_{B2pt}(t)_{ij} &= \sum_{n,a=0,1} (-1)^{at} B^n_{ai} B^n_{aj} e^{-M_{B^n_a} t} \\ C_{D^*2pt}(t)_{ij} &= \sum_{n,a=0,1} (-1)^{at} A^n_{ai} A^n_{aj} e^{-M_{D^{*n}_a} t} \\ C_{3pt}(\tau, t, 0)_{ij} &= \sum_{ab=0,1} \sum_{nm} (-1)^{a(\tau-t)+bt} A^n_{ai} B^m_{bj} \\ &\quad \times V^{nm}_{ab} e^{-M_{D^{*m}_a}(\tau-t) - M_{B^n_b} t} \end{aligned} \tag{4.12}$$

where

$$\begin{aligned} B^n_{ai} &= \frac{\langle \Omega | \mathcal{O}^i_B | B^n_a \rangle}{\sqrt{2 M_{B^n_a}}} \\ A^n_{ai} &= \frac{\langle \Omega | \mathcal{O}^i_{D^*} | {D^*}^n_a \rangle}{\sqrt{2 M_{D^{*n}_a}}} \\ V^{nm}_{ab} &= \frac{\langle {D^*}^n_a | J | B^m_b \rangle}{\sqrt{2 M_{D^{*n}_a} 2 M_{B^m_b}}} \,. \end{aligned} \tag{4.13}$$

Note that I have included contributions from opposite-parity states, which depend on imaginary time like $(-1)^t$ and arise from using staggered quarks [58], by introducing the sum over a and b. When either a or b is nonzero the corresponding term in the sum is multiplied by a sign factor which oscillates between 1 and -1 in time. I am only interested in the terms with $a = b = 0$ here; however in order to extract these, the oscillating terms must be fit away. For my choice of operators the A, B and V parameters are real [65]. I discuss my fits to these correlation functions in section 4.5.1.

4.4 One-loop Matching

A lattice current with the same matrix elements as the continuum current, to a given order, is required. The matching of lattice and continuum currents is done in [9] through $\mathcal{O}(\alpha_s, \alpha_s/am_b, \Lambda_{QCD}/m_b)$,where Λ_{QCD} is a typical QCD scale of a few hundred MeV, following the method used in [66]. Using power counting in powers of Λ_{QCD}/m_b a set of lattice currents is selected. At the order to which I work, only the following currents contribute:

$$\begin{aligned} J^{(0)i}_{\text{latt}}(x) &= \bar{\psi}_c \gamma^i \gamma^5 \Psi_b \\ J^{(1)i}_{\text{latt}}(x) &= -\frac{1}{2am_b} \bar{\psi}_c \gamma^i \gamma^5 \gamma \cdot \Delta \Psi_b \,. \end{aligned} \tag{4.14}$$

It is convenient for us to also compute the matrix elements of operators entering at $O(\alpha_s \Lambda_{QCD}/m_b)$

$$\begin{aligned} J^{(2)i}_{\text{latt}}(x) &= -\frac{1}{2am_b} \bar{\psi}_c \gamma \cdot \overleftarrow{\Delta} \gamma^0 \gamma^i \gamma^5 \Psi_b \\ J^{(3)i}_{\text{latt}}(x) &= -\frac{1}{2am_b} \bar{\psi}_c \gamma^0 \gamma^5 \Delta^i \Psi_b \,. \end{aligned} \tag{4.15}$$

This allows for a configuration-by-configuration check of the code: namely that at zero recoil, the three-point correlation functions satisfy the relation $C_{3ptJ^{(1)}} + C_{3ptJ^{(2)}} - 2C_{3ptJ^{(3)}} = 0$. This identity is derived using integration by parts and the fact that $\gamma^0 \Psi_Q = \Psi_Q$.

The full matching is a double expansion in Λ_{QCD}/m_b and in α_s. The matched current is given by

$$\mathcal{J}^i = Z[(1 + \alpha_s(\eta - \tau)) J^{(0)i}_{\text{latt}} + J^{(1)i}_{\text{latt}}] + O\left(\frac{\alpha_s \Lambda_{QCD}}{m_b}\right) \tag{4.16}$$

where Z is a multiplicative factor from the tree-level massive-HISQ wave function renormalization for the HISQ c quark. The one-loop coefficients η and τ respectively account for the renormalization of $J^{(0)i}_{\text{latt}}$ and for the mixing of $J^{(1)i}_{\text{latt}}$ into $J^{(0)i}_{\text{latt}}$. Numerical values for the perturbative coefficients relevant for the ensembles used are given in table 4.4 [9].

Table 4.4: Tree-level Z factors and one-loop matching coefficients, used in (4.16), calculated at lattice quark masses appropriate to each of our gauge-field ensembles. I also give values on each ensemble for the strong coupling constant in the V scheme at a scale of $2/a$ (from results in [9]).

Set	Z	$-\eta$	τ	$\alpha_V(2/a)$
1	0.9930	0.260(3)	0.0163(1)	0.346
2	0.9933	0.260(3)	0.0165(1)	0.344
3	0.9930	0.260(3)	0.0165(1)	0.343
4	0.9972	0.191(3)	0.0216(1)	0.311
5	0.9974	0.185(3)	0.0221(1)	0.308
6	0.9974	0.185(3)	0.0221(1)	0.307
7	0.9994	0.091(3)	0.0330(1)	0.267
8	0.9994	0.091(3)	0.0330(1)	0.267

Matrix elements of currents of order $\alpha_s^n \Lambda_{QCD}/m_b$ vanish to all orders in α_s according to Luke's theorem [67]. I will denote by V the matrix elements of the currents $J_{\rm latt}$ divided by meson mass factors, as in (4.13) with $a = b = 0$ and $n = m = 0$. Luke's theorem implies the combination

$$V_{\rm sub}^{(1)i} = V^{(1)i} - \alpha_s \tau V^{(0)i}\,, \tag{4.17}$$

which represents the physical, sub-leading matrix element, should be very small, only different from zero due to systematic uncertainties.

4.5 Analysis of numerical data

In this section I discuss the two main aspects of numerical analysis. First I present fits to the correlation functions, allowing us to determine $h_{A_1}(1)$ on each of the 8 ensembles. Second, I discuss how I infer a physical value for $h_{A_1}(1)$ with an error estimate for uncertainties associated with current matching, discretization, and dependence on quark masses.

4.5.1 Fits to correlation functions

I fit the three correlation functions defined in (4.12) simultaneously using the `corrfitter` package developed by Lepage [68, 69]. This minimises

$$\chi^2(p) = \sum_{t,t'} \Delta C(t,p)\sigma^{-2}_{t,t'}\Delta C(t',p) + \sum_i \frac{(p^i - p^i_{\text{prior}})^2}{\sigma^2_{p^i_{\text{prior}}}} \tag{4.18}$$

with respect to p. Here $\Delta C(t,p) = \overline{C}(t) - C_{\text{TH}}(t,p)$ with $C_{\text{TH}}(t,p)$ the theoretical value of the correlation function at time t computed using (4.12) with parameters p and $\overline{C}(t)$ is the measured value of the correlation function at t. p^i is the ith parameter in the theory and p^i_{prior} is its prior value with error $\sigma_{p^i_{\text{prior}}}$. The correlation matrix $\sigma_{t,t'}$ includes all correlations between data points. Fitting correlators from all smeared sources and sinks simultaneously requires the use of an SVD cut on the eigenvalues when determining the inverse of σ^2. This is implemented by replacing eigenvalues of σ^2 with magnitude less than the SVD cut with the value of the cut. The code also provides the option of removing the corresponding eigenvectors from the data and I have checked that choosing this option did not change the fit results for the matrix elements. I also exclude points close in time to the source and sink to suppress excited state contributions and speed up the fit. The number of truncated data points and SVD cuts used to obtain our results are given in table 4.5. For the D^* two point function, with symmetric boundary conditions in time, the source and sink truncations were the same. For the B two point function only the source is truncated. Also given are the truncations used for the three

Table 4.5: Values used for SVD cuts and truncations made near the source and sink.

Set	SVD	Δt^{D^*}	Δt^{B}	$\Delta t^{\mathrm{3pt}}_{D^*}$	$\Delta t^{\mathrm{3pt}}_{B}$
1	0.01	4	4	2	2
2	0.001	4	4	2	2
3	0.001	4	4	2	2
4	0.01	2	2	2	2
5	0.01	4	4	2	2
6	0.0025	4	4	1	1
7	0.0001	4	4	2	2
8	0.001	4	4	2	2

point function.

I look at the effectiveness of the various smearings by fitting each smearing diagonal, i.e. equal radii, set of two and three point correlator functions independently and comparing the result to the full fit. Figures 4.1 and 4.2 show comparisons of the fit results for $h_{A_1}(1)$ when varying numbers of exponentials; the points are normalized by the value of $h_{A_1}(1)$ taken as the result for that ensemble. Plots are shown for all 8 ensembles in figure 4.1. In each plot, I show the full fit results to the 3×3 matrix of source/sink combinations (local l, or Gaussian with 2 radii, $g2$ and $g4$), as well as "diagonal" fits where only one source/sink is used. The statistical improvement of using all the data is apparent. The flatness of the curves and the constancy of the error bars shows that, for large enough N_{exp}, the Bayesian fits are insensitive to adding further exponential terms, i.e. effects of excited states are accounted for. The final results typically come from the $N_{\mathrm{exp}} = 5$ fits to the full 3×3 matrix of correlators; however, on ensembles 3 and 7, I had to include another exponential. In these plots I only include the results of fits with $\chi^2/\mathrm{dof} < 1.2$. I give the ground state and oscillating state two point fit parameters for my full simultaneous fits in table 4.6 and table 4.7. The $C_{B2pt}(t)$ fit amplitudes, the

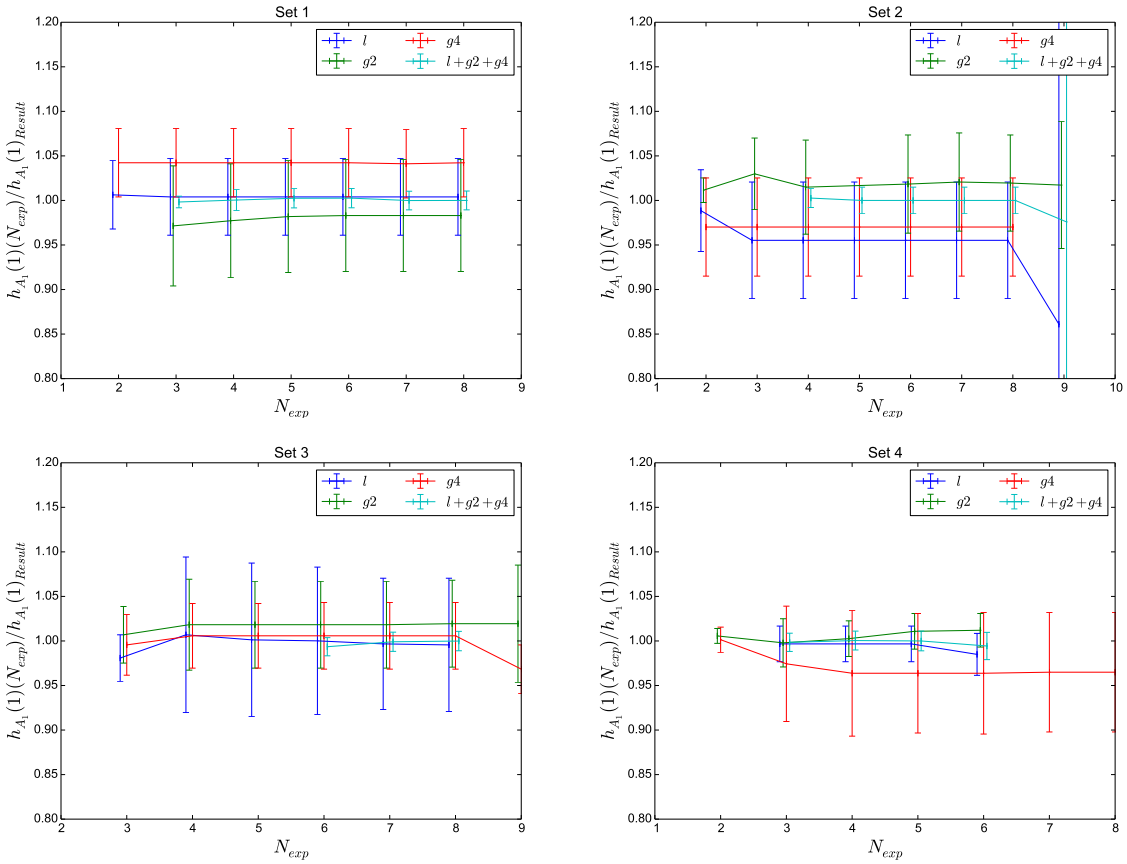

Figure 4.1: Plots of N_{exp} fit behaviour on first four ensembles for $B \to D^*$ (see table 4.1). In each plot 4 sets of data points are shown: the full fit including all 3×3 source-sink combinations, and, for comparison, separate "diagonal" fits where only one type of source-sink smearing is used. (The notation is defined in section 4.3.) A significant improvement is seen in the full fit. All diagonal fits show good agreement for $N_{\text{exp}} \geq 4$, but with the increased precision, sometimes 5 or 6 exponentials are needed to get a good 3×3 matrix fit.

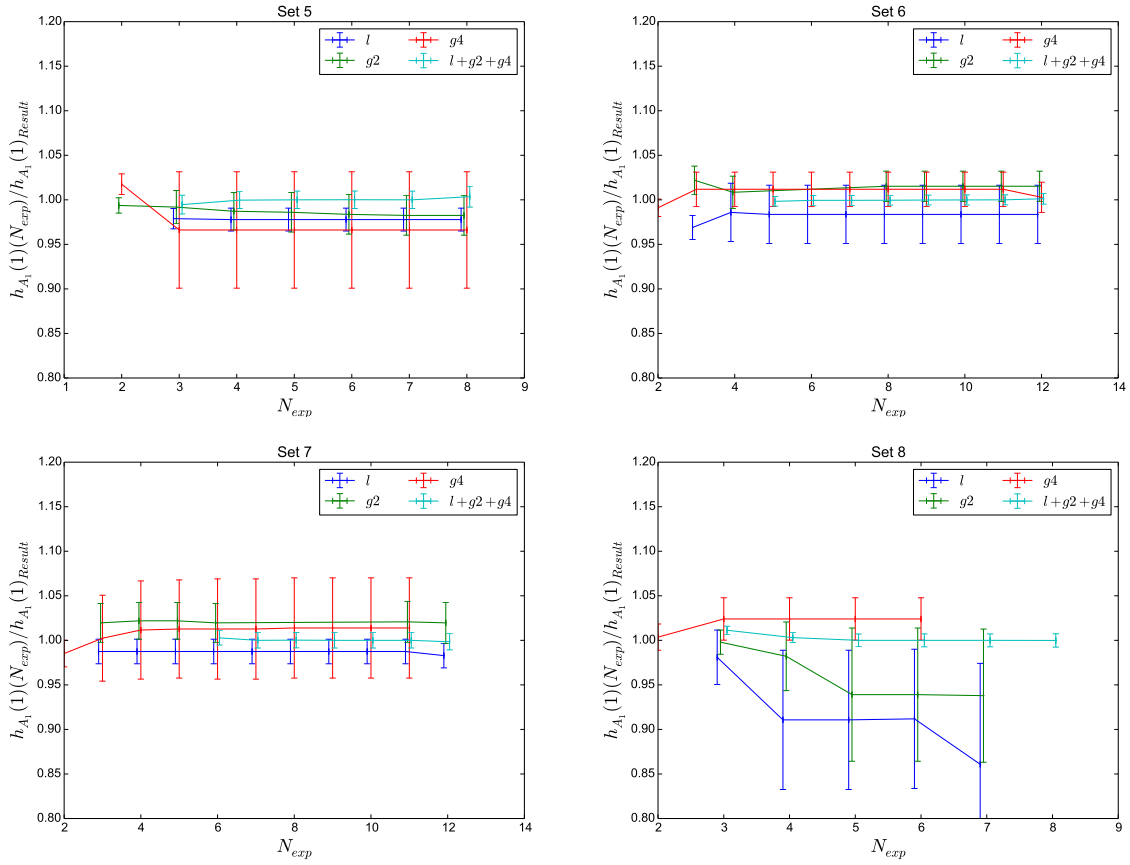

Figure 4.2: Further plots of N_{exp} fit behaviour on last four ensembles for $B \to D^*$.

energies and B^n_{ai} parameters of (4.12), are in good agreement with those in [10].

The values given in table 4.5 were chosen by trial and error, aiming to retain as much of the data as possible while maintaining a stable fit. However we could have chosen different values for these and it is good to check that our results are insensitive to such choices. As such I perform several variations of the fit, taking all combinations of $\Delta t \to \Delta t \pm 1$ for the B and D^* two point functions and the three point function as well as varying the SVD cut between a half and twice it's chosen value. Some such fits result in a χ^2/dof value greater than 1 indicating that the inclusion of the additional data includes either too large a contribution from higher energy excited states or a sufficiently singular correlation matrix to result in an unstable fit. Those fits which converge, plotted in figure 4.3, with a value of $\chi^2/\text{dof} \approx 1$ are all in agreement to within

error with the fit results I use for my analysis, demonstrating that my results are indeed robust to such variations.

Table 4.8 gives results for matrix elements corresponding to the currents $J^{(1)}_{\text{latt}}$ and $J^{(2)}_{\text{latt}}$. One can see that Luke's theorem holds, in that $V^{(1)}_{\text{sub}}$ is very small. Results are also given for $V^{(2)}$ as well as numerical values for $\alpha_s\Lambda_{\text{QCD}}/m_b$. While it is important to remember that there are absent mixing down factors from the current $J^{(0)}$ contributing at $\mathcal{O}(\alpha_s\Lambda_{\text{QCD}}/m_b)$ it is encouraging to see that $V^{(2)}$ is small compared to its expected order.

On each ensemble, I obtain a value for the zero-recoil form factors $h^{(s)}_{A_1}(1)$. As in the continuum expressions (4.3) and (4.5) we have

$$h_{A_1}(1)|_{\text{latt}} = V^{\mathcal{J}} \equiv \frac{\langle D^*|\mathcal{J}|B\rangle}{\sqrt{2M_{D^*}2M_B}} \tag{4.19}$$

and similarly for $h^s_{A_1}(1)|_{\text{latt}}$. I write $V^{\mathcal{J}}$ here to make clear that I fit combinations of three point correlators that correspond to the insertion of the current given by (4.16). Results for $h_{A_1}(1)$ on each ensemble are presented in table 4.9. I computed $h^s_{A_1}(1)$ on the physical-point lattices only, since chiral perturbation theory predicts this quantity to be much less sensitive to the sea quark mass than the spectator quark mass. (In fact it will be seen that the spectator quark mass dependence is also small).

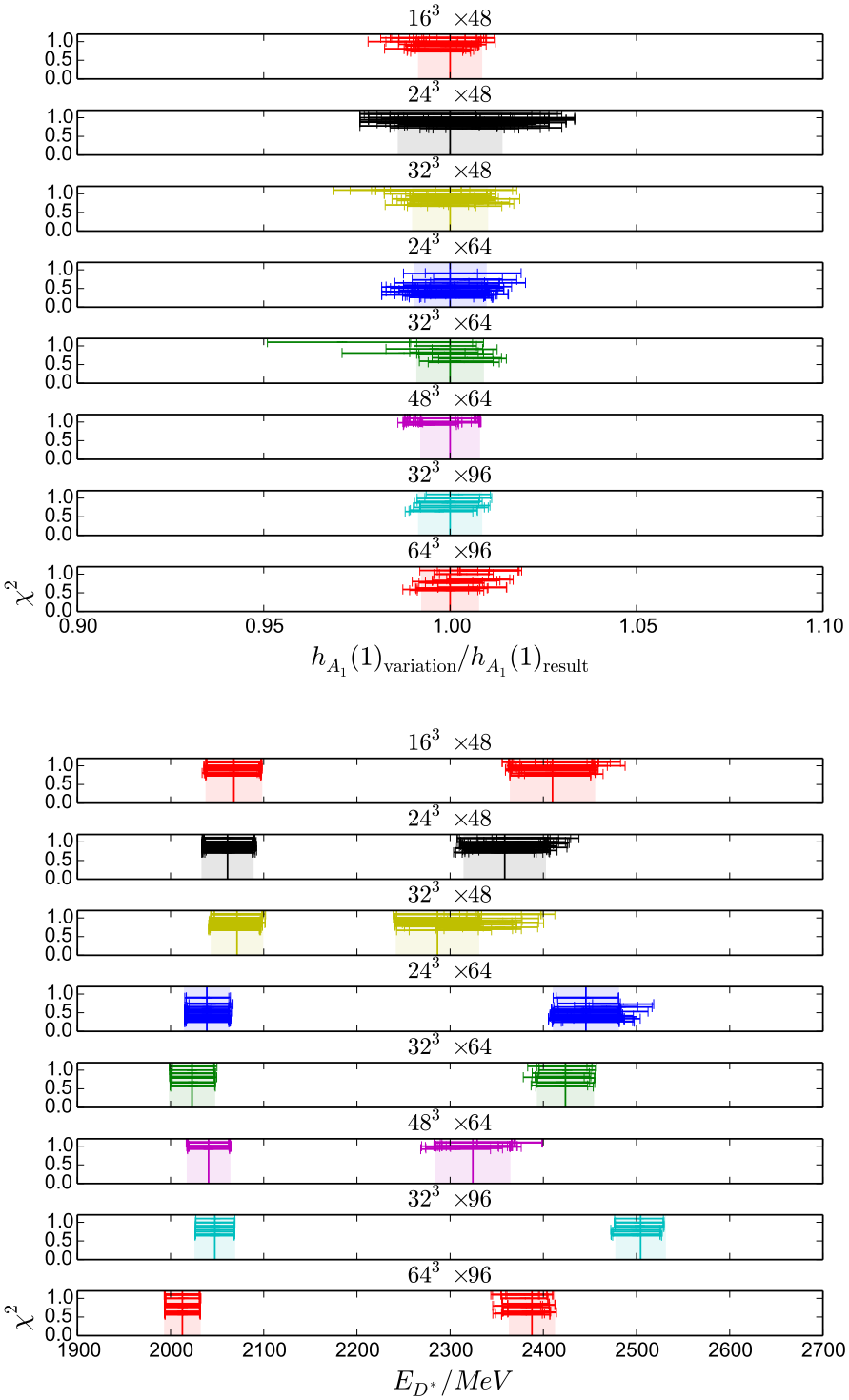

Figure 4.3: Plots showing the robustness of each fit with respect to changes in fit parameters.

Table 4.6: Ground state and oscillating state local amplitudes and masses from my fits. Note that on Set 3 I use the local vector operator, otherwise I use the point-split operator; therefore, the amplitudes A are not comparable between different operators. Also note that the tabulated B "masses" are the NRQCD "simulation energies" $aE^{\rm sim}$, representing the nonperturbative contribution to the B meson binding energy. The B parameters are in good agreement with those in [10].

Set	A^0_{0l}	A^0_{1l}	$aM_{D_0^{*0}}$	$aM_{D_1^{*0}}$
1	0.1420(12)	0.110(10)	1.5465(19)	1.815(22)
2	0.1338(17)	0.087(12)	1.5304(28)	1.742(26)
3	0.1710(14)	0.092(13)	1.5226(18)	1.675(25)
4	0.1006(23)	0.081(20)	1.2599(31)	1.499(30)
5	0.0951(14)	0.081(10)	1.2289(23)	1.459(18)
6	0.09636(52)	0.0479(87)	1.23244(99)	1.354(22)
7	0.06466(40)	0.0520(35)	0.91551(88)	1.0838(82)
8	0.05912(40)	0.0502(23)	0.89583(99)	1.0477(71)
	B^0_{0l}	B^0_{1l}	$aM_{B_0^0}$	$aM_{B_1^0}$
1	0.2287(17)	0.232(14)	0.5667(14)	0.815(13)
2	0.2171(20)	0.200(24)	0.5534(18)	0.770(18)
3	0.2099(17)	0.214(14)	0.5433(15)	0.761(14)
4	0.1700(23)	0.104(54)	0.4825(21)	0.638(46)
5	0.1611(24)	0.095(54)	0.4745(22)	0.621(42)
6	0.15739(69)	0.1674(58)	0.46809(80)	0.6523(58)
7	0.10762(64)	0.1241(35)	0.37950(76)	0.5437(40)
8	0.09884(69)	0.1131(26)	0.36473(98)	0.5042(32)

Table 4.7: Ground state and oscillating state local amplitudes and masses from my fits for the D_s^*, using the local vector operator.

	A_{0l}^{s0}	A_{1l}^{s0}	$aM_{D_{s0}^{*0}}$	$aM_{D_{s1}^{*0}}$
3	0.1987(13)	0.136(14)	1.58655(79)	1.868(14)
6	0.13689(81)	0.0918(75)	1.28341(45)	1.5094(94)
8	0.08233(40)	0.0618(23)	0.93657(49)	1.1142(50)
	B_{0l}^{s0}	B_{1l}^{s0}	$aM_{B_{s0}^0}$	$aM_{B_{s1}^0}$
3	0.25554(42)	0.2460(75)	0.60639(28)	0.8862(50)
6	0.18822(14)	0.1669(58)	0.51657(11)	0.7277(36)
8	0.11867(55)	0.1212(17)	0.40136(48)	0.5698(15)

Table 4.8: Matrix elements, with meson factors defined in (4.13), of currents contributing at $\mathcal{O}(\alpha_s \Lambda_{QCD}/m_B)$ for $B \to D^*$. Note the approximate cancellation between the mixing down term $\alpha_s \tau V^{(0)}$ and $V^{(1)}$ to give a small $V_{\rm sub}^{(1)}$ as expected from Luke's theorem. Note $V^{(2)}$ is numerically smaller than its parametric estimate $\alpha_s \Lambda_{\rm QCD}/m_b \approx 0.03$.

Set	$V_{\rm sub}^{(1)}$	$V^{(2)}$
3	−0.0050(8)	0.0138(8)
6	−0.0044(5)	0.0101(4)
8	−0.0031(7)	0.0060(8)

Table 4.9: Fit results for the zero-recoil form factor $h_{A_1}(1)_{\text{latt}} = V^{\mathcal{J}}$ for both $B \to D^*$ and $B_s \to D_s^*$.

Set	$h_{A_1}(1)_{\text{latt}}$	$h^s_{A_1}(1)_{\text{latt}}$
1	0.8606(91)	
2	0.871(13)	
3	0.8819(96)	0.8667(42)
4	0.8498(94)	
5	0.8570(84)	
6	0.8855(50)	0.8662(61)
7	0.8709(75)	
8	0.8886(63)	0.8715(44)

4.5.2 Chiral-continuum extrapolation

By carrying out the calculation using 8 ensembles, spanning 3 values of lattice spacing and 3 values of the light quark mass, many of the systematic uncertainties can be quantified by performing a least-squares fit to a function which accounts for unphysical parameters or truncation errors. Below I describe how the fits address each of these sources of uncertainty then present results of the fits.

There are two types of systematic error which must be accounted for. The first type are truncation errors about which the numerical data contain no information. In this class are the higher-order (in Λ_{QCD}/m_b) current corrections truncated in the perturbative matching described in section 4.4. The numerical data contain no information about Λ_{QCD}^2/m_b^2 or $\alpha_s\Lambda_{QCD}/m_b$ corrections, so I add to each data point nuisance terms

$$\begin{aligned} h_{A_1}(1)|_{\text{fit}} = \; & h_{A_1}(1)|_{\text{latt}} \\ & + e_4 \frac{\Lambda_{QCD}^2}{m_b^2}\left[1 + e_5\Delta_{am_b} + e_6\Delta_{am_b}^2\right] \\ & + e_7 \frac{\alpha_s\Lambda_{QCD}}{m_b}\left[1 + e_8\Delta_{am_b} + e_9\Delta_{am_b}^2\right] \end{aligned} \tag{4.20}$$

where

$$\Delta_{am_b} = (am_b - 2)/2$$

and e_4, e_5, e_6, e_7, e_8, and e_9 are Gaussian distributed variables, with mean and standard deviation $\mu(\sigma)$, with $e_4 = 0(0.5)$, $e_7 = 0(0.3)$ and $e_{5,6,8,9} = 0(1)$, 100% correlated between each data point. The e_5, e_6, e_8 and e_9 terms reflect the fact that the coefficients of the truncated Λ_{QCD}^2/m_b^2 and $\alpha_s\Lambda_{QCD}/m_b$ terms will be slowly varying functions of am_b. The choice of e_7 is motivated by the magnitude of $V^{(2)}$ and the expectation that Luke's theorem will hold at this order.

The second type of systematic uncertainties arise from truncation, discretization, or tuning errors about which we can draw inferences from the Monte Carlo calculation. Consider the unknown α_s^2 corrections to the current normalization. In contrast to the truncation of the Λ_{QCD}/m_b expansion, the numerical data is, at least in principle, sen-

sitive to $O(\alpha_s^2)$ corrections through the running of the coupling on the different lattice spacings. In addition the results have dependence on the lattice spacing and the light quark mass that can be mapped out using theoretical expectations. For the light quark mass dependence this is based on chiral perturbation theory.

4.5.3 Staggered chiral perturbation theory

The full expression for the form factor derived in staggered chiral perturbation theory is given by [70]

$$\begin{aligned} h_{A_1}(1) = 1 + \frac{X(\Lambda_\chi)}{m_c^2} + \frac{g_\pi^2}{48\pi^2 f^2}\Big[\frac{1}{16}\sum_\delta (2\bar{F}_{\pi_\delta} + \bar{F}_{K_\delta}) - \frac{1}{2}\bar{F}_{\pi_I} + \frac{1}{6}\bar{F}_{\eta_I} \\ + a^2\delta'_V\Big(\frac{M_{S_V}^2 - M_{\pi_V}^2}{(M_{\eta_V}^2 - M_{\pi_V}^2)(M_{\pi_V}^2 - M_{\eta'_V}^2)}\bar{F}_{\pi_V} + \frac{M_{\eta_V}^2 - M_{S_V}^2}{(M_{\eta_V}^2 - M_{\eta'_V}^2)(M_{\eta_V}^2 - M_{\pi_V}^2)}\bar{F}_{\eta_V} \\ + \frac{M_{S_V}^2 - M_{\eta'_V}^2}{(M_{\eta_V}^2 - M_{\eta'_V}^2)(M_{\eta'_V}^2 - M_{\pi_V}^2)}\bar{F}_{\eta'_V}\Big) + (V \to A)\Big] \end{aligned} \tag{4.21}$$

where $\bar{F}_X = F[M_X, -\Delta_{m_c}/M_X]$ as defined below.

$$\begin{aligned} F[M,x] = &\frac{M^2}{x}\Big\{x^3 \ln\frac{M^2}{\Lambda_\chi^2} + \frac{1}{3}x^3 - 4x + 2\pi \\ &- \sqrt{x^2-1}(x^2+2) \\ &\times \left(\ln\left[1 - 2x(x - \sqrt{x^2-1})\right] - i\pi\right)\Big\}. \end{aligned} \tag{4.22}$$

The masses of the η and η' are given in [41] as

$$\begin{aligned} M_{\eta_V}^2 &= \frac{1}{2}\left(M_{\pi_V}^2 + M_{S_V}^2 + \frac{3}{4}a^2\delta'_V - Z\right) \\ M_{\eta'_V}^2 &= \frac{1}{2}\left(M_{\pi_V}^2 + M_{S_V}^2 + \frac{3}{4}a^2\delta'_V + Z\right) \\ Z_V &= \sqrt{(M_{S_V}^2 - M_{\pi_V}^2)^2 - \frac{a^2\delta'_V}{2}(M_{S_V}^2 - M_{\pi_V}^2) + \frac{9(a^2\delta'_V)^2}{16}} \\ &= (M_{S_V}^2 - M_{\pi_V}^2) - \frac{a^2\delta'_V}{4} + \mathcal{O}((a^2\delta'_V)^2) \\ M_{\eta_I}^2 &= M_{\pi_I}^2/3 + 2M_{S_I}^2/3\,. \end{aligned} \tag{4.23}$$

M_{S_ξ} is the diagonal element of the mass matrix for flavour s with taste ξ, given in [71]. I take the $s\bar{s}$ pseudoscalar taste splittings equal to the pion taste splittings. This is a good approximation in the case of HISQ [56]. I then write (to order $\mathcal{O}((a^2\delta'_V)^2)$)

$$\begin{aligned} M^2_{\eta'_V} - M^2_{\pi_V} =& M^2_{S_G} - M^2_{\pi_G} + a^2\delta'_V/4 \\ M^2_{\eta_V} - M^2_{\pi_V} =& a^2\delta'_V/2 \\ M^2_{S_V} - M^2_{\pi_V} =& M^2_{S_G} - M^2_{\pi_G} \end{aligned} \tag{4.24}$$

where G indicates the taste pseudoscalar. From these I find

$$\begin{aligned} \frac{M^2_{S_V} - M^2_{\eta'_V}}{(M^2_{\eta_V} - M^2_{\eta'_V})(M^2_{\eta'_V} - M^2_{\pi_V})} &= \frac{a^2\delta'_V/4}{(M^2_{S_G} - M^2_{\pi_G})^2 - (a^2\delta'_V/4)^2} \\ \frac{M^2_{\eta_V} - M^2_{S_V}}{(M^2_{\eta_V} - M^2_{\eta'_V})(M^2_{\eta_V} - M^2_{\pi_V})} &= \frac{a^2\delta'_V/2 - (M^2_{S_G} - M^2_{\pi_G})}{(a^2\delta'_V/4 - (M^2_{S_G} - M^2_{\pi_G}))a^2\delta'_V/2} \\ \frac{M^2_{S_V} - M^2_{\pi_V}}{(M^2_{\eta_V} - M^2_{\pi_V})(M^2_{\pi_V} - M^2_{\eta'_V})} &= \frac{-(M^2_{S_G} - M^2_{\pi_G})}{((M^2_{S_G} - M^2_{\pi_G}) - a^2\delta'_V/4)a^2\delta'_V/2}\,. \end{aligned} \tag{4.25}$$

The expression for $h_{A_1}(1)$ then reduces to

$$\begin{aligned} h_{A_1}(1) = 1 + \frac{X(\Lambda_\chi)}{m_c^2} + \frac{g_\pi^2}{48\pi^2 f^2}\Bigg[& \frac{1}{16}\sum_\delta 2\bar{F}_{\pi_\delta} - \frac{1}{2}\bar{F}_{\pi_I} \\ & + \left(2 - \frac{a^2\delta'_V}{2(M^2_{S_G} - M^2_{\pi_G})}\right)\bar{F}_{\eta_V} + \left(2 - \frac{a^2\delta'_A}{2(M^2_{S_G} - M^2_{\pi_G})}\right)\bar{F}_{\eta_A} \\ & - \left(2 + \frac{a^2\delta'_V}{2(M^2_{S_G} - M^2_{\pi_G})}\right)\bar{F}_{\pi_V} - \left(2 + \frac{a^2\delta'_A}{2(M^2_{S_G} - M^2_{\pi_G})}\right)\bar{F}_{\pi_A}\Bigg] \\ & + \mathcal{O}((a^2\delta'_V)^2) \end{aligned} \tag{4.26}$$

where I have ignored terms expected to produce normal discretization errors and pion mass dependence, as these are included elsewhere in the fit. Following [6] I take $\delta'_A \approx \delta'_V \approx -\delta t$, which I implement by including $\delta'_A = \delta'_V = -\delta t \times 1.0(5)$ as priors. I use the pion masses computed in [6] together with the taste splittings for the pion, δt, given in [56].

4.5.4 Finite volume corrections

Finite volume corrections enter (4.26) through corrections to the loop integrals in the functions $\bar{F}_X$. The relevant formulae are given in [70] and are formed of polynomial terms in Δ_{m_c}/M_X and $M_X L$ exponentially suppressed by factors of $e^{-M_X L}$. The leading correction therefore goes like Δ_{m_c}/M_π. Since we keep $M_\pi L$ approximately fixed across our lattices we expect greater finite volume effects near the physical point. Evaluating these expressions on our lattices, I have found that finite volume effects are at least an order of magnitude smaller than the leading $\mathcal{O}(\alpha_s^2)$ error on the unphysical lattices. On sets 3, 6 and 8 the finite volume effects are on the order of half a percent and are significant at the order to which I work. These are incorporated into my fit by subtracting $\delta h_{A_1}(1)$, found by adding $\delta\bar{F}_X$ to each $\bar{F}_X$ appearing in (4.26), from my data. In figure 4.4 I show finite volume effects with taste splittings. In much the same way as the taste splitting washes out the cusp [70] the finite volume effects are significantly reduced.

4.5.5 Full Fit Function

Based on the discussions above the fit function for the $h_{A_1}(1)$ data takes the functional form

$$\begin{aligned} h_{A_1}(1)|_{\text{fit}} &= (1+B)\delta_a^B + C\frac{M_\pi^2}{\Lambda_\chi^2} + \delta_a^g \frac{g^2}{48\pi^2 f^2} \times \text{chiral logs} \\ &+ \gamma_1 \alpha_s^2 \left[1 + \frac{\gamma_5}{2}(am_b - 2) + \frac{\gamma_6}{4}(am_b - 2)^2\right] V^{\mathcal{J}} \end{aligned} \tag{4.27}$$

where the chiral logarithms are the $\bar{F}$ functions multiplying $g^2/48\pi^2 f^2$ in (4.26). The first term accounts for the deviation of the physical $h_{A_1}(1)$ from the static quark limit value of 1. The fit parameter B is given a prior of 0(1). I take as priors $\gamma_1 = 0(0.5)$, $\gamma_{5,6} = 0(1)$. The choice of γ_1 is motivated by the observation that the one loop matching coefficients are at most ≈ 0.25 in magnitude. We have checked that relaxing this choice to a more conservative value of $\gamma_1 = 0(1)$ does not move the central value by more than

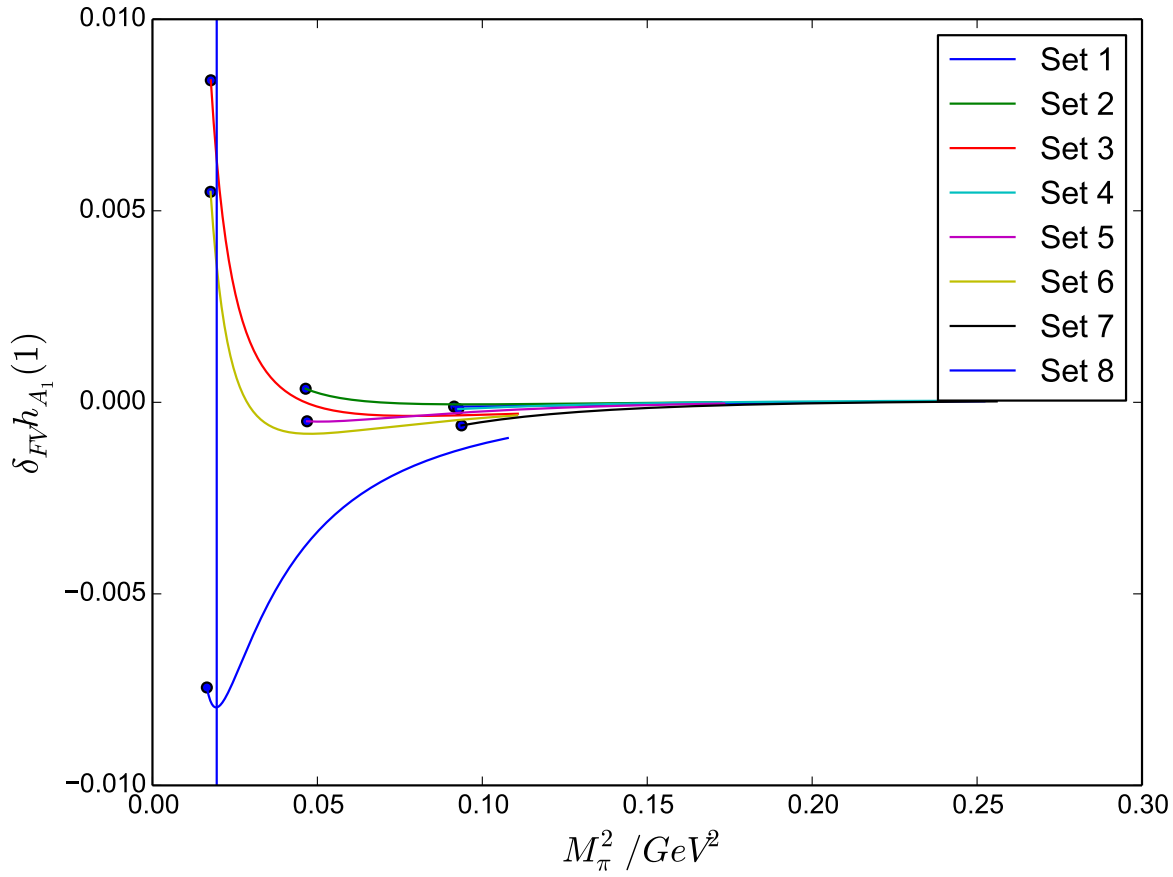

Figure 4.4: M_π^2 dependence of the finite volume corrections to the staggered chiral perturbation theory result with taste splitting effects. The vertical blue line is the physical pion mass and the solid point at the end of each curve is at the measured value of the pion mass on each lattice.

half a percent. Discretization and quark mass tuning errors are included in δ_a^B, to be described further below.

The second and third terms in (4.27) give the leading dependence on the light quark mass, parametrized by M_π^2 divided by the chiral scale Λ_χ, which I set to be 1 GeV. The coefficient of the chiral logs depends on the $D^*D\pi$ coupling g, which I take as 0.53(8) following [4], and on the pion decay constant in the chiral limit $f = 130$ MeV. The $D^* - D$ mass splitting, Δ_{m_c}, appearing in the chiral logs is taken as 142 MeV. The

uncertainties from f and Δ_{m_c} are negligible compared to the error on g and are not included. I will return to discuss δ_a^g shortly.

The fourth term in (4.27) is present in the fit since the current matching has truncation errors of $O(\alpha_s^2)$. The truncated term would have some mild dependence on am_b, which is reflected in the ansatz for this term.

The δ_a^B and δ_a^g in (4.27) parametrize how discretization and quark mass tuning errors could enter the fit form. These originate from the gauge action, the NRQCD action and the HISQ action. In all three actions discretization errors appear as even powers of a, hence I include multiplicative factors

$$\delta_a^X = \left(b_0^X + b_1^X(a\Lambda_{QCD})^2 + b_2^X(a\Lambda_{QCD})^4 + b_3^X(a\Lambda_{QCD})^6\right). \tag{4.28}$$

Each factor b_i^X, with $X = B, g$, contains a distinct sea quark tuning error dependence

$$b_i^X = \kappa_i^X \delta_b^{Xi} \delta_c^{Xi} \delta_{\text{sea}}^{Xi} \tag{4.29}$$

where the κ_i are given a Gaussian prior 0(0.5). Note that I do not include a κ_0^X term for the $\mathcal{O}(a^0)$ piece as such a term would not represent a mistuning error or discretization effect. The product on the right-hand side allows for effects of small mistunings in the sea quark masses and the valence charm and bottom quark masses. For the sea u/d and s quarks I include a multiplicative factor

$$\delta_{sea}^{Xi} = 1 + c_1^{Xi}(\delta x_{\text{sea}}/m_{\text{sea}}^{\text{phys}}) + c_2^{Xi}(\delta x_{\text{sea}}/m_{\text{sea}}^{\text{phys}})^2 \tag{4.30}$$

where $m_{\text{sea}} = 2m_l + m_s$ and $\delta x_{\text{sea}} = m_{\text{sea}} - m_{\text{sea}}^{\text{phys}}$. The physical masses are taken from [72] and are computed using the η_s mass. I take $m_l^{\text{phys}}/m_s^{\text{phys}} = 27.4$ [42]. I also include the multiplicative factor

$$\delta_c^{Xi} = 1 + d_1^{Xi}(\delta m_c/m_c^{\text{phys}}) + d_2^{Xi}(\delta m_c/m_c^{\text{phys}})^2 \tag{4.31}$$

where $\delta m_c = m_c - m_c^{\text{phys}}$, with physical mass taken from [7], and the factor

$$\delta_b^{Xi} = 1 + f_1^{Xi}(\delta m_b/m_b^{\text{phys}}) + f_2^{Xi}(\delta m_b/m_b^{\text{phys}})^2 \tag{4.32}$$

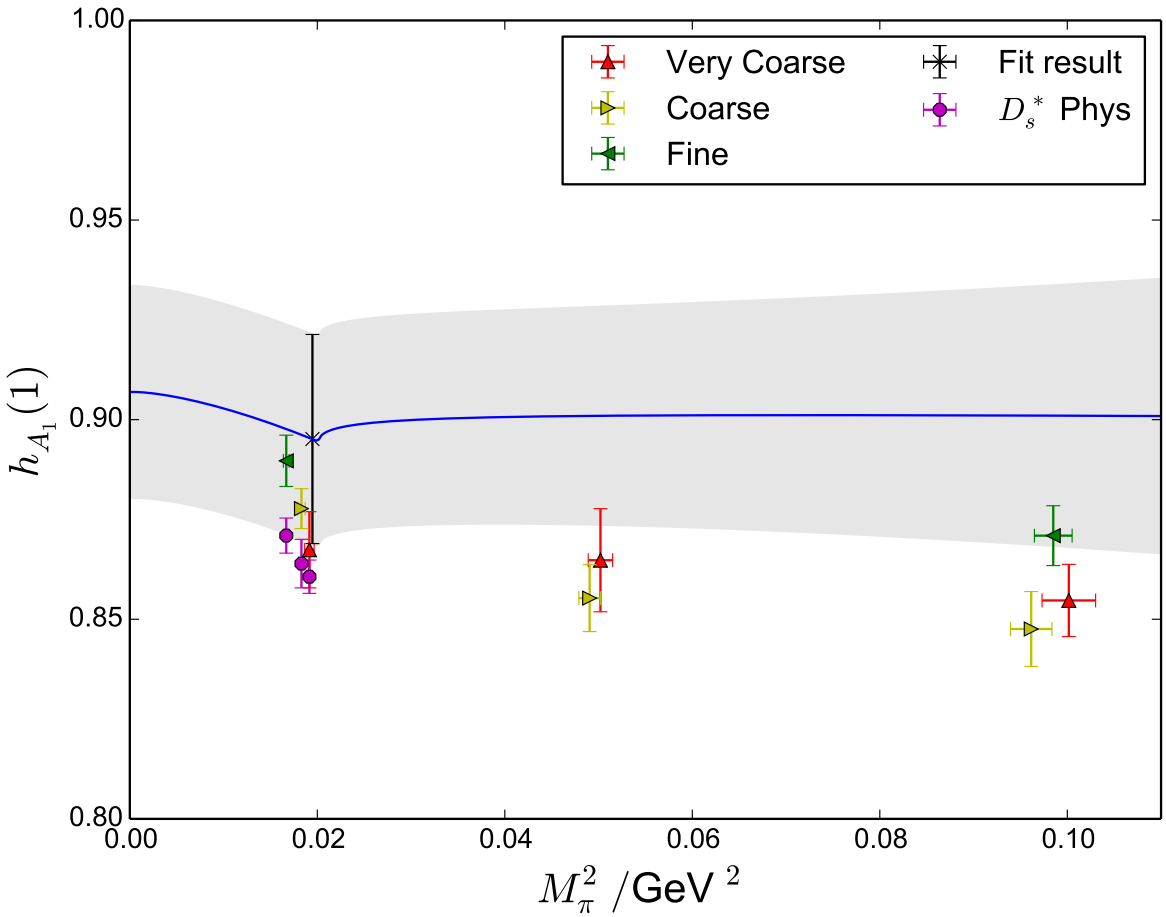

Figure 4.5: Fit to my data using staggered chiral perturbation theory. The blue line and grey band are the continuum chiral perturbation theory result and error extrapolated from my lattice data. The error band includes systematic errors coming from matching uncertainties and hence has a much larger error than any of the data points, which are only shown with their statistical error. The points labelled D_s^* Phys are the values of $h^s_{A_1}(1)$ computed for $B_s \to D_s^*$ on the physical point lattices.

with $\delta m_b = m_b - m_b^{\text{phys}}$ where m_b^{phys} is determined from the spin-averaged kinetic mass of the Υ and η_b[5]. c_i, d_i, and f_i are given prior values of 0(0.5). I neglect the effects of the very small mistuning of the light quark masses from their physical value, which we expect to be small.

The calculation on each ensemble of the form factor for $B_s \to D_s^*$ decay is equivalent to

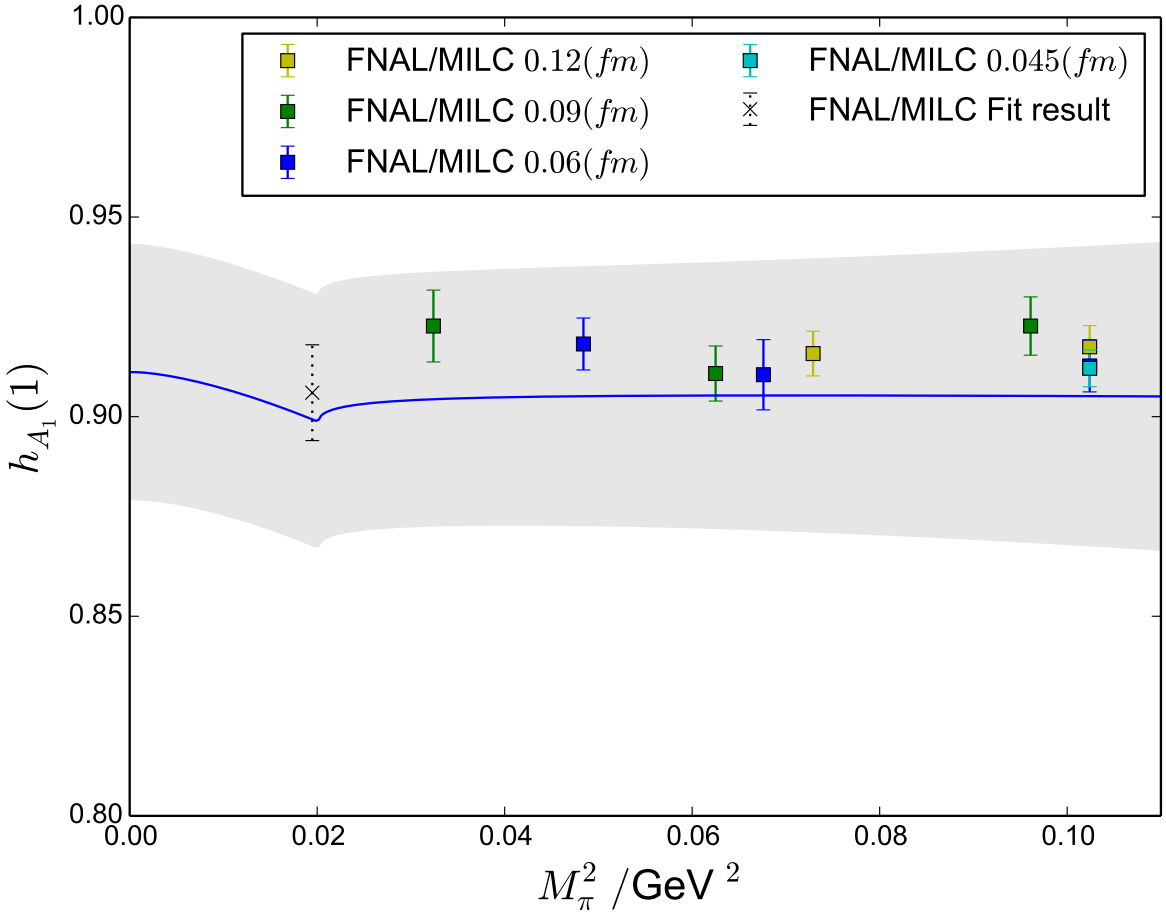

Figure 4.6: Comparison showing data points from the Fermilab Lattice and MILC collaborations [4] against our chiral continuum fit.

the $B \to D^*$ calculation, with the light quark propagator replaced with a strange quark propagator. The analysis is substantially more straightforward, both because the data is less noisy and because no chiral extrapolation is required. Before fitting the lattice data, I include a term to account for the absence of $O(\Lambda_{QCD}^2/m_b^2)$ and $O(\alpha_s\Lambda_{QCD}/m_b)$ effects, as in (4.20), using the same Gaussian variables e_4, e_5, e_6, e_7, e_8, and e_9.

For the continuum-chiral fit to the $h^s_{A_1}(1)$ I take the functional form to be the following,

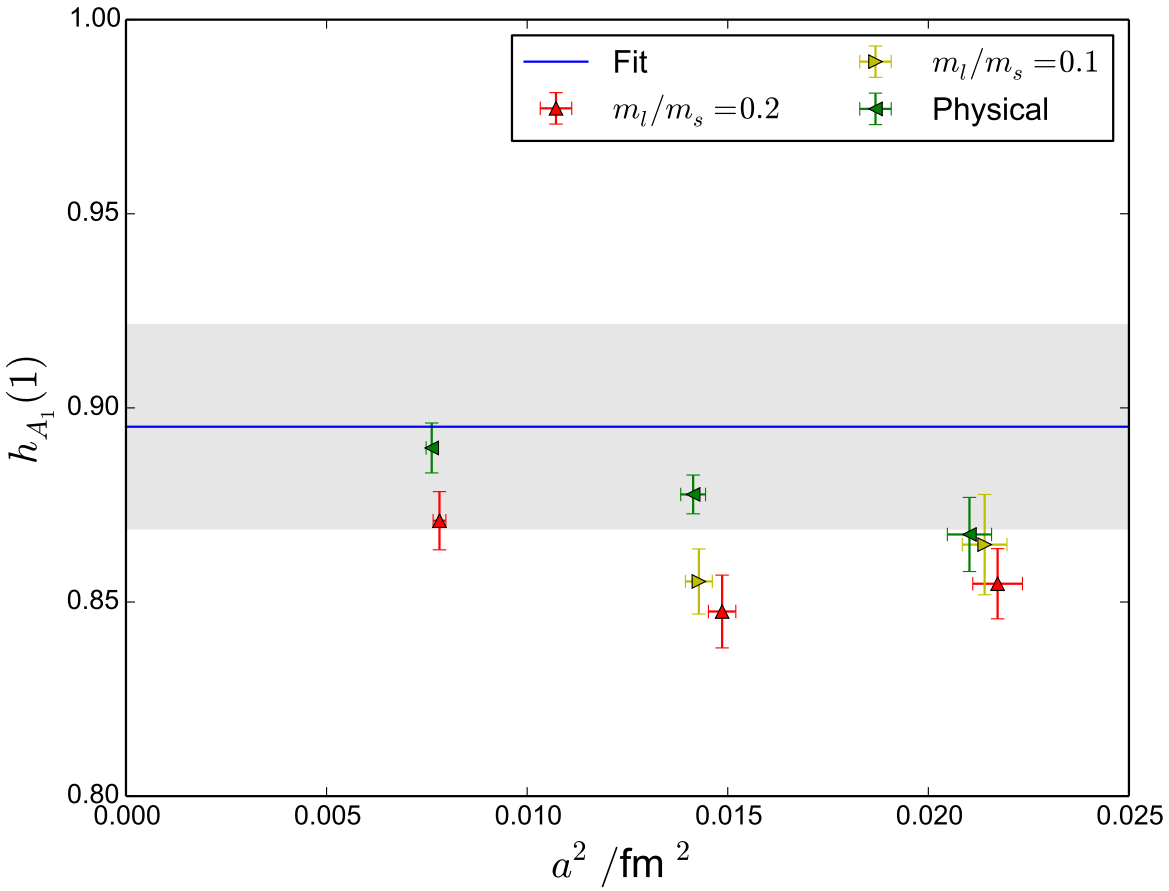

Figure 4.7: Plot showing the a^2 dependence of data extracted from the fit. The blue line with grey error band shows the physical result for the form factor determined by the fit described in the text.

where $\delta_a^{sB} B^s$ has the same form and priors as the term included for the $B \to D^*$:

$$h^s_{A_1}(1)\big|_{\text{fit}} = (1 + B^s)\delta_a^{sB} + \gamma_1 \alpha_s^2 \Big[1 + \frac{\gamma_5}{2}(am_b - 2) + \frac{\gamma_6}{4}(am_b - 2)^2\Big] V^{(0)} \tag{4.33}$$

where γ_1, γ_5 and γ_6 are the same as in (4.27) because these terms represent the same higher order matching corrections. I run the $B_s \to D_s^*$ fit simultaneously with the $B \to D^*$ fit.

The NRQCD and HISQ systematics are the same as before, and we expect negligible isospin breaking and finite volume effects. In Figure 4.5 I show the M_π^2 dependence of

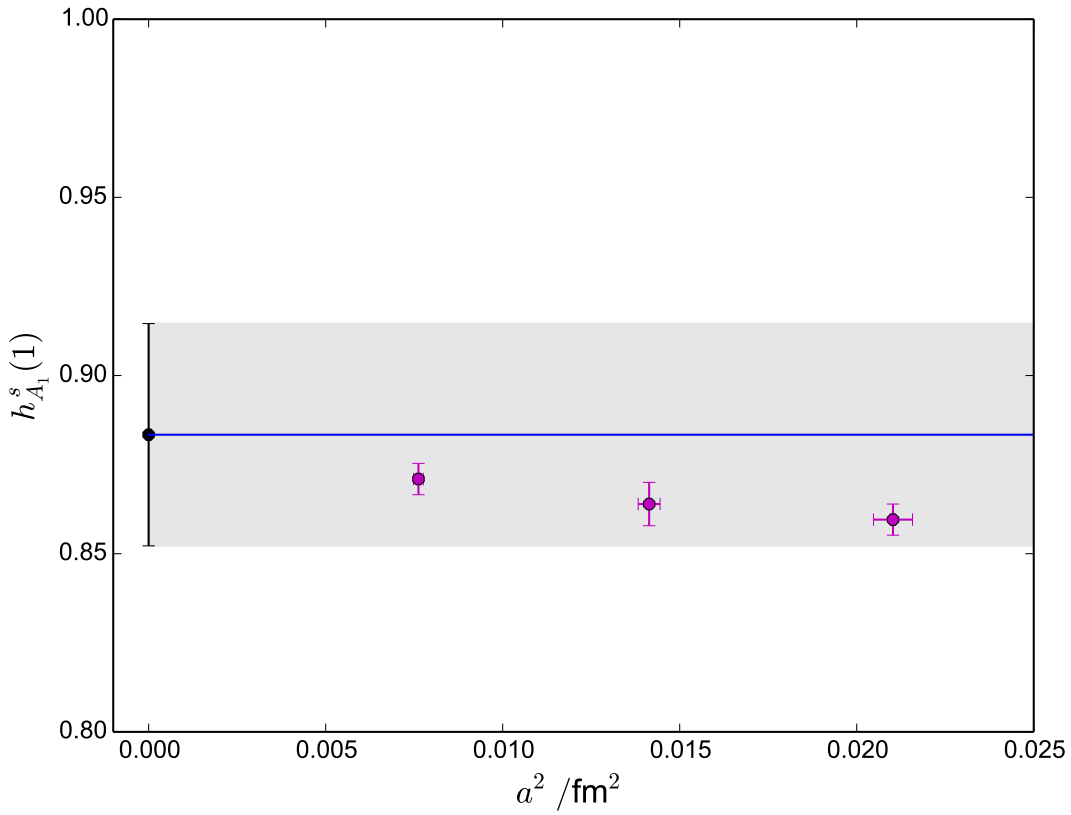

Figure 4.8: Lattice spacing dependence of my results for the $B_s \to D_s^*$ zero recoil form factor. The blue line with grey error band shows the physical result for the form factor determined by the fit described in the text.

my $B \to D^*$ data and the extrapolated continuum chiral form.

I present results for the $h_{A_1}(1)$ and $h^s_{A_1}(1)$ fit parameters B, γ_i, κ_i, c_i, d_i, f_i in table 4.10. Plots showing the a^2 dependence of my $B \to D^*$ and $B_s \to D_s^*$ data are shown in Figures 4.7 and 4.8 respectively, together with the result of my fit. The $\mathcal{O}(a^4)$ and $\mathcal{O}(a^6)$ parameters default to their prior values, while the $\mathcal{O}(a^2)$ parameters are consistent with zero. Table 4.11 presents a summary and combination of the uncertainties in the results for $h_{A_1}(1)$ and $h^s_{A_1}(1)$.

In table 4.12 I give fit results for plausible variations on the chosen fit function as a demonstration of stability under such nontrivial choices. Neglecting different powers of

Table 4.10: Results for parameters in the chiral-continuum fits, Eq. (4.27) and (4.33). Terms not listed retain their prior values and are not shown while $\kappa_1^B = -0.17(25)$ and $\kappa_1^B = -0.05(42)$ for $h_{A_1}(1)$ and $h^s_{A_1}(1)$ respectively.

	c_1^{B0}	c_2^{B0}	d_1^{B0}	d_2^{B0}	f_1^{B0}	f_2^{B0}
$h_{A_1}(1)$	−0.15(12)	0.27(29)	0.24(40)	0.0(5)	0.24(40)	0.0(5)
$h^s_{A_1}(1)$	−0.03(22)	0.05(35)	0.0(5)	0.0(5)	0.0(5)	0.0(5)
	B	C	g	γ_1	γ_5	γ_6
$h_{A_1}(1)$	−0.091(27)	−0.02(24)	0.521(78)	−0.14(44)	0(1)	-0.15(97)
$h^s_{A_1}(1)$	−0.117(31)	–	–	−0.14(44)	0(1)	-0.15(97)

Table 4.11: Partial errors (in percentages) for $h^{(s)}_{A_1}(1)$. A full accounting of the breakdown of systematic errors is made difficult by the fact that smaller priors not well constrained by the data are mixed in a correlated way by the fitter; these are reflected in the total systematic uncertainty. Note that the uncertainty from missing α_s^2 terms in the matching for $h_{A_1}(1)$ and $h^s_{A_1}(1)$ is constrained somewhat by the fit; a naive estimate would give 3.5% on the fine lattices.

Uncertainty	$h_{A_1}(1)$	$h^s_{A_1}(1)$	$h_{A_1}(1)/h^s_{A_1}(1)$
α_s^2	2.1	2.5	0.4
$\alpha_s\Lambda_{QCD}/m_b$	0.9	0.9	0.0
$(\Lambda_{QCD}/m_b)^2$	0.8	0.8	0.0
a^2	0.7	1.4	1.4
$g_{D^*D\pi}$	0.2	0.03	0.2
Total systematic	2.7	3.2	1.7
Data	1.1	1.4	1.4
Total	2.9	3.5	2.2

Table 4.12: Fit results for $h_{A_1}(1)$ for different chiral-continuum fit functions.

Fit function	$h_{A_1}(1)$	$h^s_{A_1}(1)$
Eq. (4.26)	0.895(26)	0.883(31)
excluding hairpin terms	0.895(26)	0.883(31)
continuum χPT formula	0.897(25)	0.882(31)
$\Lambda_{QCD} = 750$ MeV	0.900(35)	0.882(38)
$\Lambda_{QCD} = 250$ MeV	0.897(24)	0.890(23)
excluding polynomial $\mathcal{O}(a^6)$ terms	0.895(26)	0.883(31)
excluding polynomial $\mathcal{O}(a^4)$ terms	0.895(26)	0.883(31)
excluding polynomial $\mathcal{O}(a^2)$ terms	0.898(26)	0.891(25)
excluding polynomial M_π^2 dependence	0.895(27)	0.883(31)
excluding $(\Lambda/m_b)^2$ uncertainty	0.895(25)	0.883(31)
totally correlated $(\Lambda_{QCD}/m_b)^2$ errors	0.895(27)	0.883(31)

a^2 we see that the result is only sensitive to leading $\mathcal{O}(a^2)$ errors. The M_π^2 dependence I included does not affect the central value if removed, nor do changes in the assumed correlations between NRQCD systematics between ensembles. Removing taste splitting terms in the chiral perturbation theory result down to the continuum formula results in only a small change to the central value. Adding $\alpha_s\Lambda_{QCD}/m_b$, which I have excluded from my fit due to Luke's theorem, results in a slight increase in the central value as well as the expected increase in error. The result is also only mildly sensitive to different choices of Λ_{QCD} which I vary by $\pm 50\%$. Note that taken collectively no tested variations result in more than a 0.25σ change to the central value.

4.5.6 Isospin breaking effects

The effects of electromagnetic interactions and $m_u \neq m_d$ on $h_{A_1}(1)$ are negligible compared to the dominant uncertainties quoted in table 4.11. I find only a variation of

0.25% in the chiral-continuum fits to $h_{A_1}(1)$ whether the π^0 or π^+ mass is used as the input value for the physical limit. Electroweak and Coulomb effects in the decay rate (4.1) are presently accounted for at leading order by a single multiplicative factor $\bar{\eta}_{EW}$. As lattice QCD uncertainties are reduced in the future, it will be desirable to more directly calculate the effects of electromagnetism in a lattice QCD+QED calculation, where $m_u \neq m_d$ can also be implemented.

4.6 Results and Discussion

I have calculated the zero recoil form factor for $B \to D^* \ell \nu$ decay using the most physically realistic gluon field configurations currently available along with quark discretizations that are highly improved. The final result for the form factor, including all sources of uncertainty, is

$$\mathcal{F}^{B\to D^*}(1) = h_{A_1}(1) = 0.895(10)_{\text{stat}}(24)_{\text{sys}} \,. \tag{4.34}$$

It is clear from this treatment that the dominant source of uncertainty is the $\mathcal{O}(\alpha_s^2)$ uncertainty coming from the perturbative matching calculation. In principle this could be reduced by a two-loop matching calculation; however, such calculations in lattice NRQCD have not been done before. It is worth noting that for this calculation the uncertainty is somewhat constrained by the fit, as is reflected in table 4.11. It has also been suggested [44] that it could be estimated using heavy-HISQ b quarks on 'ultrafine' lattices with $a = 0.045$ fm and $m_b a < 1$. There we can use the nonperturbative PCAC relation and the absolute normalization of the pseudoscalar current to normalise $J^{(0)}$, using $(m_b + m_c)\hat{P} = Z\partial_\mu \hat{A}^\mu$ to find the matching coefficient Z and then comparing matrix elements of this normalized current to the result using perturbation theory.

Within errors, the result presented here agrees with the result from the Fermilab Lattice and MILC Collaborations [4], $h_{A_1}(1) = 0.906(4)(12)$. The higher precision achieved in this work is due to the use of the same lattice discretization for the b and c quarks. This enabled them to avoid the larger current-matching uncertainties present in this NRQCD-b, HISQ-c work. Nevertheless, the value of providing a completely independent lattice QCD result using different formalisms is self-evident.

After combining the statistical and systematic errors in quadrature, a weighted average of the two lattice results yields $h_{A_1}(1) = 0.900(11)$.

My result for the $B_s \to D_s^*$ zero-recoil form factor is

$$\mathcal{F}^{B_s\to D_s^*}(1) = h^s_{A_1}(1) = 0.883(12)_{\text{stat}}(28)_{\text{sys}} \,. \tag{4.35}$$

This is the first lattice QCD calculation of this quantity. No significant difference between the result for $B \to D^*$ and $B_s \to D_s^*$ is seen, showing that spectator quark mass effects are very small. Correlated systematic uncertainties cancel in the ratio, which I find to be

$$\frac{\mathcal{F}^{B\to D^*}(1)}{\mathcal{F}^{B_s\to D_s^*}(1)} = \frac{h_{A_1}(1)}{h^s_{A_1}(1)} = 1.013(14)_{\text{stat}}(17)_{\text{sys}}\,. \tag{4.36}$$

No significant U-spin ($d \leftrightarrow s$) breaking effect is found at the few percent level.

4.7 Implications for V_{cb}

Until recently, one would simply combine a world average of lattice data for $h_{A_1}(1)$ with the latest HFLAV result for the $\bar{B}^0 \to D^{*+}\ell^-\nu$ differential branching fraction extrapolated to zero recoil: $\bar{\eta}_{EW}\mathcal{F}(1)|V_{cb}| = 35.61(11)(44) \times 10^{-3}$ [47]. Doing so with the weighted average of the Fermilab/MILC result and the one presented here yields

$$|V_{cb}|_{HFLAV} = (38.9 \pm 0.7) \times 10^{-3}, \tag{4.37}$$

where the estimated charge-averaged value of $\bar{\eta}_{EW} = 1.015(5)$ [4] has been used. The uncertainty in $|V_{cb}|_{HFLAV}$ is due in equal parts to lattice and experimental error. This method of determining V_{cb} relies upon the extrapolation of experimental data to zero recoil which in turn depends in a non-trivial way upon the choice or parameterisation, and in fact recent work [73, 74, 75, 76, 77, 78] has brought into question the accuracy of the CLN [79] method of extrapolation and suggests that the tension between inclusive and exclusive measurement may be resolved by using a different parameterisation scheme, one proposed by Boyd, Grinstein, and Lebed (BGL) [80].

4.8 Non-zero recoil

One can also, in principle, compute V_{cb} in a model independent way by computing form factors away from zero recoil. Such a calculation is complicated considerably by the number of matrix elements one must compute in order to access all the relevant form factors, as well as the added complication that one must fit multiple q^2 values simultaneously in order to account for the large correlations in the data.

4.8.1 Form factor isolation

The relevant form factors are those given in (4.2), which I present again here for convenience,

$$\begin{aligned}
\langle D^*(p',\epsilon)|\bar{c}\gamma^\mu b|B(p)\rangle &= \frac{2iV(q^2)}{M_B+M_{D^*}}\,\epsilon^{\mu\nu\rho\sigma}\epsilon^*_\nu p'_\rho p_\sigma \\
\langle D^*(p',\epsilon)|\bar{c}\gamma^\mu\gamma^5 b|B(p)\rangle &= 2M_{D^*}A_0(q^2)\frac{\epsilon^*\cdot q}{q^2}q^\mu \\
&+ (M_B+M_{D^*})A_1(q^2)\Big[\epsilon^{*\mu}-\frac{\epsilon^*\cdot q}{q^2}q^\mu\Big] \\
&- A_2(q^2)\frac{\epsilon^*\cdot q}{M_B+M_{D^*}}\Big[p^\mu+p'^\mu-\frac{M_B^2-M_{D^*}^2}{q^2}q^\mu\Big]
\end{aligned} \tag{4.38}$$

where $q = p - p'$. I will also need the identities

$$\langle\Omega|\bar{u}\gamma^\nu c|D^*(p,\epsilon(p,\lambda))\rangle = \frac{\sqrt{Z_{D^*}}}{2M_{D^*}}\epsilon^\nu(p,\lambda) \tag{4.39}$$

and

$$\sum_\lambda \epsilon_\nu(p,\lambda)\epsilon^*_\mu(p,\lambda) = g_{\nu\mu} - \frac{p_\nu p_\mu}{M^2}. \tag{4.40}$$

The computational aspects of the calculation proceed in much the same way as for zero recoil, the only significant choices are how I distribute the momenta between the two mesons. For the sake of simplicity I choose to put the momenta on the D^*, this allows us to use twisted boundary conditions (TBC) on the inversion of the charm propagator and to easily insert momenta in a continuous fashion, rather than being restricted to multiples of $2\pi/L$. I will discuss TBC shortly. For the vector current it is easy to choose momenta and polarisations to extract $V(q^2)$. The ground state amplitudes and matrix element appearing in the three point function have the form

$$\begin{aligned}
&\langle\Omega|\bar{u}\gamma^\nu c|D^*(p',\epsilon(p',\lambda))\rangle\langle D^*(p',\epsilon)|\bar{c}\gamma^\mu b|B(p)\rangle\langle B(p)|\bar{b}\gamma^5 u|\Omega\rangle \\
&\quad= \sum_\lambda \frac{\sqrt{Z_B}}{2E_B}\frac{\sqrt{Z_{D^*}}}{2E_{D^*}}\epsilon^\nu(p',\lambda)\frac{2iV(q^2)}{M_B+M_{D^*}}\epsilon^{\mu\kappa\rho\sigma}\epsilon(p',\lambda)^*_\kappa p'_\rho p_\sigma
\end{aligned} \tag{4.41}$$

I have chosen to put the B meson at rest, so only $\sigma = 0$ contributes. Using 4.40, 4.41 becomes

$$\begin{aligned}\langle\Omega|\bar{u}\gamma^\nu c|D^*(p',\epsilon(p',\lambda))\rangle\langle D^*(p',\epsilon)|\bar{c}\gamma^\mu b|B(p)\rangle\langle B(p)|\bar{b}\gamma^5 u|\Omega\rangle \\ = \frac{\sqrt{Z_B}}{2M_B}\frac{\sqrt{Z_{D^*}}}{2E_{D^*}}\frac{2iV(q^2)}{M_B+M_{D^*}}\epsilon^{\mu\kappa\rho\sigma}(\delta^\nu_\kappa - p'^\nu p'_\kappa/M^2_{D^*})p'_\rho p_\sigma. \qquad (4.42)\end{aligned}$$

The antisymmetric sum over $p'_\kappa p'_\rho$ vanishes, leaving

$$\begin{aligned}\langle\Omega|\bar{u}\gamma^\nu c|D^*(p,\epsilon(p,\lambda))\rangle\langle D^*(p',\epsilon)|\bar{c}\gamma^\mu b|B(p)\rangle\langle B(p)|\bar{b}\gamma^5 u|\Omega\rangle \\ = \frac{\sqrt{Z_B}}{2M_B}\frac{\sqrt{Z_{D^*}}}{2E_{D^*}}\frac{2iV(q^2)}{M_B+M_{D^*}}\epsilon^{\mu\nu\rho 0}p'_\rho p_0 \qquad (4.43)\end{aligned}$$

thus all that is needed is to choose μ and ν to be two distinct spatial directions such that $p'_i \neq 0$ for $i \neq \mu \neq \nu$ and the form factor can be read off from the matrix element in the fit by dividing out the factor of $2iM_B p'_i/(M_B + M_{D^*})$, assuming the matrix element already includes the normalisation factors $\sqrt{2M_B}$ and $\sqrt{2E_{D^*}}$.

The other form factors may be accessed through more elaborate combinations. In my calculation I split the momenta equally between the x and y directions, and take the D^* operator with $\nu = 1, 3$. The first observation that can be made is that taking the inner product of the pseudovector expression in (4.2) with q eliminates all but the first term. We are then left with

$$\begin{aligned}q_\mu\langle\Omega|\bar{u}\gamma^\nu c|D^*(p,\epsilon(p,\lambda))\rangle\langle D^*(p',\epsilon)|\bar{c}\gamma^\mu\gamma^5 b|B(p)\rangle\langle B(p)|\bar{b}\gamma^5 u|\Omega\rangle \\ = \sum_\lambda \frac{\sqrt{Z_B}}{2M_B}\frac{\sqrt{Z_{D^*}}}{2E_{D^*}}\epsilon^\nu(p',\lambda)2M_{D^*}A_0(q^2)\epsilon(p',\lambda)^\kappa q_\kappa \\ = \frac{\sqrt{Z_B}}{2M_B}\frac{\sqrt{Z_{D^*}}}{2E_{D^*}}2M_{D^*}A_0(q^2)(g^{\nu\kappa} - p'^\nu p'^\kappa/M^2_{D^*})q_\kappa. \qquad (4.44)\end{aligned}$$

Then choosing spatial ν such that $p'^\nu \neq 0$ the expression $(g^{\nu\kappa} - p'^\nu p'^\kappa/M^2_{D^*})q_\kappa$ evaluates to $-p'^\nu E_{D^*}M_B/M^2_{D^*}$ and again the form factor can be read off by dividing the product of q and the matrix element by the factor

$$-2p'^\nu E_{D^*}M_B/M_{D^*}. \qquad (4.45)$$

Before I continue it should be noted that a complication has arisen. Ideally one would fit to the combinations of various three point functions defined here such that by fitting a single three point function each form factor could be read off. However this is not possible in this case as prior to the fit q_0 is unknown, since the D^* energy has not yet been measured. In order to minimise the amount of data I attempt to fit I define three reduced currents, from which the form factors can be recovered after fitting. The first two, which are relevant here, are

$$\begin{aligned} M^A_{X,0} &= \langle\Omega|\bar{u}\gamma^1 c|D^*(p,\epsilon(p,\lambda))\rangle\langle D^*(p',\epsilon)|\bar{c}\gamma^0\gamma^5 b|B(p)\rangle\langle B(p)|\bar{b}\gamma^5 u|\Omega\rangle \\ M^A_{X,\vec{q}} &= \vec{q}_j\langle\Omega|\bar{u}\gamma^1 c|D^*(p,\epsilon(p,\lambda))\rangle\langle D^*(p',\epsilon)|\bar{c}\gamma^j\gamma^5 b|B(p)\rangle\langle B(p)|\bar{b}\gamma^5 u|\Omega\rangle \end{aligned} \tag{4.46}$$

and the final definition, which will be useful later, is

$$M^A_{Z,3} = \langle\Omega|\bar{u}\gamma^3 c|D^*(p,\epsilon(p,\lambda))\rangle\langle D^*(p',\epsilon)|\bar{c}\gamma^3\gamma^5 b|B(p)\rangle\langle B(p)|\bar{b}\gamma^5 u|\Omega\rangle. \tag{4.47}$$

Once I have done the fit I may take the ground state matrix elements for $M^A_{X,0}$ and $M^A_{X,\vec{q}}$ and combine them to find $A_0(q^2)$

$$-\frac{M_{D^*}}{2p'^1 E_{D^*} M_B}\left[(M_B - E_{D^*})M^A_{X,0} + M^A_{X,\vec{q}}\right] \tag{4.48}$$

again assuming the normalisation factors are already incorporated. Accessing A_1 is far more straightforward. Choosing μ in (4.2) such that $p'^\mu = p^\mu = 0$, ie $\mu = 3$ in this case,

$$\begin{aligned} &\langle\Omega|\bar{u}\gamma^\nu c|D^*(p,\epsilon(p,\lambda))\rangle\langle D^*(p',\epsilon)|\bar{c}\gamma^\mu\gamma^5 b|B(p)\rangle\langle B(p)|\bar{b}\gamma^5 u|\Omega\rangle \\ &\quad = \sum_\lambda \frac{\sqrt{Z_B}}{2M_B}\frac{\sqrt{Z_{D^*}}}{2M_{D^*}}\epsilon^\nu(p',\lambda)(M_B + M_{D^*})A_1(q^2)\epsilon^{*3}(p',\lambda). \end{aligned} \tag{4.49}$$

Taking $\nu = 3$ the matrix element coming from this three point function simply reduces to $-(M_B + M_{D^*})A_1(q^2)$. Therefore to extract $A_1(q^2)$ from the ground state matrix element of $M^A_{Z,3}$ I simply take $-M^A_{Z,3}/(M_B + M_{D^*})$. The final form factor, A_2, is considerably messier to access directly. Instead, following [14] I compute the combination

$$A_{12}(q^2) = \frac{(M_B + M_{D^*})^2(M_B^2 + M_{D^*}^2 - q^2)A_1(q^2) - \lambda A_2(q^2)}{16 M_B M_{D^*}^2(M_B + M_{D^*})} \tag{4.50}$$

where $\lambda = \big((M_B + M_{D^*})^2 - q^2\big)\big((M_B - M_{D^*})^2 - q^2\big)$. In order to project this I take $\zeta = (|\vec{q}|, q^0\vec{q}/|\vec{q}|)$, for which $\zeta_\mu q^\mu = 0$, and compute

$$\begin{aligned}
&\zeta_\mu \langle \Omega | \bar{u}\gamma^\nu c | D^*(p, \epsilon(p,\lambda))\rangle \langle D^*(p',\epsilon)|\bar{c}\gamma^\mu\gamma^5 b|B(p)\rangle\langle B(p)|\bar{b}\gamma^5 u|\Omega\rangle \\
&\quad = \sum_\lambda \frac{\sqrt{Z_B}}{2M_B}\frac{\sqrt{Z_{D^*}}}{2M_{D^*}}\Big[\zeta_\mu \epsilon^\nu(p',\lambda)\epsilon^{*\mu}(p',\lambda)(M_B + M_{D^*})A_1(q^2)) \\
&\qquad\qquad - \frac{2A_2(q^2)\epsilon^\nu(p',\lambda)\epsilon^{*\kappa}(p',\lambda)q_\kappa \zeta_\mu p^\mu}{M_B + M_{D^*}}\Big] \\
&= \frac{\sqrt{Z_B}}{2M_B}\frac{\sqrt{Z_{D^*}}}{2M_{D^*}}\frac{8M_B q^v E_{D^*}}{2|q|}\Big[\frac{(M_B + M_{D^*})^2(M_B^2 - M_{D^*}^2 - q^2)}{16M_B M_{D^*}^2(M_B + M_{D^*})}A_1(q^2) \\
&\qquad\qquad - \frac{\lambda}{16M_B M_{D^*}^2(M_B + M_{D^*})}A_2\Big]
\end{aligned} \tag{4.51}$$

where in the last two lines I have used the choice of $\nu = 1$. I therefore compute

$$A_{12}(q^2) = \frac{|q|}{8M_B q^1 E_{D^*}}\left(|q|M^A_{X,0} + \frac{q^0}{|q|}M^A_{X,\vec{q}}\right). \tag{4.52}$$

4.8.2 Twisted boundary conditions

In order to put momentum on the charm propagator I use twisted boundary conditions [81]. If instead of taking period boundary conditions we impose the boundary conditions

$$\psi'(x + L\hat{\mu}) = e^{i2\pi\theta_\mu}\psi'(x) \tag{4.53}$$

which in fourier space gives the condition $(p_\mu - 2\pi\theta_\mu/L)L = 1$. Momentum is thus discretised and takes values

$$p_\mu = 2\pi(N_\mu + \theta_\mu)/L. \tag{4.54}$$

In order to implement this we rewrite the field with twisted boundary conditions in terms of a unitary transformation of fields with periodic boundary conditions

$$\psi'(x) \to e^{i2\pi\theta\cdot x}\psi(x). \tag{4.55}$$

This transformation takes

$$\bar{\psi}'(x)D(x,y)\psi'(y) \to \bar{\psi}(x)e^{-i2\pi\theta\cdot x}D(x,y)e^{i2\pi\theta\cdot y}\psi(y) = \bar{\psi}(x)D_\theta(x,y)\psi(y) \tag{4.56}$$

which does not affect the value of the fermionic determinant and can therefore be used with sea quarks with periodic boundary conditions. All we need to do is compute propagators using the inverse of D_θ rather than D. For my preliminary investigation I choose values of q^2 in the full range. The maximum value of q^2 is given by the mass of the product leptons $q^2_{\rm min} = (m_{\nu_l} + m_l)^2$ while the maximum value of q^2 is given at zero recoil when the D^* is at rest $q^2_{\rm max} = (M_B - M_{D^*})^2$.

The maximum value of $|\vec{q}|$ can be computed easily by considering on shell energies and momentum conservation. The result is

$$\max[|\vec{q}|] = \Big[\left(\frac{M_B^2 + M_{D^*}^2 - (m_{\nu_l} + m_l)^2}{2M_B} \right)^2 - M_{D^*}^2 \Big]^{-\frac{1}{2}} = 2.26\text{GeV} \tag{4.57}$$

where the numerical value is taken neglecting the lepton masses. Initially I take five values of q^2 including the zero recoil point, in order to investigate what range of possible q^2 values might be probed effectively.

4.8.3 Fitting nonzero recoil data

An important aspect of fits to nonzero recoil data is the retention of correlations between different q^2 values and different currents - if correlations are neglected then any further processing of the fit results will contain artificially large errors. However a full simultaneous fit to the data is made difficult by the large numbers of parameters and the tendency of the fitting code to stall in such circumstances. As such I employ whatever tricks I can to simplify the fit. I use the fact that the two point functions have real amplitudes to average between transpose elements in the matrix of correlators indexed by source and sink smearings. I also manually exclude highly correlated data points.

For this calculation I use only set 1, specified in table 4.1, with 960 configurations using only a single time source on each. Since I insert spatial momentum aiming for specific values of q^2 without prior knowledge of the B or D^* energies on the lattice, I expect to miss the intended q^2 by a small amount for large recoil. In fact, on the very coarse lattice care must be taken as the lowest value of q^2 corresponds to $|q|a = 1.66 > \pi/2$

Table 4.13: Tree-level Z factors and one-loop matching coefficients [9].

Set	Z	$-\eta$	τ	$\alpha_V(2/a)$
A^j	0.9930	0.260(3)	0.0165(1)	0.343
A^0	0.9930	0.232(5)	-0.01269(1)	0.343
V^j	0.9930	0.118(5)	0.0423(1)	0.343
V^0	0.9930	0.148(3)	-0.0494(1)	0.343

which has the potential to cause taste changing effects. I negate this effect by splitting the momenta equally between the x and y directions, such that even on the very coarse lattices all chosen momenta lie within the first quarter with $-\pi/2a < q^i < \pi/2a$.

When I assemble lattice currents into the fully matched currents it is worth noting that the matching coefficients differ for spatial and timelike components of the current. Matching coefficients for the vector and axial currents following the notation of 4.16 are given in table 4.13 and where the vector lattice currents are found from the axial vector lattice currents given in 4.14 by making the replacement $\gamma^i\gamma^5 \to \gamma^i$.

4.8.4 Results

Since this preliminary nonzero recoil calculation uses only a single time source on each configuration I am not concerned by the increase in error compared to the zero recoil calculation. I am primarily interested in the relative precision with which each form factor can be extracted and at what value of q^2 the error becomes too large. I also consider the size of the matrix element of $J^{(2)i}_{\text{latt}}$ which is expected to grow considerably as the momentum on the charm quark increases. Figure 4.9 shows plots of the four form factors, in lattice units, against q^2, as well as the D^* ground state energy. Based on this it might be reasonable to use a range roughly between q^2_{max} and $q^2_{\text{max}}/2$, aiming to keep errors to the same order of magnitude as the zero recoil calculation with respect to A_1.

In figure 4.10 I show the computed magnitude of the contribution of $J^{(2)i}_{\text{latt}}$ to the

Table 4.14: Results for the four form factors defined in 4.2, in lattice units.

q^2	A_0	A_1	A_{12}	V	E_{D^*}
5.572(11)	–	-0.799(39)	–	–	1.5196(24)
5.290(14)	-0.63(20)	-0.829(43)	-0.424(51)	0.18(14)	1.5560(30)
4.491(28)	-0.47(23)	-0.928(88)	-0.374(85)	0.25(17)	1.6582(63)
3.164(36)	-0.59(20)	-1.09(14)	-0.490(92)	0.07(17)	1.8390(87)
1.198(73)	-1.14(42)	-1.33(49)	-0.63(18)	0.26(47)	2.154(21)

form factors, divided by the fully matched form factor result. These results imply that the uncertainty coming from the omission of this matched current should be less than approximately 3% over the proposed range of q^2 for the A_1 and A_{12} form factors while an uncertainty of roughly 5% would be expected for A_0. The vector current on the other hand appears to be considerably more noisy.

4.8.5 Outlook

We have performed the first lattice QCD calculation of these form factors away from zero recoil. The calculation is complicated numerically by the increased number of matrix elements required to extract the various form factors. This increases both the complexity of the fit as well as the computing time spent evaluating correlation functions. In order to ease this increase in complexity a study of optimising a single choice of smearing would be valuable. The covariant gaussian smearing used in MILC introduces issues related to normalisation as well as having an undesirably large overlap with excited states and replacing the three smearings used with a single smearing chosen to produce maximum overlap with the D^* ground state with minimal excited state contamination would reduce the number of propagators and contractions required as well as simplifying the bayesian fitting. I have also investigated the momentum dependence of the uncertainty associated with $J^{(2)i}_{\text{latt}}$ and determined approximately an appropriate range of q^2 to investigate.

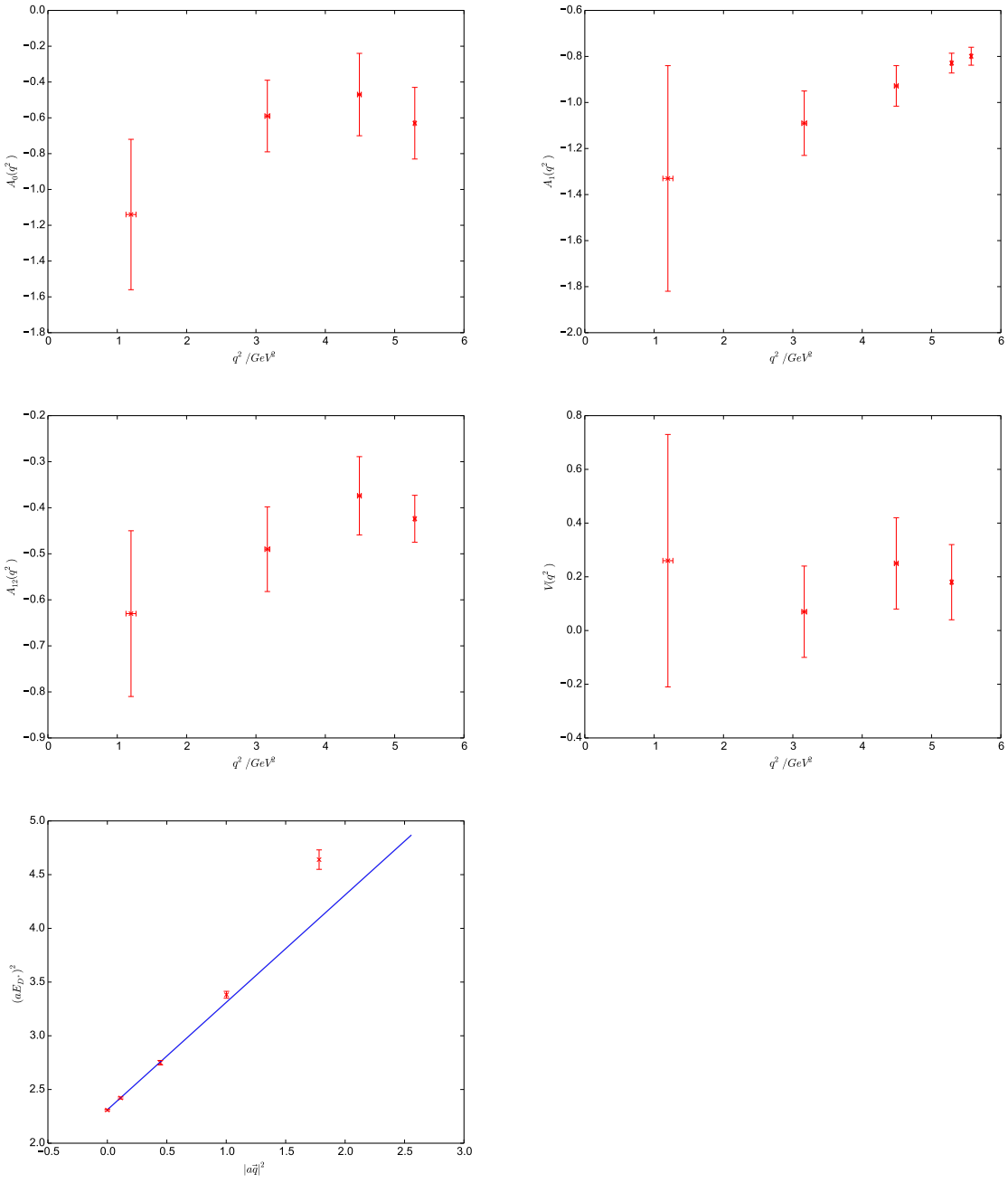

Figure 4.9: Plots of each form factor against aq^2 as well as the D^* energy squared against $|a\vec{q}|^2$. Using a simple linear fit to $aE^2_{D^*}$ it is not possible to fit all of the data, while excluding the value at maximum $|a\vec{q}|$ gives a reasonable fit with $\chi^2/\text{dof} = 1.4$, indicating that above $|aq| \approx 1$ discretisation effects become significant.

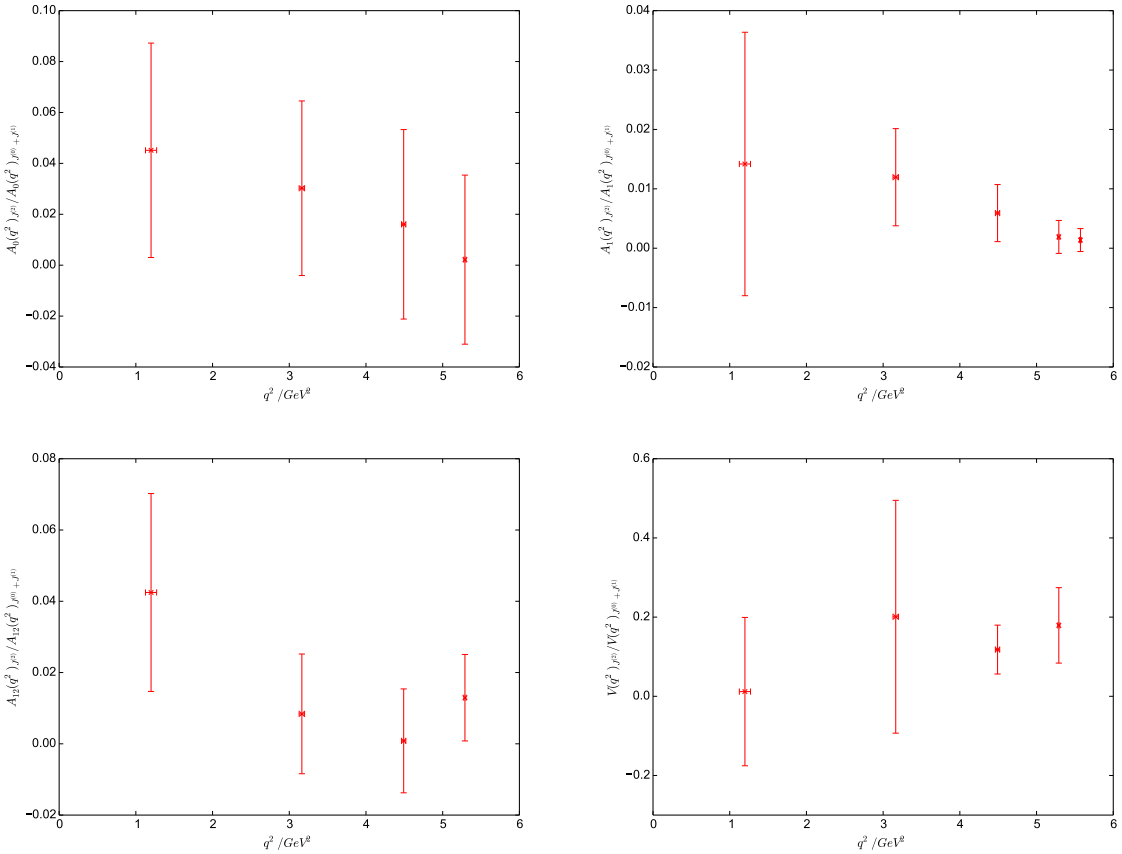

Figure 4.10: Plots of the contribution of $\alpha J^{(2)}$ to the uncertainty of each form factor, using a matching coefficient of 1, divided by the form factor computed from the known matched current against q^2.

Another theoretical hurdle is how to deal with the chiral perturbation theory and finite volume effects away from zero recoil. As I have demonstrated in the zero recoil calculation, such effects are significant. To my knowledge the calculation of the form factors away from zero recoil in rooted staggered chiral perturbation theory has not been done.

Chapter 5

Radiative Improvement and Kinetic Couplings

5.1 Matching procedure

As discussed in section 3.5.3 one must tune the parameters appearing in (3.86), which we restate here for convenience:

$$S = a^3 \sum_x \Big[\psi^\dagger(x)\psi(x) \\ -\psi^\dagger(x+a\hat{t})\Big(1-\frac{aH_0}{2n}\Big)^n\Big(1-\frac{a\delta H}{2}\Big)U_t^\dagger(x)\Big(1-\frac{a\delta H}{2}\Big)\Big(1-\frac{aH_0}{2n}\Big)^n\psi(x)\Big].$$

with

$$aH_0 = -\Delta^{(2)}/2am \tag{5.1}$$

$$a\delta H = a\delta H_{v^4} + a\delta H_{v^6} \tag{5.2}$$

$$\begin{aligned} a\delta H_{v^4} =& -c_1\frac{(\Delta^{(2)})^2}{8(am)^3} + c_2\frac{ig}{8(am)^2}\big(\Delta^{(\pm)}\cdot\tilde{E} - \tilde{E}\cdot\Delta^{(\pm)}\big) \\ & - c_3\frac{g}{8(am)^2}\sigma\cdot\big(\tilde{\Delta}^{(\pm)}\times\tilde{E} - \tilde{E}\times\tilde{\Delta}^{(\pm)}\big) \\ & - c_4\frac{g}{2am}\sigma\cdot\tilde{B} + c_5\frac{a^2\Delta^{(4)}}{24am} - c_6\frac{a(\Delta^{(2)})^2}{16n(am)^2} \end{aligned} \tag{5.3}$$

$$\begin{aligned} \delta H_{v^6} =& -f_1\frac{g}{8(am)^3}\Big\{\Delta^{(2)}, \sigma\cdot\tilde{B}\Big\} \\ & - f_2\frac{3g}{64(am)^4}\Big\{\Delta^{(2)}, \sigma\cdot\big(\tilde{\Delta}^{(\pm)}\times\tilde{E} - \tilde{E}\times\tilde{\Delta}^{(\pm)}\big)\Big\} \\ & - f_3\frac{ig^2}{8(am)^3}\sigma\cdot\tilde{E}\times\tilde{E}. \end{aligned} \tag{5.4}$$

This tuning is necessary in order to ensure that the effective theory reproduces the results of continuum QCD, a typical procedure is to compare a number of quantities computed in both in order to constrain the parameters c_i. c_1, c_5 and c_6 are known as "kinetic couplings", and since c_1 and c_6 have the same form only two free parameters require tuning. The remaining c_i parameters correct for radiative processes, and must also be tuned in order for the theory to correctly reproduce QCD to the desired order.

A convenient method for computing these parameters is to use perturbation theory to compute the coefficients of terms in the effective action in background field gauge in the continuum, and to match these to those computed using lattice perturbation theory and NRQCD. The use of background field gauge restricts the number of possible terms appearing in the effective action to those which are gauge invariant. At the end of section 2.3.1 it was noted that the use of BFG results in a finite 1PI vertex function, since the coupling g only receives renormalisation contributions from the gauge field renormalisation. This is critical for our matching procedure as it means we are free to mix UV regulators between the two calculations. The matching calculation is performed using the Minkowski actions for both continuum and lattice NRQCD and do the integral over temporal momentum as a contour integral. We use tree level on shell spinors for the matching, which must be corrected for at one loop by considering the expansion of the one loop on shell matching $p = (i(E_0 + \vec{p}^2/2m_b), \vec{p})$ where $E_0(p) = \Sigma(p)$ is $\mathcal{O}(\alpha)$, where $\Sigma(p)$ is the quark self energy. Throughout this chapter I use m in equations, suppressing the b subscript on the b quark mass m_b.

5.2 Automated Perturbation Theory

The application of automated perturbation theory to lattice gauge theories was first developed by Lüscher and Weisz [82] and the algorithm I used here, based on this, is set out in [83]. For completeness I outline the basic methodology.

A generic lattice fermion action may be expanded in the gauge fields $U_\mu(x) = \sum_r (agA_\mu(x+$

$\frac{a}{2}e_\mu))^r/r!$ as

$$S[\psi,A] = \sum_r \frac{g^r}{r!} \sum_{k_1,\mu_1,a_1} ... \sum_{k_r,\mu_r,a_r} A^{a_1}_{\mu_1}(k_1)...A^{a_r}_{\mu_r}(k_r)\times \sum_{p,q,b,c} \bar{\psi}^b(p)\psi^c(q)V_{F,r}(p,b;q,c;k_1,\mu_1,a_1;...k_r,\mu_r,a_r) \tag{5.5}$$

where, separating colour factors, the symmetrised vertex is given by

$$V_{F,r}(p,b;q,c;k_1,\mu_1,a_1;...k_r,\mu_r,a_r) = \frac{1}{r!}\sum_{\sigma\in S_r} \sigma\cdot C_{F,r}(b,c;a_1...a_r)\sigma\cdot Y_{F,r}(p,q;k_1,\mu_1;...k_r,\mu_r) \tag{5.6}$$

with σ an element of the permutation group of r elements. C here is the Clebsch-Gordon colour factor, given by $C = \left(T^{a_1}\times ...T^{a_r}\right)_{b,c}$ and Y, the reduced vertex function, is given by

$$Y_{F,r}(p,q;k_1,\mu_1;...k_r,\mu_r) = \sum_{n=1}^{n_r(\{\mu\})} \Gamma^{\{\mu\}}_n f^{\{\mu\}}_n e^{\frac{i}{2}\left(p\cdot x+q\cdot y\sum_{j=1}^r \vec{k}_j\cdot\vec{v}^{\{\mu\}}_{n,j}\right)} \tag{5.7}$$

where for a given combination of r Lorentz indices there are $n_r(\{\mu\})$ terms coming from the number of ways of selecting those indices from the expansion of the links, with $\vec{v}^{\{\mu\}}_{n,j}$ the position vector of the mid point of the link from which the j^{th} Lorentz index originated. $\Gamma^{\{\mu\}}_n$ and $f^{\{\mu\}}_n$ are a spin algebra factor and an amplitude respectively. We encode the Feynman rules as an ordered list of entities, implemented in python, of the form

$$E = (\tau,\mu_1,...,\mu_r : x,y;\vec{v}_1,...\vec{v}_r,f). \tag{5.8}$$

The variable $0\leq\tau\leq 15$ indexes the element of the spin algebra basis to which the corresponding monomial,f, corresponds. The set of entities is refered to as a field. From the field it is trivial to reconstruct the Feynman rule for a particular vertex by summing $f\cdot\exp(\frac{i}{2}(p\cdot x+q\cdot y+\sum_j k_j\vec{v}_j))$ over the entities with a given set of Lorentz indices. Originally presented in [84] the `HiPPy` and `HPsrc` packages generalise the original algorithm conceived by Lüscher and Weisz [82] for closed traced Wilson loops. These freely available packages have since been generalised to include fermions and background fields

[85]. The packages are implemented with provisions for diagrammatic differentiation making them highly suitable for calculations, such as those I perform here, involving many derivatives of multiple variables. The Feynman rules, encoded in vertex files by `HiPPy`, are fed into `HPsrc`, written in fortran, which constructs the integrands for each diagram and performs the momentum integrals over the Brillouin zone using the Monte Carlo integration package `Vegas` [86].

5.3 c_4

The parameter c_4 in (5.1) appears multiplying the chromomagnetic operator:

$$-c_4\frac{g}{2am}\sigma\cdot\tilde{B}. \tag{5.9}$$

Radiative corrections to the chromomagnetic operator occur in both QCD and NRQCD and differences between the corrections must be tuned using c_4. Nonperturbative studies have shown that the impact of this term on the hyperfine splitting of bottomonium goes like the square of c_4 [87], which has contributions at $\mathcal{O}(\alpha)$. These corrections have been calculated [11] but omit $\mathcal{O}(\alpha)$ corrections from the use of tree level on shell quarks due to the timelike gauge link appearing in the NRQCD action. This originally missed correction has since been computed independently and incorporated, though for the v^6 action c_4 has only been calculated for three values of am_b. As such it is desirable to compute a full set of c_4 over a wide range of am_b using the v^6 action.

5.3.1 Continuum calculation

In the continuum the effective action takes the form

$$\Gamma = Z_2^{-1}\bar{\psi}(\partial\!\!\!/ + A\!\!\!/)\psi + \delta Z_\sigma\bar{\psi}\frac{\sigma_{\mu\nu}F^{\mu\nu}}{m}\psi + ... \tag{5.10}$$

which after the FWT transformation (3.79) and multiplicative renormalisation contains the chromomagnetic term

$$(1+\delta Z_\sigma Z_2 Z_m)g{\Psi^\dagger}_R\frac{\sigma\cdot B}{2m_R}\Psi_R. \tag{5.11}$$

As noted above in BFG the renormalisaton of the coupling g comes only from the wavefunction renormalisation of the gauge field. As such the 1PI vertex can be computed using the unrenormalised coupling and background gauge field to acquire a UV finite result. Since QCD is renormalisable the combination $\delta Z_\sigma Z_2 Z_m$ is also UV finite, meaning we can directly compare between different UV regularisation schemes. Since the action

contains no terms of the form (5.11) the term δZ_σ has no tree level piece and is $\mathcal{O}(\alpha)$. This means that at one loop, in the continuum, the contribution of Z_2 and Z_m can be disregarded. Note that the tree level piece coming from $\bar{\psi}\not{A}\psi$ automatically contains the renormalised mass as the gordon decomposition is performed between on shell spinors.

The continuum QCD calculation proceeds straightforwardly, and includes the abelian and nonabelian diagrams. The nonabelian diagram includes a contribution to the vertex from the gauge fixing term as well as the conventional piece from the gauge action. The result is [88]

$$\delta Z_\sigma^{(1)} = \frac{3\alpha}{2\pi}\log\frac{\mu}{m} + \frac{13}{6\pi}\alpha \tag{5.12}$$

where μ is a gluon mass introduced as an IR regulator. To one loop the diagrams contain no ghosts, so this is a valid IR regulator.

5.3.2 NRQCD calculation

In NRQCD the effective action contains the term

$$\Gamma_{c_4}^{\mathrm{NRQCD}} = c_4 Z_\sigma^{NRQCD} g\Psi^\dagger \frac{\sigma\cdot B}{2m}\Psi \tag{5.13}$$

which after renormalisation becomes

$$\Gamma_{c_4}^{\mathrm{NRQCD}} = c_4 Z_\sigma^{NRQCD} Z_m^{NRQCD} Z_2^{NRQCD} g{\Psi^\dagger}_R \frac{\sigma\cdot B}{2m_R}\Psi_R. \tag{5.14}$$

The matching requirement then reads

$$c_4 Z_\sigma^{NRQCD} Z_m^{NRQCD} Z_2^{NRQCD} = 1 + \delta Z_\sigma. \tag{5.15}$$

to $\mathcal{O}(\alpha)$ this gives

$$c_4^{(0)} = 1 \tag{5.16}$$

$$c_4^{(1)} = \delta Z_\sigma^{(1)} - Z_m^{NRQCD(1)} - Z_2^{NRQCD(1)} - Z_\sigma^{NRQCD(1)}. \tag{5.17}$$

Contributions to each of the NRQCD renormalisations may be seen as coming from two sources: normal diagrammatic contributions such as those in figure 5.1 and tadpole

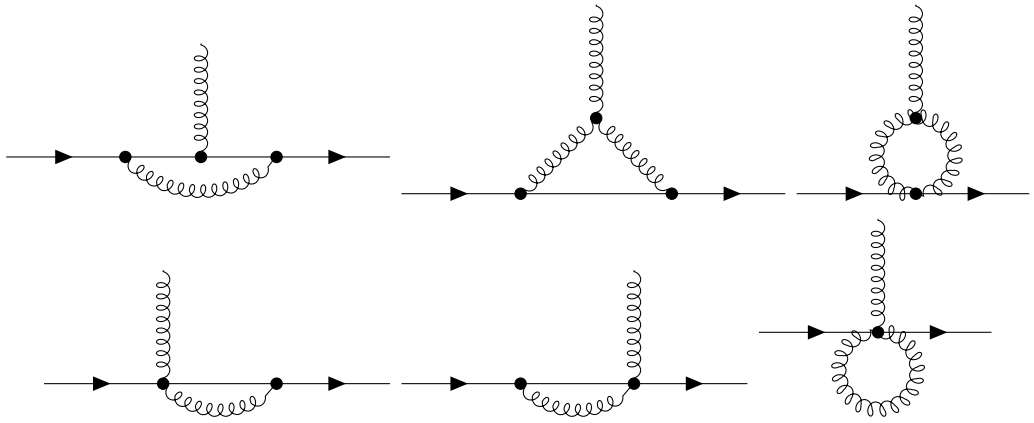

Figure 5.1: Diagrams contributing to the radiative correction, clockwise from top left: abelian, nonabelian, algae, ankh, and two swordfish diagrams.

contributions, arising from the substitution $U \to U/u_0$ with $u_0 = 1 - \alpha u_0^{(1)}$. The tadpole terms have been calculated in [88], using mathematica, and depend on the specific details of the NRQCD action used, such as the stability parameter n. The tadpole factors relevant for $c_4^{(1)}$, for the v^6 action, are

$$Z_\sigma^{\mathrm{tad}(1)} = \left(\frac{13}{3} + \frac{13}{4am} - \frac{3}{8n(am)^2} + \frac{3}{(am)^2} - \frac{3}{4(am)^3} \right) u_0^{(1)} \tag{5.18}$$

$$Z_m^{\mathrm{tad}(1)} = -\left(\frac{2}{3} + \frac{3}{(am)^2} \right) u_0^{(1)} \tag{5.19}$$

and there is no tadpole contribution to Z_2^{NRQCD}.

The diagrammatic contributions to $c_4^{(1)}$ are given in figure 5.1. I generate Feynman rules for the relevant vertices automatically using the `HiPPy` package, for the v^6 NRQCD action. I evaluate the diagrams using the `HPsrc` code, which makes use of the `Vegas` Monte Carlo integration routines. For c_4 the diagrams contain only logarithmic divergences in μ, as I will discuss shortly, which produce sufficiently little noise in the integral that I may just compute diagrams at several different values of μ and fit the logarithms away afterwards. Later when I compute $c_2^{(1)}$, which is strongly IR divergent, a subtraction function must be added to the integrals.

Each integral in figure 5.1 is projected onto the corresponding Z by considering the

explicit form of the term in the effective action, before renormalisation of the mass and fields,

$$\Gamma_{c4} = Z_{\sigma}^{NRQCD} g\Psi^{\dagger}(p+q)\frac{i\epsilon_{ijk}\sigma^{j}q^{k}A^{i}(q)}{2m}\Psi(p). \tag{5.20}$$

Each integral contributes something of the form

$$\Gamma_{c4}^{\text{diag}} = \Psi^{\dagger}(p+q)\mathcal{M}(p,q)_{i}A^{i}(q)\Psi(p). \tag{5.21}$$

I may therefore project out its contribution to Z by taking

$$gZ^{\text{diag}} = m\text{Tr}\left[\frac{\partial}{\partial q^{1}}\mathcal{M}(p,q)_{2}|_{\vec{p}=q=0}\sigma^{3}\right] \tag{5.22}$$

where p_0 is chosen so that the heavy quark is on shell. This is done using the tree level equation of motion and so must be corrected for at one loop. I discuss the treatment of poles in the numerical evaluation of diagrams in Appendix B.

I split each Z into an IR finite piece indicated by $\tilde{Z}$ as well as an IR divergent logarithm $A\log(a\mu)$. The IR divergences are known from analytic results, and are given by [89]

$$Z_{2}^{NRQCD(1)} + Z_{\sigma}^{NRQCD(1)} = \tilde{Z}_{2}^{NRQCD(1)} + \tilde{Z}_{\sigma}^{NRQCD(1)} + \frac{3}{2\pi}\log(a\mu) \tag{5.23}$$

$$Z_{m}^{NRQCD(1)} = \tilde{Z}_{m}^{NRQCD(1)}. \tag{5.24}$$

I compute the sum of all diagrammatic renormalisation factors simultaneously and fit the result to

$$\frac{3}{2\pi}\log(a\mu) + \tilde{Z}_{\text{diag}}^{(1)} \tag{5.25}$$

in order to find the diagrammatic contribution. I use values of $a\mu$ between 10^{-2} and 10^{-4} so that any lattice artefact μ dependence is negligible. In order to make the calculation as efficient as possible, I compute the ankh diagram, which converges quickly but takes a lot of time due to the size of the vertex, seperately from the remaining diagrams.

There is one more subtle contribution which must be included, this originates from the point splitting in time of the tree level vertex, introducing a factor of e^{ip0} in the

Feynman rules. Since I use tree level on shell external quark momenta, the result must be adjusted at one loop to recover the on shell value to this order. The one loop on shell condition reads $p = (i(-E_0 + p^2/2m), \vec{p})$ which yields a correction to $c_4^{(1)}$ of $+E_0^{(1)}$. $E_0^{(1)}$ has both diagrammatic and tadpole contributions. I include the diagrammatic contribution, $E_0^{\mathrm{diag}(1)} = \Sigma(0)$, along with the others in the monte carlo integral. The tadpole contribution is given by

$$E_0^{\mathrm{tad}(1)} = \left(1 + \frac{7}{2m} - \frac{3}{4nm^2} - \frac{3}{2m^2}\right) u_0^{(1)} \tag{5.26}$$

and is included in the analysis. Values for tadpole factors, as well as fit results for the diagrammatic contributions, are given in table 5.1.

5.3.3 Results

Figure 5.2 shows fits to (5.25), using only a single parameter for $\tilde{Z}^{(1)}_{\mathrm{diag}}$ with gaussian prior $-3(3)$. It can be seen that relatively few points are necessary to extract the IR finite piece since $a\mu$ is small and polynomial terms are suppressed. Table 5.1 gives the mass, diagrammatic, and tadpole contributions as well as the computed value of $c_4^{(1)}$. Figure 5.3 shows the am_b dependence of $c_4^{(1)}$, the divergent behaviour around $am_b \approx 0.6$ can be explained by considering the high momentum behaviour of the fermion propagator. The momentum k in the numerical integrals is restricted to the Brillouin zone $-\pi < k < \pi$, and when $am_b < am_{\mathrm{crit}}$ the pole $w_f = \left(1 - \frac{aH_0(k)}{2n}\right)^{-2n}$ goes to infinity and becomes negative for some values of k. This critical value can easily be found considering the maxiumum value of $k = \pi$ and setting $w_f^{-1} = 0$ to find

$$\begin{aligned}
\left(1 - \frac{aH_0(\pi)}{2n}\right) &= 0 \\
1 - \frac{\pi^2}{4nm_{\mathrm{crit}}} &= 0 \\
m_{\mathrm{crit}} &= \pi^2/4n.
\end{aligned}$$

Table 5.1: Tadpole and diagrammatic contributions to $c_4^{(1)}$. The error coming from the computed value of $u_0^{(1)} = 0.750275(5)$ is not tabulated in $Z_\sigma^{\mathrm{tad}(1)}$, though this is included in the analysis and the given value of $c_4^{(1)}$.

am_b	$E_0^{\mathrm{tad}(1)}$	$Z_\sigma^{\mathrm{tad}(1)}$	$Z_m^{\mathrm{tad}(1)}$	$\tilde{Z}_{\mathrm{diag}}^{(1)}$	$c_4^{(1)}$
0.6	−0.4741	10.767	−6.752	−5.67(3)	2.112(26)
0.8	1.614	8.607	−4.017	−1.32(3)	−0.858(28)
1.0	2.110	7.307	−2.751	−1.30(3)	−0.459(26)
1.25	2.184	6.309	−1.940	−1.55(1)	−0.051(12)
1.5	2.104	5.679	−1.501	−1.64(1)	0.066(11)
1.9	1.929	5.056	−1.124	−1.72(1)	0.1046(99)
2.8	1.618	4.374	−0.7872	−1.861(6)	0.0908(57)
3.4	1.481	4.142	−0.6949	−1.925(9)	0.0643(89)
5.0	1.260	3.822	−0.5902	−2.050(8)	0.0002(80)

I use a value for the stability parameter of $n = 4$ and so the smallest value of am_b I should use is $\pi^2/16 = 0.61685$. This could easily be remedied by choosing a different stability parameter, but $am_b = 0.6$ is already comparable to charm masses on the coarse lattices and it is likely that in such circumstances relativistic approaches to simulating the bottom quark, such as heavy-HISQ, would be favourable.

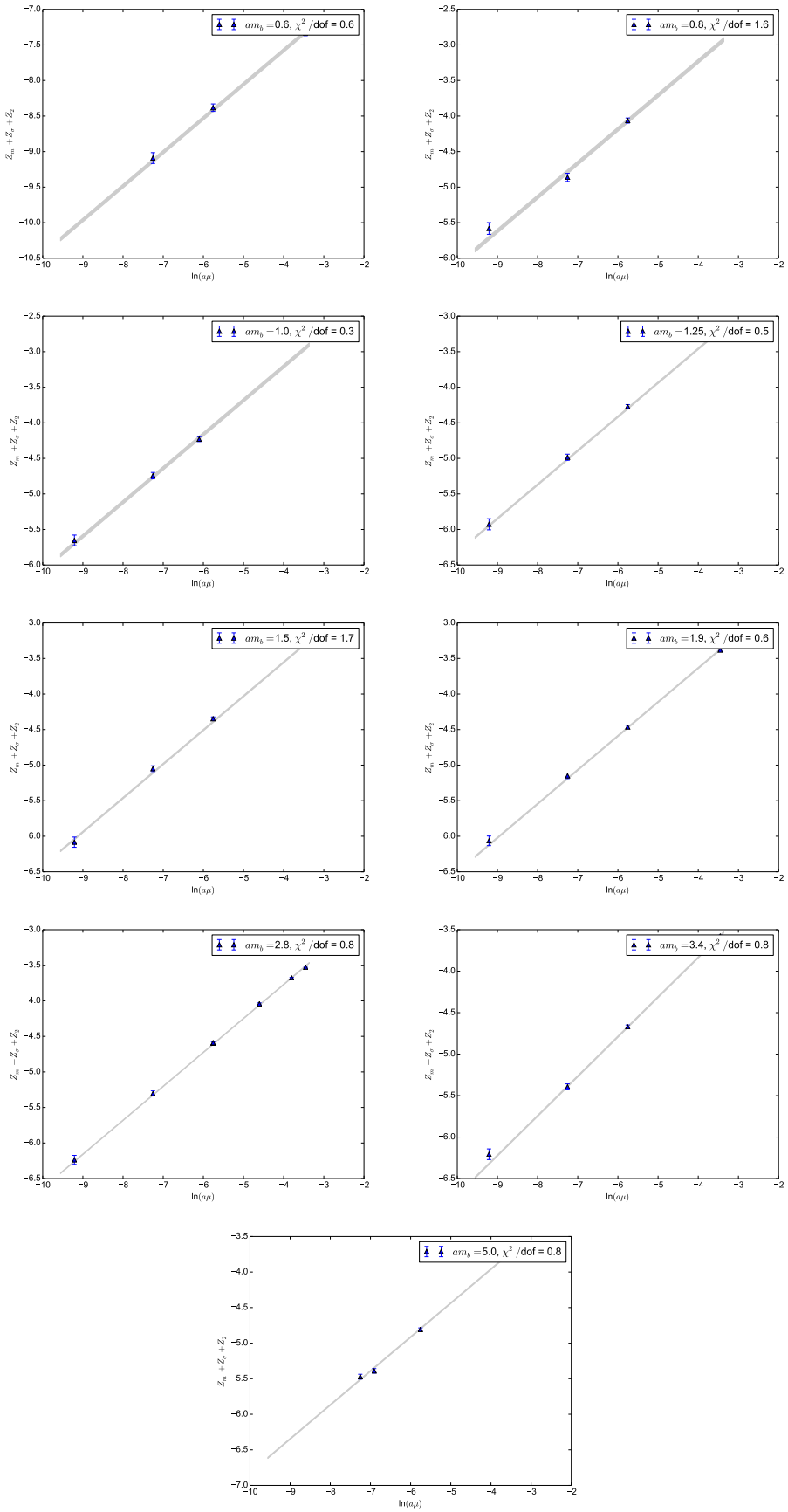

Figure 5.2: Plots of fits to (5.25) for various am_b.

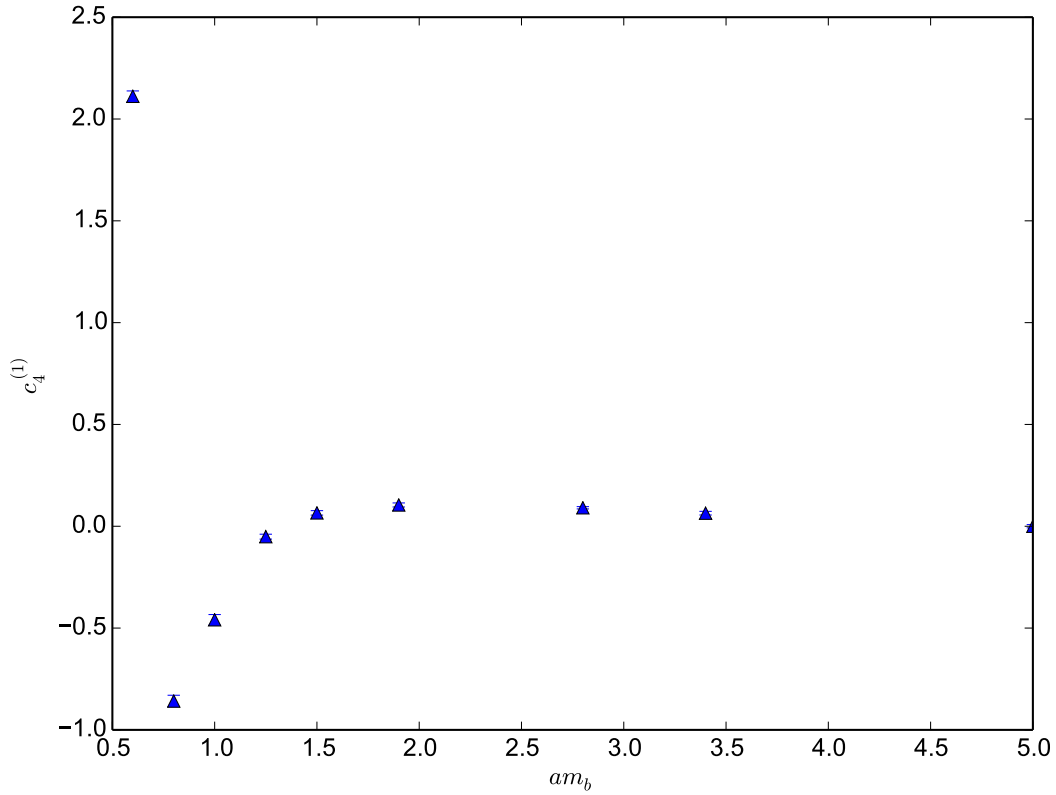

Figure 5.3: Plots of $c_4^{(1)}$ against am_b.

5.4 c_2

The parameter c_2 in (5.1) multiplies what is refered to as the "Darwin operator":

$$c_2 \frac{ig}{8(am)^2}\left(\Delta^{(\pm)} \cdot \tilde{E} - \tilde{E} \cdot \Delta^{(\pm)}\right). \tag{5.27}$$

The Darwin operator also receives renormalisations from the diagrams in figure 5.1. The Darwin operator is responsible for shifting the energy of s-wave states. Nonperturbative studies [5] of the effect of varying c_2 on these shifts suggests that the $\mathcal{O}(\alpha)$ corrections to c_2 are not significant, however the calculation of c_2 to this order is still desirable for completeness, as well as to eliminate the need to estimate systematic errors resulting from its omission.

5.4.1 Continuum calculation

The continuum effective action contains the terms detailed in (5.10). Following the FWT transformation, the terms containing A_0 are

$$\Gamma^{A_0} = Z_2^{-1}(q^2)\Psi^\dagger\left(gA_0 - \frac{g}{8m^2}q^2A_0 + ...\right)\Psi + \delta Z_\sigma(q^2)\Psi^\dagger\left(-\frac{g}{4m^2}q^2A_0 + ...\right)\Psi. \tag{5.28}$$

After renormalisation we isolate the Darwin term

$$\Gamma^{\text{darwin}} = \left(1 - 8m^2 Z_2^{-1\prime}(0) + 2\delta Z_\sigma(0)\right)\Psi_R^\dagger\left[-\frac{g}{8m_R^2}q^2A_0\right]\Psi_R. \tag{5.29}$$

Details of the analytic calculation of $Z_2^{-1\prime}(0)$ and $\delta Z_\sigma(0)$ can be found in [90]. The total contribution to the darwin term from continuum QCD is

$$Z_D = 1 - \alpha\left(\frac{1}{\pi} + \frac{7m}{4\mu} + \frac{m^2}{\pi\mu^2} + \left(\frac{6}{\pi} - \frac{4}{9\pi}\right)\log(\mu/m)\right). \tag{5.30}$$

The $1/\mu$ and $1/\mu^2$ IR divergences must match and cancel between the continuum and NRQCD calculations. These are problematic for the vegas integral and in practice they must be subtracted prior to integration.

5.4.2 NRQCD calculation

After renormalisation the NRQCD effective action contains the piece

$$\Gamma_{c_2}^{\rm NRQCD} = -c_2 Z_D^{\rm NRQCD} Z_2^{\rm NRQCD} Z_m^{\rm NRQCD2} g \Psi_R^\dagger \frac{q^2 A_0}{8m_R^2} \Psi_R. \tag{5.31}$$

I work in the Breit frame in which $\vec{p} = -\vec{q}/2$. The NRQCD projection for the $\mathcal{O}(\alpha)$ vertex is

$$V_0(p,q)^R = Z_D^{\rm NRQCD} q^2/8m^2 \tag{5.32}$$

using the on shell condition we then have

$$Z_D^{\rm NRQCD} = 8m^2 \frac{d}{d(q^2)} V_0(p,q)|_{p=q=0} = \left(\frac{4m^2}{3} \frac{\partial^2}{\partial q_i^2} + im \frac{\partial}{\partial p_0} \right) V_0(p,q)|_{p=q=0}. \tag{5.33}$$

Including both 1 particle irreducible and 1 particle reducible diagrams in the calculation of $V_0(p,q)$, $Z_D^{\rm NRQCD}$ automatically includes the contributions from the wavefunction renormalisations of the tree level iA_0 and Darwin vertices. The projection operator (5.33) should therefore also be applied to these pieces, and the contribution of the iA_0 tree level term is non-trivial. Its contribution is

$$Z_D^{A_0,NRQCD} = -\left(\frac{m^2}{3} \frac{\partial^2}{\partial p_i^2} + im \frac{\partial}{\partial p_0} \right) \left(\Sigma(p) - i \frac{\partial}{\partial p_0} \Sigma(p) \right) \Big|_{p=0} \tag{5.34}$$

which I include when I evaluate and project the diagrams in figure 5.1. To make this distinction clear I write

$$Z_D^{\rm NRQCD} = Z_D^{1PI,NRQCD} + Z_D^{A_0,NRQCD}. \tag{5.35}$$

As mentioned above a subtraction function must be included in the vegas integral in order to remove IR divergences. I opt to use the subtraction function given in [11]

$$I_{\rm sub}(\mu) = \tilde{Z}_{\rm sub} + \frac{7m}{4\mu} + \frac{21}{4\pi} \log(a\mu) + \frac{m^2}{\pi\mu^2} \tag{5.36}$$

where $\tilde{Z}_{\rm sub}$ includes some polynomial in $a\mu$. This function cancels the leading IR divergences pointwise, and contributes a continuum like logarithm. For each value of m I use

to calculate c_2 I therefore need to also independently compute $I_{\rm sub}$ for several values of $a\mu$ and perform a fit in order to determine $\tilde{Z}_{\rm sub}$.

The total quantity computed in the numerical integral is then

$$Z_D^{1PI,NRQCD(1)} + Z_D^{A_0,NRQCD(1)} + I_{\rm sub} + Z_2^{(1)} - E_0^{(1)} + 2Z_m^{(1)} = \tilde{Z}_D^{1PI,NRQCD(1)} + \tilde{Z}_D^{A_0,NRQCD(1)} + \tilde{Z}_{\rm sub} + \tilde{Z}_2^{(1)} - E_0^{(1)} + 2\tilde{Z}_m^{(1)} + \left[\frac{4}{9\pi} + \frac{21}{4\pi} - \frac{6}{\pi}\right]\log(a\mu). \tag{5.37}$$

Care has been taken to ensure the terms omitted from [89], the factor of 2 from the mass squared and the projection operator applied to Z_2, have been included. In order to fit the subtraction function for each value of am I took a quadratic in μ. The parameters of the resultant fits are given in figure 5.4. Having done the fit to $I_{\rm sub}$ I remove its polynomial and logarithmically divergent piece analytically from the results for the numerical integral (5.37). Adding in tadpole pieces as I did for c_4 the final result is then

$$c_2^{(1)} = -\frac{1}{\pi} - \Big[\tilde{Z}_D^{1PI,NRQCD(1)} + \tilde{Z}_D^{A_0,NRQCD(1)} + \tilde{Z}_D^{\rm tad} + \tilde{Z}_2^{(1)} - E_0^{(1)} - E_0^{\rm tad(1)} + 2\tilde{Z}_m^{(1)} + 2\tilde{Z}_m^{\rm tad(1)} + \left[\frac{4}{9\pi} - \frac{6}{\pi}\right]\log(am)\Big] \tag{5.38}$$

where

$$\tilde{Z}_D^{\rm tad} = \left(\frac{10}{3} + 2 - \frac{3}{4(am)^3} - \frac{3}{32(am)^2} + \frac{13}{4am}\right) u_0^{(1)} \tag{5.39}$$

and

$$E_0^{\rm tad(1)} = \left(1 + \frac{7}{2am} - \frac{3}{2(am)^3} - \frac{3}{16(am)^2}\right) u_0^{(1)}. \tag{5.40}$$

5.4.3 Results

v^6 Action

Defining

$$\tilde{Z}_\Sigma^{(1)} = \tilde{Z}_D^{A_0,NRQCD(1)} + \tilde{Z}_2^{(1)} - E_0^{(1)} + 2\tilde{Z}_m^{(1)} \tag{5.41}$$

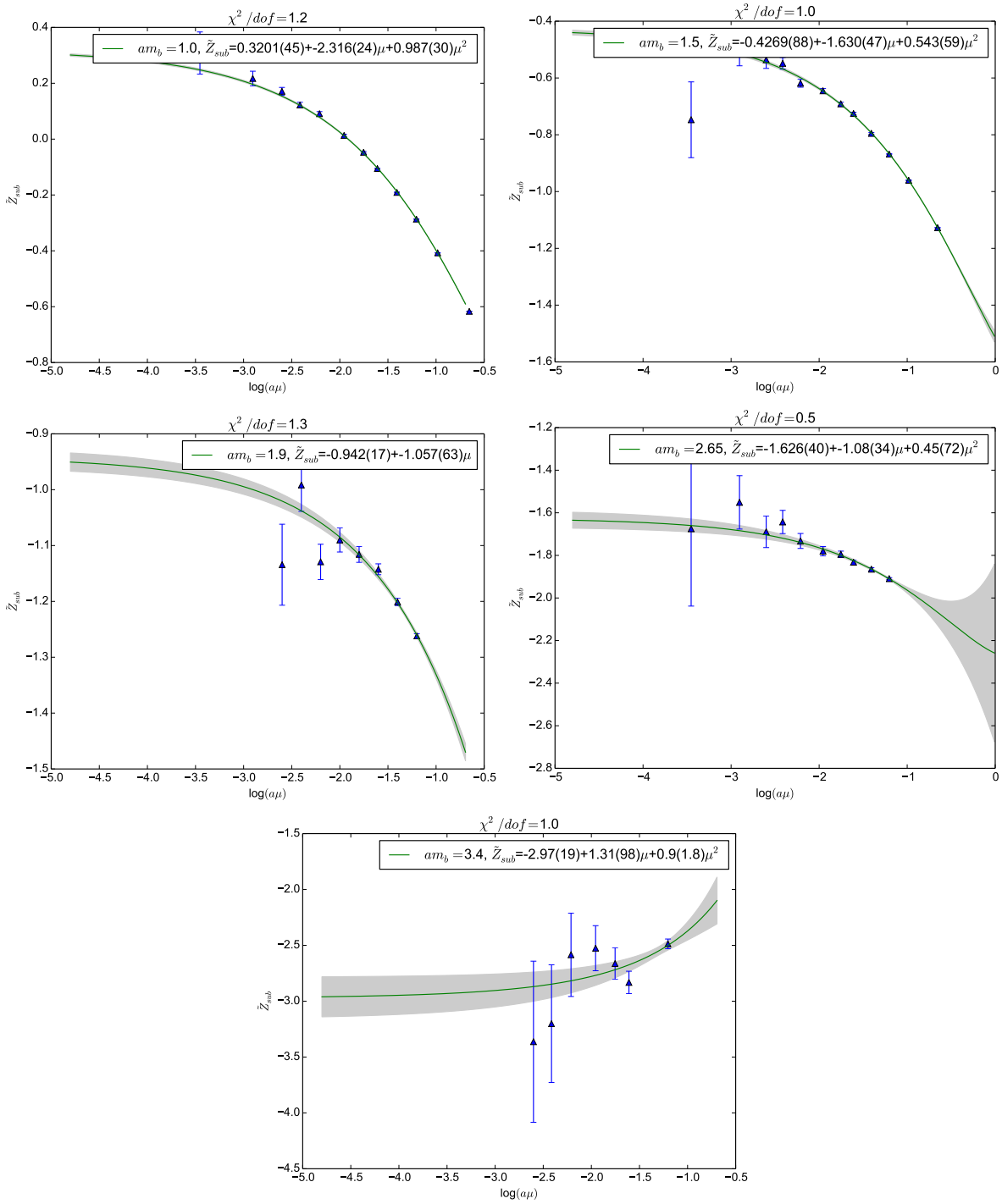

Figure 5.4: Plots of fits to $\tilde{Z}_{\rm sub}$ defined in (5.36).

Table 5.2: Numerical results for the calculation of c_2 for the v^6 action.

am_b	$\tilde{Z}_{\rm sub}(0)$	$Z_D^{\rm tad(1)}$	$\tilde{Z}_\Sigma^{(1)}$	$\tilde{Z}_D^{1PI,NRQCD(1)} + \tilde{Z}_\Sigma^{(1)}$	$c_2^{(1)}$
1.0	0.3201 (45)	5.806819(36)	–	-0.774(51)	2.261(51)
1.5	-0.4269 (88)	5.429076(34)	–	-1.825(55)	1.901(55)
1.9	-0.942 (17)	5.183311(32)	4.719(40)	-1.273(76)	1.083(76)
2.65	-1.626 (40)	4.881364(31)	3.718(40)	-0.12(11)	-0.05(11)
3.4	-2.97 (19)	4.698242(29)	–	1.78(19)	-1.76(19)

Table 5.3: Numerical results for the calculation of c_2 for the v^4 action, using table IV of [11] as input together with my computed values of $\tilde{Z}_\Sigma^{(1)}$.

am_b	$Z_D^{\rm tad(1)}$	$\tilde{Z}_\Sigma^{(1)}$	$\tilde{Z}_D^{1PI,NRQCD(1)}$	$c_2^{(1)}$
1.9	5.183311(32)	4.961(34)	-5.95(8)	0.679(87)
2.65	4.881364(31)	3.874(34)	-3.71(10)	-0.41(11)
3.4	4.698242(29)	3.135(31)	-1.73(12)	-1.45(11)

which is the sum of IR finite pieces of diagrammatic pieces calculated from $\Sigma(p)$.

Table 5.2 gives fit results for $\tilde{Z}_D^{1PI,NRQCD(1)} + \tilde{Z}_\Sigma^{(1)}$ and $\tilde{Z}_{\rm sub}(0)$ as well as the numerical values of $Z_D^{\rm tad(1)}$ on the full v^6 NRQCD action. For $am_b = 1.9, 2.65$ I also give values for $\tilde{Z}_\Sigma^{(1)}$. This was done in order to check my computed values for $\tilde{Z}_D^{1PI,NRQCD(1)}$ against those given in [11], with which I am in good agreement.

v^4 Action

Having confirmed their diagrammatic pieces are correct, I perform the much simpler calculation of the quantity $\tilde{Z}_\Sigma^{(1)}$ using the v^4 action and combine this with results for the IR finite part of the diagrammatic contribution in [11] to obtain a revised value for c_2 on the v^4 action.

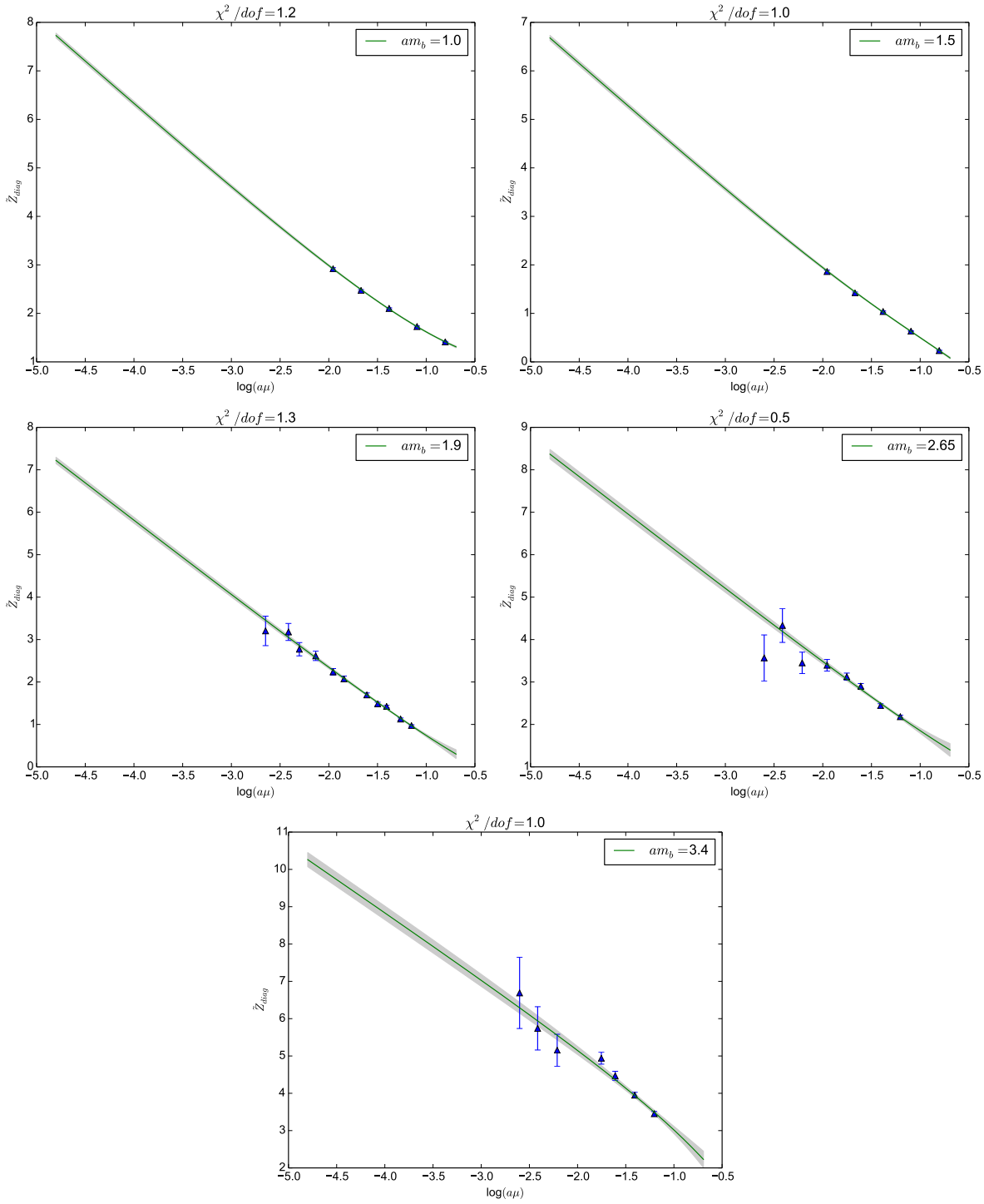

Figure 5.5: Plots of fits to $\tilde{Z}_D^{1PI,NRQCD(1)} + \tilde{Z}_D^{A_0,NRQCD(1)} + \tilde{Z}_2^{(1)} - E_0^{(1)} + 2\tilde{Z}_m^{(1)} + \left(\frac{4}{9\pi} - \frac{6}{\pi}\right)\log(a\mu)$ including polynomial terms in μ, which is the IR finite and logarithmic piece of (5.37) following removal of the IR finite and logarithmic piece of the subtraction function.

am_b Dependence of c_2

It is interesting to check whether c_2 has any dependence upon $(am_b)^2$. In principle redefinitions of the gauge fields can generate contributions to c_2 going as $(am_b)^2$, coming from the tree level vertex. Therefore I have tried fitting my results to various fit functions with and without quadratic pieces and find no evidence for a piece going as $(am_b)^2$.

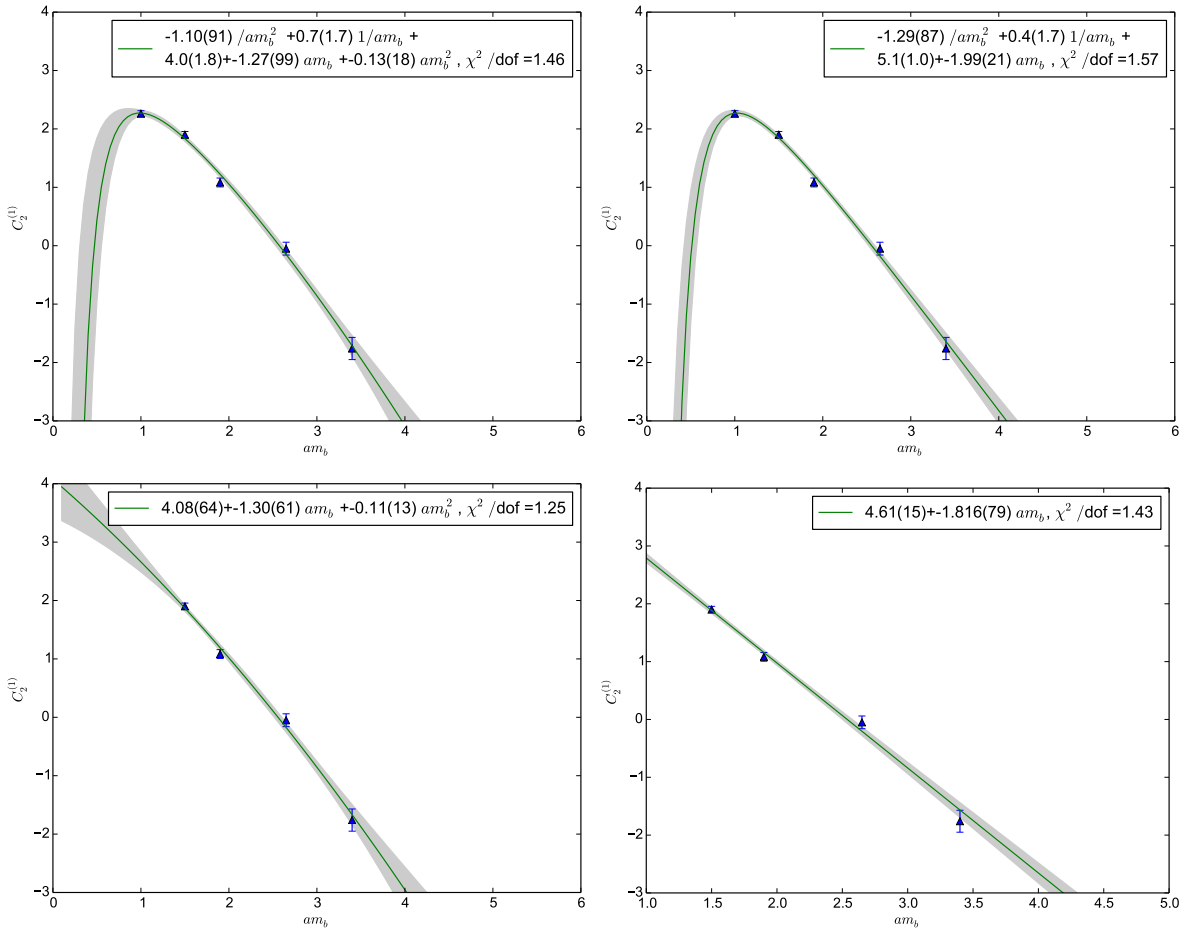

Figure 5.6: Plots of fits to c_2, using a polynomial in am_b. The top two plots include terms going as $1/am_b$ and $1/(am_b)^2$ and the $am_b = 1.0$ point while the bottom two do not.

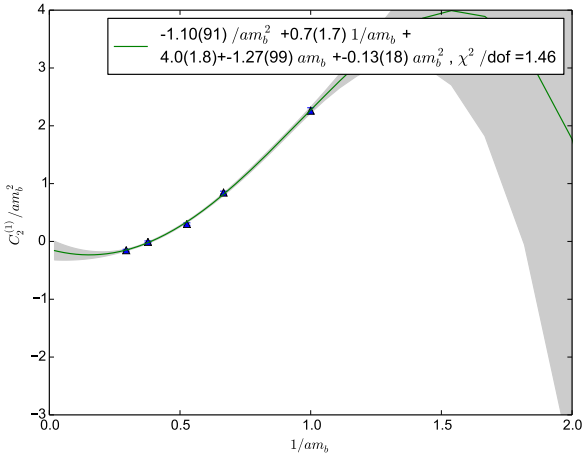

Figure 5.7: Plot of $c_2/(am_b)^2$ for the top left fit function of figure 5.6, going to 0 as $am_b \to \infty$.

5.5 c_1 and c_5

c_1 and c_5 multiply the two independent kinetic terms in the NRQCD action:

$$c_5 \frac{a^2 \Delta^{(4)}}{24am}, \; - c_1 \frac{(\Delta^{(2)})^2}{8(am)^3}. \tag{5.42}$$

The $-c_6 \frac{a(\Delta^{(2)})^2}{16n(am)^2}$ term is proportional to the c_1 term and it is conventional to absorb them together, as we do later. They correct the dispersion relation by removing terms which do not obey the rotational symmetry of the continuum theory such as $\sum_{i=1,2,3} p_i^4$ as well as correcting the coefficients of those functions of p^2 which do not match the continuum.

5.5.1 1-loop, on shell dispersion relation

The one loop improvement of the kinetic couplings c_1, c_5 and c_6 appearing in 3.86 is done by matching the NRQCD one loop on shell dispersion relation to the continuum relativistic expansion order by order in $\mathbf{p}^2$. There is no need for an IR regulator as all the relevant quantities are IR finite. The inverse heavy quark propagator may be written

$$G(p)^{-1} = G^{(0)}(p)^{-1} - \alpha \Sigma(p) \tag{5.43}$$

where $G^{(0)}(p)$ is the tree level propagator obtained from 3.86 as

$$G^{(0)}(p)^{-1} = \left[1 - e^{-ip_4} F(\mathbf{p})^{2n} F_1(\mathbf{p})^2\right] \tag{5.44}$$

$$F(\mathbf{p}) = 1 - \frac{1}{nm}\sum_j \sin^2(\mathbf{p}_j/2) \tag{5.45}$$

$$\begin{aligned} F_1(\mathbf{p}) = 1 &- \frac{c_5}{3m}\sum_j \sin^4(\mathbf{p}_j/2) \\ &+ \frac{\tilde{c}_1}{m^3}\left(1+\frac{m}{2n}\right)\left[\sum_j \sin^2(\mathbf{p}_j/2)\right]^2 \\ &- \frac{2c_{(p^2)^3}}{m^5}\left(1-\frac{m^2}{6n^2}\right)\left[\sum_j \sin^2(\mathbf{p}_j/2)\right]^3 \\ &- \frac{8c_{p^6}}{45m}\sum_j \sin^6(\mathbf{p}_j/2) \\ &+ \frac{2c_{p^2p^4}}{3m^3}\sum_{j,k} \sin^2(\mathbf{p}_j/2)\sin^4(\mathbf{p}_k/2) \end{aligned} \tag{5.46}$$

with $\tilde{c}_1 = (c_1 + c_6 m/2n)/(1 + m/2n)$ and $c_1 = c_6$. The on shell energy $\omega(\mathbf{p})$ is the value of $-ip_4$ which produces a pole in the full propagator, found by setting 5.43 equal to zero

$$\omega(\mathbf{p}) = -\log[F(\mathbf{p})^{2n} F_1(\mathbf{p})^2] - \alpha\Sigma(\omega_0(\mathbf{p}), \mathbf{p}) \tag{5.47}$$

where $\omega_0(\mathbf{p})$ is the tree level on shell energy

$$\begin{aligned} \omega_0(\mathbf{p}) = &\frac{\mathbf{p}^2}{2m} - \frac{(\mathbf{p}^2)^2}{8m^3} + \frac{(\mathbf{p}^2)^3}{16m^5} \\ &+ \alpha\left[c_5^{(1)}\frac{\mathbf{p}^4}{24m} - \tilde{c}_1^{(1)}\Big(\frac{1}{m}+\frac{1}{2n}\Big)\frac{(\mathbf{p}^2)^2}{8m^2}\right]. \end{aligned} \tag{5.48}$$

The self energy is expanded in small $\mathbf{p}$ as

$$\Sigma(p) = \Sigma_0(\omega) + \Sigma_1(\omega)\frac{\mathbf{p}^2}{2m} + \Sigma_2(\omega)\frac{(\mathbf{p}^2)^2}{8m^2} + \Sigma_3(\omega)\mathbf{p}^4 \tag{5.49}$$

where

$$\Sigma_0(\omega) = \Sigma(\omega, \mathbf{p})\Big|_{\mathbf{p}=0} \tag{5.50}$$

$$\Sigma_1(\omega) = m\frac{\partial^2}{\partial p_z^2}\Sigma(\omega, \mathbf{p})\Big|_{\mathbf{p}=0} \tag{5.51}$$

$$\Sigma_2(\omega) = m^2\frac{\partial^4}{\partial p_z^2 \partial p_y^2}\Sigma(\omega, \mathbf{p})\Big|_{\mathbf{p}=0} \tag{5.52}$$

$$\Sigma_3(\omega) = \frac{1}{24}\left[\frac{\partial^4}{\partial p_z^4} - 3\frac{\partial^4}{\partial p_z^2 \partial p_y^2}\right]\Sigma(\omega, \mathbf{p})\Big|_{\mathbf{p}=0} \tag{5.53}$$

$$\Sigma_m^{(l)} = (-i)^l \frac{1}{l!}\frac{\partial^l}{\partial p_4^l}\Sigma_m(p_4)\Big|_{p_4=0}. \tag{5.54}$$

Using this $\Sigma(\omega_0(\mathbf{p}), \mathbf{p})$ is expanded as

$$\begin{aligned}\Sigma(\omega_0(\mathbf{p}), \mathbf{p}) = W_0 + \frac{\mathbf{p}^2}{2m}Z_m^{(1)} \\ + \frac{(\mathbf{p}^2)^2}{8m^2}\left[W_1 - \frac{3Z_m^{(1)}}{m}\right] + W_2\mathbf{p}^4\end{aligned} \tag{5.55}$$

where we have defined

$$Z_m^{(1)} = \Sigma_0^{(1)} + \Sigma_1^{(0)} \tag{5.56}$$

$$W_0 = \Sigma_0^{(0)} \tag{5.57}$$

$$W_1 = 2\Sigma_0^{(2)} + 2\Sigma_1^{(1)} + \Sigma_2^{(0)} + \frac{2}{m}\Sigma_0^{(1)} + \frac{3}{m}\Sigma_1^{(0)} \tag{5.58}$$

$$W_2 = \Sigma_3^{(0)}. \tag{5.59}$$

Substituting 5.55 into 5.47, to one loop

$$\begin{aligned}\omega(\mathbf{p}) = \frac{\mathbf{p}^2}{2m}(1 - \alpha Z_m^{(1)}) - \frac{(\mathbf{p}^2)^2}{8m^3}(1 - 3Z_m^{(1)}) + \frac{(\mathbf{p}^2)^3}{16m^5} \\ + \alpha\left[c_5^{(1)}\frac{\mathbf{p}^4}{24m} - \tilde{c}_1^{(1)}\Big(\frac{1}{m} + \frac{1}{2n}\Big)\frac{(\mathbf{p}^2)^2}{8m^2}\right] \\ - \alpha\left(W_0 + \frac{(\mathbf{p}^2)^2}{8m^2}W_1 + W_2\mathbf{p}^4\right).\end{aligned} \tag{5.60}$$

Identifying $(1 + \alpha Z_m^{(1)})m = m^r$, the renormalised mass, we write to $\mathcal{O}(\alpha\mathbf{p}^4, \mathbf{p}^6)$

$$\omega(\mathbf{p}) = \frac{\mathbf{p}^2}{2m^r} - \frac{(\mathbf{p}^2)^2}{8m^{r3}} + \frac{(\mathbf{p}^2)^3}{16m^{r5}} + \alpha\left[W_0 + \mathbf{p}^4\Big(\frac{c_5^{(1)}}{24m} - W_2\Big) - \frac{(\mathbf{p}^2)^2}{8m^2}\Big(\tilde{c}_1^{(1)}\Big(\frac{1}{m}+\frac{1}{2n}\Big) + W_1\Big)\right]. \quad (5.61)$$

In order to match the continuum relativistic dispersion relation I therefore take

$$\tilde{c}_1^{(1)} = -\Big(\frac{1}{m}+\frac{1}{2n}\Big)^{-1} W_1 \quad (5.62)$$

$$c_5^{(1)} = 24mW_2. \quad (5.63)$$

As for c_4 and c_2 there are tadpole contributions to $\tilde{c}_1$ and c_5. These are computed in mathematica by inserting factors of $1/u$ into the momentum space kinetic part of the action wherever a gauge link appears, replacing $u \to 1-x$ and then taking the coefficient of x in an expansion about $x = 0$. The tadpole factors are given by

$$\frac{\tilde{c}_1^{\mathrm{tad}(1)}}{u_0^{(1)}} = -\frac{1}{8}\Big(1+\frac{m}{2n}\Big)^{-1}\Big[\frac{6}{m^3} + \frac{6}{m^2 n} - \frac{72}{m^2} + \frac{3}{2mn^2} - \frac{2}{m} + \frac{12}{n^2} - \frac{1}{n}\Big] \quad (5.64)$$

$$\frac{c_5^{\mathrm{tad}(1)}}{u_0^{(1)}} = -\frac{3}{4m^3} - \frac{3}{8m^2 n} + \frac{3}{m^2} + \frac{1}{4m} - \frac{4}{3}. \quad (5.65)$$

The full expressions for $\tilde{c}_1$ and c_5 are then

$$\tilde{c}_1^{(1)} = -\Big(\frac{1}{m}+\frac{1}{2n}\Big)^{-1} W_1 + \tilde{c}_1^{\mathrm{tad}(1)} \quad (5.66)$$

$$c_5^{(1)} = 24mW_2 + \tilde{c}_5^{\mathrm{tad}(1)}. \quad (5.67)$$

5.5.2 Results

Table 5.4 gives results for $\tilde{c}_1^{(1)}$ and $c_5^{(1)}$ using the v^6 NRQCD action. Much smaller values of am_b are not expected to be needed as these lattices would be sufficiently fine for heavy-HISQ methods to be used for the bottom quark.

Figure 5.8 shows plots of the fit am_b dependence of $\tilde{c}_1$ and c_5. The results I present here were calculated using `Vegas` with periodic boundary conditions. However, it is

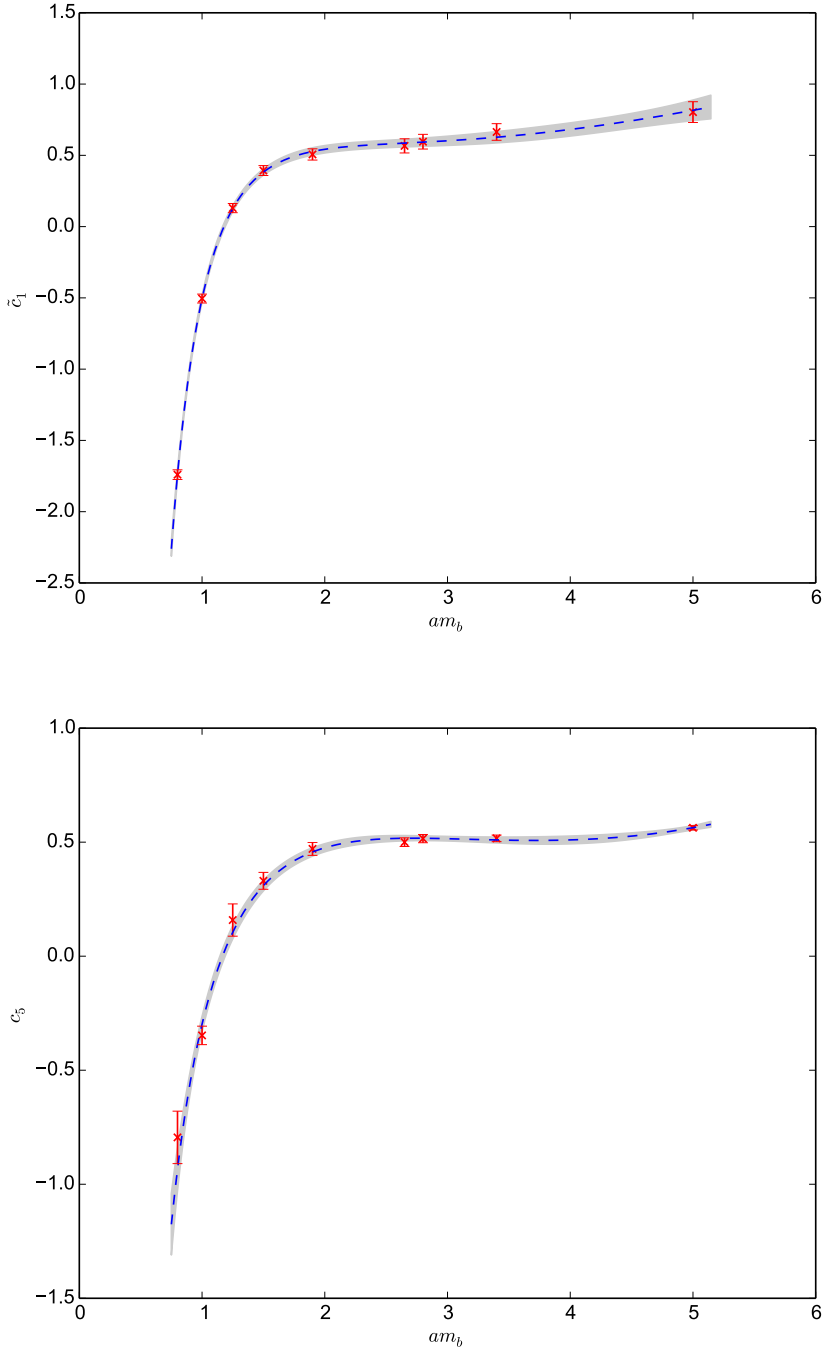

Figure 5.8: Plots of $\tilde{c}_1$ (top) and c_5 (bottom), including the tadpole corrections, against am_b. The dashed blue line shows the result of a fit of the am_b dependence of each coupling and the shaded portion shows the error.

Table 5.4: Results for the kinetic couplings $\tilde{c}_1^{(1)}$ and $c_5^{(1)}$ using the v^6 action.

am_b	$\tilde{c}_1^{(1)}$	$c_5^{(1)}$
0.8	−1.740(34)	−0.79(11)
1.0	−0.505(31)	−0.347(41)
1.25	0.130(32)	0.158(71)
1.5	0.393(35)	0.330(37)
1.9	0.506(39)	0.471(28)
2.65	0.566(50)	0.500(19)
2.8	0.596(52)	0.516(18)
3.4	0.664(58)	0.517(15)
5.0	0.803(73)	0.5630(96)

also possible to do the calculation of the kinetic couplings, and in principle all of the matching coefficients, using twisted boudary conditions [82] to perform the integrals. Using twisted boundary conditions introduces a twist as an IR regulator and means that the sum over momentum may be performed as an exact sum. The IR divergeances of individual pieces cancel exactly in such a case to give a finite result. Being an exact sum there are no statistical errors and uncertainty arises purely from the fit to $1/L$ that must be performed in order to remove the IR regulator. In parallel to the PBC calculation presented here, $\tilde{c}_1^{(1)}$ and $c_5^{(1)}$ were also calculated using twisted boundary conditions [2] and the results were found to be in good agreement.

5.6 Summary

Table 5.5 summarises my results for the v^6 NRQCD action. The calculation of the bottomonium hyperfine splittings, originally calculated in [91], can now proceed using our correct values for the $\mathcal{O}(\alpha_s v^4, v^6)$ improved couplings. These results also represent a step towards the extension of NRQCD to investigations of exotic bottomonium states, motivated by experimental evidence for such states in the charmonium spectrum [92].

Table 5.5: Results for the 1-loop couplings, c_i, I have computed for the v^6 action.

am_b	$\tilde{c}_1^{(1)}$	$c_5^{(1)}$	$c_2^{(1)}$	$c_4^{(1)}$
0.6	–	–	–	2.112(26)
0.8	−1.740(34)	−0.79(11)	2.261(51)	−0.858(28)
1.0	−0.505(31)	−0.347(41)	–	−0.459(26)
1.25	0.130(32)	0.158(71)	–	−0.051(12)
1.5	0.393(35)	0.330(37)	1.901(55)	0.066(11)
1.9	0.506(39)	0.471(28)	1.083(76)	0.1046(99)
2.65	0.566(50)	0.500(19)	−0.05(11)	–
2.8	0.596(52)	0.516(18)	–	0.0908(57)
3.4	0.664(58)	0.517(15)	−1.76(19)	0.0643(89)
5.0	0.803(73)	0.5630(96)	–	–

Chapter 6

Conclusions and Outlook

6.1 Conclusions and Outlook

This thesis covers several projects using lattice QCD to make predictions for hadronic quantities involving b quarks. I have performed the calculation of the $B \to D^*$ zero recoil form factor using highly improved staggered quarks and nonrelativistic lattice QCD and produced a result in good agreement with the literature and with a comparable error. I have also carried out an exploratory calculation of the nonzero recoil form factor on a small lattice with physically tuned parameters, demonstrating the viability of the statistical analysis as well as highlighting potential difficulties.

The calculation of the NRQCD action parameters c_1, c_5, c_2 and c_4 using automated perturbation theory completes the intended $\mathcal{O}(\alpha)$ improvement of the v^6 NRQCD action. As finer lattices become available the use of HISQ quarks using masses heavier than the charm, approaching that of the bottom quark, will allow extrapolation to the physical heavy quark mass of form factors relevant to weak and electromagnetic decays. Such calculations will evade uncertainties arising from matching currents, but will introduce new uncertainties associated with the extrapolation to heavier masses. In order to test and improve our understanding of these uncertainties, a highly improved non-relativistic action is highly desirable, and moving from the v^4 action to the v^6 action represents a significant step. In the future it would be desirable to improve further upon these calculations by computing the radiative corrections using TBC, though this will require some means of matching IR regulators between the continuum and lattice calculations.

Bibliography

[1] **HPQCD** Collaboration, J. Harrison, C. T. H. Davies, and M. Wingate, "Lattice QCD calculation of the $B_{(s)} \to D^*_{(s)}\ell\nu$ form factors at zero recoil and implications for $|V_{cb}|$," *Phys. Rev. D* **97** (2018) 054502.

[2] Hughes, Ciaran and Davies, Christine T. H. and Harrison, Judd and Horgan, Ronald R. and von Hippel, Georg M. and Wingate, Matthew, "Improving the kinetic couplings in lattice non-relativistic QCD,".

[3] Davies, Christine and Harrison, Judd and Lepage, G Peter and Monahan, Christopher and Shigemitsu, Junko and Wingate, Matthew, "Improving the theoretical prediction for the $B_s - \bar{B}_s$ width difference: matrix elements of next-to-leading order $\Delta B = 2$ operators," *EPJ Web Conf.* **175** (2018) 13023.

[4] J. A. Bailey *et al.*, "Update of $|V_{cb}|$ from the $\bar{B} \to D^*\ell\bar{\nu}$ form factor at zero recoil with three-flavor lattice QCD," *Phys. Rev. D* **89** no. 11, (2014) 114504, `arXiv:1403.0635 [hep-lat]`.

[5] **HPQCD** Collaboration, Dowdall, R. J. and Colquhoun, B. and Daldrop, J. O. and Davies, C. T. H. and Kendall, I. D. and Follana, E. and Hammant, T. C. and Horgan, R. R. and Lepage, G. P. and Monahan, C. J. and Müller, E. H., "The Upsilon spectrum and the determination of the lattice spacing from lattice QCD including charm quarks in the sea," *Phys. Rev. D* **85** (2012) 054509.

[6] R. J. Dowdall, C. T. H. Davies, G. P. Lepage, and C. McNeile, "V_{us} from and K decay constants in full lattice QCD with physical u, d, s, and c quarks," *Phys. Rev. D* **88** (2013) 074504.

[7] **HPQCD** Collaboration, Chakraborty, Bipasha and Davies, C. T. H. and Galloway, B. and Knecht, P. and Koponen, J. and Donald, G. C. and Dowdall, R. J. and Lepage, G. P. and McNeile, C., "High-precision quark masses and QCD coupling from $n_f = 4$ lattice QCD," *Phys. Rev. D* **91** (2015) 054508.

[8] J. Harrison, C. Davies, and M. Wingate, "$|V_{cb}|$ from the $\bar{B}^0 \to D^{*+}\ell^-\bar{\nu}$ zero-recoil form factor using $2+1+1$ flavour HISQ and NRQCD," *Proc. Sci.* **LATTICE2016** (2016) 287, `arXiv:1612.06716 [hep-lat]`.

[9] Monahan, Christopher and Shigemitsu, Junko and Horgan, Ron, "Matching lattice and continuum axial-vector and vector currents with nonrelativistic QCD and highly improved staggered quarks," *Phys. Rev. D* **87** (2013) 034017.

[10] B. Colquhoun, C. T. H. Davies, R. J. Dowdall, J. Kettle, J. Koponen, G. P. Lepage, and A. T. Lytle, "B-meson decay constants: a more complete picture from full lattice QCD," *Phys. Rev. D* **91** no. 11, (2015) 114509, `arXiv:1503.05762 [hep-lat]`.

[11] T. C. Hammant, A. G. Hart, G. M. von Hippel, R. R. Horgan, and C. J. Monahan, "Radiative improvement of the lattice nonrelativistic QCD action using the background field method with applications to quarkonium spectroscopy," *Phys. Rev. D* **88** (2013) 014505.

[12] K. G. Wilson, "Confinement of quarks," *Phys. Rev. D* **10** (1974) 2445–2459.

[13] **HPQCD** Collaboration, E. B. Gregory, C. T. H. Davies, I. D. Kendall, J. Koponen, K. Wong, E. Follana, E. Gámiz, G. P. Lepage, E. H. Müller, H. Na, and J. Shigemitsu, "Precise B, B_s, and B_c meson spectroscopy from full lattice QCD," *Phys. Rev. D* **83** (2011) 014506.

[14] R. R. Horgan, Z. Liu, S. Meinel, and M. Wingate, "Lattice QCD calculation of form factors describing the rare decays $B \to K^* \ell^+ \ell^-$ and $B_s \to \phi \ell^+ \ell^-$," *Phys. Rev. D* **89** (2014) 094501.

[15] **Fermilab Lattice - MILC** Collaboration, A. Bazavov, C. Bernard, C. M. Bouchard, C. DeTar, M. Di Pierro, A. X. El-Khadra, R. T. Evans, E. D. Freeland, E. Gámiz, S. Gottlieb, U. M. Heller, J. E. Hetrick, R. Jain, A. S. Kronfeld, J. Laiho, L. Levkova, P. B. Mackenzie, E. T. Neil, M. B. Oktay, J. N. Simone, R. Sugar, D. Toussaint, and R. S. Van de Water, "B- and D-meson decay constants from three-flavor lattice QCD," *Phys. Rev. D* **85** (2012) 114506.

[16] G. K. Cheung, C. O'Hara, G. Moir, M. Peardon, S. M. Ryan, C. E. Thomas, and D. Tims, "Excited and exotic charmonium, D_s and D meson spectra for two light quark masses from lattice QCD," *Journal of High Energy Physics* **2016** no. 12, (2016) 89.

[17] Z. Fodor and C. Hoelbling, "Light hadron masses from lattice QCD," *Rev. Mod. Phys.* **84** (2012) 449–495.

[18] **HPQCD** Collaboration, B. Chakraborty, C. T. H. Davies, B. Galloway, P. Knecht, J. Koponen, G. C. Donald, R. J. Dowdall, G. P. Lepage, and C. McNeile, "High-precision quark masses and QCD coupling from $n_f = 4$ lattice QCD," *Phys. Rev. D* **91** (2015) 054508.

[19] **Fermilab Lattice - MILC** Collaboration, A. Bazavov, C. Bernard, C. M. Bouchard, C. C. Chang, C. DeTar, D. Du, A. X. El-Khadra, E. D. Freeland, E. Gámiz, S. Gottlieb, U. M. Heller, A. S. Kronfeld, J. Laiho, P. B. Mackenzie, E. T. Neil, J. Simone, R. Sugar, D. Toussaint, R. S. Van de Water, and R. Zhou, "$B^0_{(s)}$-mixing matrix elements from lattice QCD for the Standard Model and beyond," *Phys. Rev. D* **93** (2016) 113016.

[20] **ETM** Collaboration, C. Alexandrou, S. Bacchio, P. Dimopoulos, J. Finkenrath, R. Frezzotti, K. Jansen, B. Kostrzewa, M. Mangin-Brinet, F. Sanfilippo, S. Simula, C. Urbach, and U. Wenger, "Pion vector form factor from lattice QCD at the physical point," *Phys. Rev. D* **97** (2018) 014508.

[21] **Budapest-Marseille-Wuppertal** Collaboration, Dürr, Stephan and Fodor, Zoltán and Hoelbling, Christian and Krieg, Stefan and Kurth, Thorsten and Lellouch, Laurent and Lippert, Thomas and Malak, Rehan and Métivet, Thibaut and Portelli, Antonin and Sastre, Alfonso and Szabó, Kálmán, "Lattice QCD at the physical point meets $SU(2)$ chiral perturbation theory," *Phys. Rev. D* **90** (2014) 114504.

[22] V. Gimnez and J. Reyes, "Calculation of the continuum-lattice HQET matching for the complete basis of four-fermion operators: reanalysis of the B^0B^0 mixing," *Nuclear Physics B* **545** no. 1, (1999) 576606.

[23] S. Weinberg, *The Quantum Theory of Fields, Volume II.*

[24] C. Itzykson and J. Zuber, *Quantum Field Theory.*

[25] I. Montvay and G. Munster, *Quantum Fields on a Lattice.*

[26] G. P. Lepage, "Two-particle states on a torus and their relation to the scattering matrix," *Nuclear Physics B* **354** (1991) 531–578.

[27] P. Guo, J. J. Dudek, R. G. Edwards, and A. P. Szczepaniak, "Coupled-channel scattering on a torus," *Phys. Rev. D* **88** (2013) 014501.

[28] K. Rummukainen and S. Gottlieb, "Resonance scattering phase shifts on a non-rest-frame lattice," *Nuclear Physics B* **450** no. 1, (1995) 397 – 436.

[29] C.-J. Lin, G. Martinelli, C. Sachrajda, and M. Testa, "K decays in a finite volume," *Nuclear Physics B* **619** no. 1, (2001) 467 – 498.

[30] M. Döring, U. G. Meißner, E. Oset, and A. Rusetsky, "Unitarized chiral perturbation theory in a finite volume: Scalar meson sector," *The European Physical Journal A* **47** no. 11, (2011) 139.

[31] C. Gattringer and C. Lang , *Quantum Chromodynamics on the Lattice*.

[32] M. Alford, W. Dimm and G.P. Lepage, "Lattice QCD on Small Computers," `arXiv:9507010 [hep-lat]`.

[33] Christof Gattringer, Roland Hoffmann, Stefan Schaefer, "Setting the scale for the luscher-weisz action," `arXiv:hep-lat/0112024 [hep-lat]`.

[34] P. M. G. Peter Lepage, "On the Viability of Lattice Perturbation Theory," `arXiv:9209022 [hep-lat]`.

[35] G. P. Lepage, "Redesigning Lattice QCD," `arXiv:hep-lat/9607076 [hep-lat]`.

[36] A. Hart, G. M. von Hippel, and R. R. Horgan, "Radiative corrections to the lattice gluon action for highly improved staggered quarks and the effect of such corrections on the static potential," *Phys. Rev. D* **79** (2009) 074008.

[37] **HPQCD** Collaboration, E. Follana, Q. Mason, C. Davies, K. Hornbostel, G. P. Lepage, J. Shigemitsu, H. Trottier, and K. Wong, "Highly improved staggered quarks on the lattice with applications to charm physics," *Phys. Rev. D* **75** (2007) 054502.

[38] H. Nielsen and M. Ninomiya, "Absence of neutrinos on a lattice: (I). Proof by homotopy theory," *Nuclear Physics B* **185** no. 1, (1981) 2040.

[39] S. R. Sharpe, "Rooted staggered fermions: Good, bad or ugly?," *PoS* **LAT2006** (2006) 022, `arXiv:hep-lat/0610094 [hep-lat]`.

[40] R. Dowdall, C. Davies, T. Hammant, and R. Horgan, "Precise heavy-light meson masses and hyperfine splittings from lattice QCD including charm quarks in the sea," *Phys. Rev. D* **86** (2012) 094510, `arXiv:1207.5149 [hep-lat]`.

[41] C. Aubin and C. Bernard, "Pion and kaon masses in staggered chiral perturbation theory," *Phys. Rev. D* **68** (2003) 034014.

[42] **Fermilab Lattice - MILC** Collaboration, A. Bazavov, C. Bernard, J. Komijani, C. M. Bouchard, C. DeTar, J. Foley, L. Levkova, D. Du, J. Laiho, A. X. El-Khadra, E. D. Freeland, E. Gámiz, S. Gottlieb, U. M. Heller, J. Kim, D. Toussaint, A. S. Kronfeld, P. B. Mackenzie, J. N. Simone, R. S. Van de Water, R. Zhou, E. T. Neil, and R. Sugar, "Charmed and light pseudoscalar meson decay constants from four-flavor lattice qcd with physical light quarks," *Phys. Rev. D* **90** (2014) 074509.

[43] G. P. Lepage, "Flavor-symmetry restoration and Symanzik improvement for staggered quarks," *Phys. Rev. D* **59** (1999) 074502.

[44] A. Lytle, "Semileptonic B_c decays from full lattice QCD," `arXiv:1605.05645 [hep-lat]`.

[45] G. P. Lepage, L. Magnea, C. Nakhleh, U. Magnea, and K. Hornbostel, "Improved nonrelativistic QCD for heavy-quark physics," *Phys. Rev. D* **46** (1992) 4052–4067.

[46] **ARGUS** Collaboration, H. Albrecht *et al.*, "Measurement of the Decay $B_0 \to D^*$- Lepton+ Neutrino," *Phys. Lett. B* **197** (1987) 452–456.

[47] **Heavy Flavor Averaging Group (HFAG)** Collaboration, Y. Amhis *et al.*, "Averages of b-hadron, c-hadron, and τ-lepton properties as of summer 2016," `arXiv:1612.07233 [hep-ex]`.

[48] A. J. Bevan *et al.*, "The Physics of the B Factories," *Eur. Phys. J. C* **74** (2014) 3026, `arXiv:1406.6311 [hep-ex]`.

[49] A. Alberti, P. Gambino, K. J. Healey, and S. Nandi, "Precision Determination of the Cabibbo-Kobayashi-Maskawa Element V_{cb}," *Phys. Rev. Lett.* **114** no. 6, (2015) 061802, `arXiv:1411.6560 [hep-ph]`.

[50] J. A. Bailey *et al.*, "$B \to D\ell\nu$ form factors at nonzero recoil and $|V_{cb}|$ from 2+1-flavor lattice QCD," *Phys. Rev. D* **92** no. 3, (2015) 034506, arXiv:1503.07237 [hep-lat].

[51] H. Na *et al.*, "$B \to Dl\nu$ form factors at nonzero recoil and extraction of $|V_{cb}|$," *Phys. Rev. D* **92** no. 5, (2015) 054510, arXiv:1505.03925 [hep-lat].

[52] C. G. Boyd, B. Grinstein, and R. F. Lebed, "Constraints on form-factors for exclusive semileptonic heavy to light meson decays," *Phys. Rev. Lett.* **74** (1995) 4603–4606, arXiv:hep-ph/9412324 [hep-ph].

[53] C. Bourrely, L. Lellouch, and I. Caprini, "Model-independent description of $B \to \pi\ell\nu$ decays and a determination of $|V(ub)|$," *Phys. Rev. D* **79** (2009) 013008, arXiv:0807.2722 [hep-ph].

[54] **FLAG** Collaboration, S. Aoki *et al.*, "Review of lattice results concerning low-energy particle physics," *Eur. Phys. J. C* **77** no. 2, (2017) 112, arXiv:1607.00299 [hep-lat].

[55] **MILC** Collaboration, A. Bazavov *et al.*, "Scaling studies of QCD with the dynamical HISQ action," *Phys. Rev. D* **82** (2010) 074501, arXiv:1004.0342 [hep-lat].

[56] **MILC** Collaboration, A. Bazavov *et al.*, "Lattice QCD ensembles with four flavors of highly improved staggered quarks," *Phys. Rev. D* **87** no. 5, (2013) 054505, arXiv:1212.4768 [hep-lat].

[57] **MILC** Collaboration, A. Bazavov *et al.*, "Gradient flow and scale setting on MILC HISQ ensembles," *Phys. Rev. D* **93** no. 9, (2016) 094510, arXiv:1503.02769 [hep-lat].

[58] **HPQCD** Collaboration, E. Follana *et al.*, "Highly Improved Staggered Quarks on the Lattice, with Applications to Charm Physics," *Phys. Rev. D* **75** (2007) 054502, arXiv:hep-lat/0610092.

[59] G. P. Lepage, L. Magnea, C. Nakhleh, U. Magnea, and K. Hornbostel, "Improved nonrelativistic QCD for heavy quark physics," *Phys. Rev. D* **46** (1992) 4052–4067, `hep-lat/9205007`.

[60] A. Sirlin, "Large m(W), m(Z) Behavior of the O(alpha) Corrections to Semileptonic Processes Mediated by W," *Nucl. Phys. B* **196** (1982) 83–92.

[61] E. S. Ginsberg, "Radiative corrections to k-e-3-neutral decays and the delta-i=1/2 rule. (erratum)," *Phys. Rev.* **171** (1968) 1675. [Erratum: Phys. Rev. **174**, 2169 (1968)].

[62] D. Atwood and W. J. Marciano, "Radiative Corrections and Semileptonic B Decays," *Phys. Rev.* **D41** (1990) 1736.

[63] MILC Code Repository, https://github.com/milc-qcd.

[64] I. D. Kendall, *Lattice QCD studies of Upsilon physics*. PhD thesis, University of Glasgow, 2010.

[65] J. J. Dudek, R. G. Edwards, and D. G. Richards, "Radiative transitions in charmonium from lattice QCD," *Phys. Rev. D* **73** (2006) 074507.

[66] C. J. Morningstar and J. Shigemitsu, "Perturbative matching of lattice and continuum heavy-light currents with nrqcd heavy quarks," *Phys. Rev. D* **59** (1999) 094504.

[67] M. E. Luke, "Effects of subleading operators in the heavy quark effective theory," *Phys. Lett. B* **252** (1990) 447–455.

[68] G. P. Lepage *et al.*, "Constrained curve fitting," *Nucl. Phys. Proc. Suppl.* **106** (2002) 12–20, `hep-lat/0110175`.

[69] G.P. Lepage, "Corrfitter Version 4.1.". github.com/gplepage/corrfitter.git.

[70] J. Laiho, R.S. Van de Water, "$B \to D^* l\nu$ and $B \to Dl\nu$ form factors in staggered chiral perturbation theory," *Phys. Rev. D* **73** (2006) 054501.

[71] C. Aubin and C. Bernard, "Pseudoscalar decay constants in staggered chiral perturbation theory," *Phys. Rev. D* **68** (2003) 074011.

[72] R. J. Dowdall, C. T. H. Davies, R. R. Horgan, C. J. Monahan, and J. Shigemitsu, "B-meson decay constants from improved lattice NRQCD and physical u, d, s and c sea quarks," *Phys. Rev. Lett.* **110** no. 22, (2013) 222003, arXiv:1302.2644 [hep-lat].

[73] F. U. Bernlochner, Z. Ligeti, M. Papucci, and D. J. Robinson, "Combined analysis of semileptonic B decays to D and D^*: $R(D^{(*)})$, $|V_{cb}|$, and new physics," *Phys. Rev.* **D95** no. 11, (2017) 115008, arXiv:1703.05330 [hep-ph].

[74] D. Bigi, P. Gambino, and S. Schacht, "A fresh look at the determination of $|V_{cb}|$ from $B \to D^* \ell\nu$," *Phys. Lett. B* **769** (2017) 441–445, arXiv:1703.06124 [hep-ph].

[75] B. Grinstein and A. Kobach, "Model-Independent Extraction of $|V_{cb}|$ from $\bar{B} \to D^* \ell\overline{\nu}$," *Phys. Lett. B* **771** (2017) 359–364, arXiv:1703.08170 [hep-ph].

[76] D. Bigi, P. Gambino, and S. Schacht, "$R(D^*)$, $|V_{cb}|$, and the Heavy Quark Symmetry relations between form factors," arXiv:1707.09509 [hep-ph].

[77] S. Jaiswal, S. Nandi, and S. K. Patra, "Extraction of $|V_{cb}|$ from $B \to D^{(*)} \ell\nu_\ell$ and the Standard Model predictions of $R(D^{(*)})$," arXiv:1707.09977 [hep-ph].

[78] F. U. Bernlochner, Z. Ligeti, M. Papucci, and D. J. Robinson, "Tensions and correlations in $|V_{cb}|$ determinations," arXiv:1708.07134 [hep-ph].

[79] I. Caprini, L. Lellouch, and M. Neubert, "Dispersive bounds on the shape of anti-$B \to D(*)$ lepton anti-neutrino form-factors," *Nucl. Phys. B* **530** (1998) 153–181, arXiv:hep-ph/9712417 [hep-ph].

[80] C. G. Boyd, B. Grinstein, and R. F. Lebed, "Precision corrections to dispersive bounds on form-factors," *Phys. Rev. D* **56** (1997) 6895–6911, arXiv:hep-ph/9705252 [hep-ph].

[81] C. Sachrajda and G. Villadoro, "Twisted boundary conditions in lattice simulations," *Physics Letters B* **609** no. 1, (2005) 73 – 85.

[82] M. Lscher and P. Weisz, "Efficient numerical techniques for perturbative lattice gauge theory computations," *Nuclear Physics B* **266** no. 2, (1986) 309 – 356.

[83] A. Hart and G.M. von Hippel and R.R. Horgan and E.H. Müller, "Automated generation of lattice QCD Feynman rules," *Computer Physics Communications* **180** no. 12, (2009) 2698 – 2716. 40 YEARS OF CPC: A celebratory issue focused on quality software for high performance, grid and novel computing architectures.

[84] A. Hart, G. von Hippel, R. Horgan, and L. Storoni, "Automatically generating feynman rules for improved lattice field theories," *Journal of Computational Physics* **209** no. 1, (2005) 340 – 353.

[85] Hammant, T.C. and Horgan, R.R. and Monahan, C.J. and Hart, A.G. and Müller, E.H. and Gray, A. and Sivalingham, K. and von Hippel, G.M., "Improved automated lattice perturbation theory in background field gauge," *arXiv:1011.2696* .

[86] G. P. Lepage, "A new algorithm for adaptive multidimensional integration," *Journal of Computational Physics* **27** no. 2, (1978) 192 – 203.

[87] S. Meinel, "Bottomonium spectrum at order v^6 from domain-wall lattice QCD: Precise results for hyperfine splittings," *Phys. Rev. D* **82** (2010) 114502.

[88] Hammant, T. C. and Hart, A. G. and von Hippel, G. M. and Horgan, R. R. and Monahan, C. J., "Radiative improvement of the lattice nonrelativistic QCD action using the background field method with applications to quarkonium spectroscopy," *Phys. Rev. D* **88** (2013) 014505.

[89] T. Hammant, A. Hart, G. von Hippel, R. Horgan, and C. Monahan, "Radiative improvement of the lattice NRQCD action using the background field method and application to the hyperfine splitting of quarkonium states," *Phys. Rev. Lett.* **107** (2011) 112002, `arXiv:1105.5309 [hep-lat]`.

[90] T. C. Hammant, *Perturbative Calculations in Lattice Gauge Theories and the Application of Statistical Mechanics to Soft Condensed Matter Systems*. PhD thesis, University of Cambridge, DAMTP.

[91] **HPQCD** Collaboration, Dowdall, R. J. and Davies, C. T. H. and Hammant, T. and Horgan, R. R., "Bottomonium hyperfine splittings from lattice nonrelativistic QCD including radiative and relativistic corrections," *Phys. Rev. D* **89** (2014) 031502.

[92] **Particle Data Group** Collaboration, Olive, K. A. and others, "Review of Particle Physics," *Chin. Phys.* **C38** (2014) 090001.

Appendix A

Explicit Correlation Function Contractions

For real, symmetric, stride-2 smearings Δ, suppressing Dirac indices for the moment, and summing over repeated indices and spatial coordinates for zero recoil:

$$\begin{aligned}
C_{3pt}(x_0, y_0, z_0) =& \langle \bar{u}_a(x) M_{st} c_a(x + \sigma_1 + \delta_{st}) \bar{c}_b(y) \Gamma b_b(y) \bar{b}_c(z + \sigma_2) \gamma u_c(z) \rangle \Delta_1(\sigma_1) \Delta_2(\sigma_2) \\
=& \mathrm{tr}\left[\Omega^\dagger(x) M_{st} \Omega(x + \delta_{st}) S^c_{ab}(x + \sigma_1 + \delta_{st}, y) \Omega^\dagger(y) \Gamma \right] \\
& \times \left[G^b_{bc}(y, z + \sigma_2) \gamma \Omega(z) S^l_{ca}(z, x) \right] \Delta_1(\sigma_1) \Delta_2(\sigma_2) \\
=& \mathrm{tr}\left[\xi^*_{ea}(x) \Omega^\dagger(x) M_{st} \Omega(x + \delta_{st}) S^c_{eb}(x + \sigma_1 + \delta_{st}, y) \Omega^\dagger(y) \Gamma \right] \\
& \times \left[G^b_{bc}(y, z + \sigma_2) \gamma \Omega(z) S^l_{cd}(z, x') \xi_{da}(x') \right] \Delta_1(\sigma_1) \Delta_2(\sigma_2)
\end{aligned} \tag{A.1}$$

where it is understood that when we add δ_{st} it is modulo the hypercube. I have used the noise condition:

$$\xi^*_{ab}(z) \xi_{cb}(y) = \delta_{ac} \delta_{xy} \tag{A.2}$$

to insert the random walls. Setting

$$\mathrm{Ext}_{ba}(y) = G^b_{bc}(y, z + \sigma_2) \gamma \Omega(z) S^l_{cd}(z, x') \xi_{da}(x') \Delta_2(\sigma_2) \tag{A.3}$$

this becomes

$$\begin{aligned}
C_{3pt}(x_0, y_0, z_0) =& \mathrm{tr}\left[\xi^*_{ea}(x) \Omega^\dagger(x) M_{st} \Omega(x + \delta_{st}) S^c_{eb}(x + \sigma_1 + \delta_{st}, y) \Omega^\dagger(y) \Gamma \mathrm{Ext}_{ba}(y) \right] \Delta_1(\sigma_1) \\
=& \mathrm{tr}\left[\xi^*_{ea}(x - \sigma_1) \Omega^\dagger(x) M_{st} \Omega(x + \delta_{st}) S^c_{eb}(x + \delta_{st}, y) \Omega^\dagger(y) \Gamma \mathrm{Ext}_{ba}(y) \right] \Delta_1(\sigma_1) \,.
\end{aligned} \tag{A.4}$$

Now, we do not have $S^c_{ab}(x,y)$, we have $S^c_{ab}(y,x)$ so we can use:

$$S^*_{ba}(x,y) = (-1)^y S_{ab}(y,x)(-1)^x \tag{A.5}$$

where $(-1)^x$ is shorthand for $(-1)^{x_0+x_1+x_2+x_3}$. Now

$$\begin{aligned} C_{3pt}(x_0,y_0,z_0) =& \mathrm{tr}\left[\Omega^\dagger(y)(-1)^y S^{c*}_{bc}(y,x+\delta_{st})(-1)^{x+\delta_{st}}\beta_M(x)\xi^*_{ca}(x-\sigma_1)\Gamma \mathrm{Ext}_{ba}(y)\right] \\ & \times \Delta_1(\sigma_1) \end{aligned} \tag{A.6}$$

where $\beta_M(x) = \Omega^\dagger(x) M_{st} \Omega(x+\delta_{st})$ is the local spin-taste phase. Inserting Dirac indices:

$$\begin{aligned} C_{3pt}(x_0,y_0,z_0) =& \Omega^\dagger_{\alpha\beta}(y)(-1)^y S^{c*}_{bc}(y,x)(-1)^x \beta_M(x+\delta_{st})\xi^*_{ca}(x-\sigma_1+\delta_{st})\Delta_1(\sigma_1) \\ & \times \Gamma_{\beta\kappa}\mathrm{Ext}_{ba,\kappa\alpha}(y) \\ =& \pm\left[\Omega_{\beta\alpha}(y)(-1)^y S^c_{bc}(y,x)(-1)^x \beta_M(x)\xi_{ca}(x-\sigma_1+\delta_{st})\Delta_1(\sigma_1)\right]^* \\ & \times \Gamma_{\beta\kappa}\mathrm{Ext}_{ba,\kappa\alpha}(y)\,. \end{aligned} \tag{A.7}$$

We recognise $S^c_{bc}(y,x)(-1)^x\beta_M(x)\xi_{ca}(x-\sigma_1+\delta_{st})\Delta_1(\sigma_1)$ as the MILC KS propagator. The naive active quark that gets made in NRQCD is then:

$$\mathrm{Active}_{ab,\alpha\beta}(y) = \Omega_{\alpha\beta}(y)(-1)^y S^c_{ac}(y,x)(-1)^x\beta_M(x)\xi_{cb}(x-\sigma_1+\delta_{st})\Delta_1(\sigma_1) \tag{A.8}$$

and the contractions to do are

$$\begin{aligned} \mathrm{Current}_{ab,\alpha\beta}(y) &= \mathrm{Active}^*_{ba,\kappa\alpha}(y)\Gamma_{\kappa\beta} \\ C_{3pt} &= \mathrm{Current}_{ab,\alpha\beta}(y)\mathrm{Ext}_{ba,\beta\alpha}(y)\,. \end{aligned} \tag{A.9}$$

Appendix B

Treatment of Poles in Vegas Integration

When evaluating the diagrams in figure (5.1) we take the integral over k_4 as an integral over a circle in the complex plane $w = e^{ik_4}$. In order to prevent poles crossing this contour as we vary the spatial momentum $\vec{k}$ it is necessary to vary the radius of the contour. Considering first the abelian diagram there are two fermionic poles occuring at

$$w_{f_1}^{-1} = 1 - G^{-1}(p-k)|_{k_4=0} = \left(1 - \frac{aH_0(p-k)}{2n}\right)^{2n} e^{-ip_4} \tag{B.1}$$

and

$$w_{f_2}^{-1} = 1 - G^{-1}(p-k+q)|_{k_4=0} = \left(1 - \frac{aH_0(p-k+q)}{2n}\right)^{2n} e^{-i(p_4+q_4)} \tag{B.2}$$

where the two RHS expressions illustrate the result for the unimproved NRQCD action. The gluon poles are given by

$$w_g^{\pm} = \frac{1}{2}\left[2 + \hat{k}^2 + \mu^2 \pm \sqrt{(\hat{k}^2+\mu^2)(\hat{k}^2+\mu^2+4)}\right] \tag{B.3}$$

with

$$\hat{k}^2 = \sum_{j=1,3} 4\sin^2(k_j/2) \tag{B.4}$$

and μ an infra red gluon mass regulator. For large k w_{f_1}, w_{f_2} and w_g^+ move away from the unit circle on the outside while w_g^- moves towards zero. However for intermediate values of k the fermionic poles may move inside of the unit circle. We therefore shift

the contour of integration to ensure that no poles cross it as we vary k. We move the contour to cross through the average of w_g^- and the left most right moving pole of w_{f_1}, w_{f_2} and w_g^+.

In the case of the nonabelian diagram there are four gluon poles and a single fermionic pole. The gluon poles are given by

$$w_{1g}^{\pm} = \frac{e^{-ip_4}}{2}\left[2 + (p \hat{-} k)^2 + \mu^2 \pm \sqrt{\left((p \hat{-} k)^2 + \mu^2\right)\left((p \hat{-} k)^2 + \mu^2 + 4\right)}\right] \tag{B.5}$$

$$w_{2g}^{\pm} = \frac{e^{-i(p_4+q_4)}}{2}\left[2 + (p - \hat{k} + q)^2 + \mu^2 \pm \sqrt{\left((p - \hat{k} + q)^2 + \mu^2\right)\left((p - \hat{k} + q)^2 + \mu^2 + 4\right)}\right] \tag{B.6}$$

and the fermion pole is given by

$$w_f^{-1} = 1 - G^{-1}(k)|_{k_4=0} = \left(1 - \frac{aH_0(k)}{2n}\right)^{2n}. \tag{B.7}$$

Again it is necessary to shift the contour between the rightmost leftmoving pole and the leftmost rightmoving pole. The two swordfish diagrams require similar treatment. The algae and ankh diagrams have simpler pole structure with only gluon poles appearing and moving in opposite directions away from the unit circle, as such no contour shift is needed.